

Graph-Structured Topic Modeling for Documents with Spatial or Covariate Dependencies

Yeo Jin Jung

*Department of Statistics
The University of Chicago
Chicago, IL 60637, USA*

YEOJINJUNG@UCHICAGO.EDU

Claire Donnat

*Department of Statistics
The University of Chicago
Chicago, IL 60637, USA*

CDONNAT@UCHICAGO.EDU

Abstract

We address the challenge of incorporating document-level metadata into topic modeling to improve topic mixture estimation. To overcome the computational complexity and lack of theoretical guarantees in existing Bayesian methods, we extend probabilistic latent semantic indexing (pLSI), a frequentist framework for topic modeling, by incorporating document-level covariates or known similarities between documents through a graph formalism. Modeling documents as nodes and edges denoting similarities, we propose a new estimator based on a fast graph-regularized iterative singular value decomposition (SVD) that encourages similar documents to share similar topic mixture proportions. We characterize the estimation error of our proposed method by deriving high-probability bounds and develop a specialized cross-validation method to optimize our regularization parameters. We validate our model through comprehensive experiments on synthetic datasets and three real-world corpora, demonstrating improved performance and faster inference compared to existing Bayesian methods.

Keywords: Topic Modeling, Latent Dirichlet Allocation, Total Variation Penalty, Graph Regularization, Graph Cross Validation;

1 Introduction

Consider a corpus of n documents, each composed of words (or more generally, terms) from a vocabulary of size p . This corpus can be represented by a *document-term* matrix $D \in \mathbb{N}^{n \times p}$, where each entry D_{ij} denotes the number of times term j appears in document i . The objective of topic modeling is to retrieve low-dimensional representations of the data by representing each document as a mixture of latent topics, defined as distributions over term frequencies.

In this setting, each document $D_i \in \mathbb{R}^p$ is usually assumed to be sampled from a multinomial distribution with an associated probability vector $M_i \in \mathbb{R}^p$ that can be decomposed as a mixture of K topics. In other words, letting N_i denote the length of document i :

$$\forall i = 1, \dots, n, \quad D_i \sim \text{Multinomial}(N_i, M_i), \quad \text{with } M_i = \sum_{k=1}^K W_{ik} A_k. \quad (1)$$

In the previous equation, W_{ik} corresponds to the proportion of topic k in document i , and the vector W_i provides a low-dimensional representation of document i in terms of its topic composition. Each entry A_{kj} of the vector $A_k \in \mathbb{R}^p$ corresponds to the expected frequency of word j in topic k . Since document lengths $\{N_i\}_{i=1}^n$ are usually treated as nuisance variables, most topic modeling approaches work in fact directly with the word frequency matrix $X = \text{diag}(\{\frac{1}{N_i}\}_{i=1 \dots n})D$, which can be written in a “signal + noise” form as:

$$X = M + Z = WA + Z. \quad (2)$$

Here, $M \in \mathbb{R}^{n \times p}$ is the true signal whose entry M_{ij} denotes the expected frequency of word i in document j , while $Z = X - M$ denotes some centered multinomial noise. The objective of topic modeling is thus to estimate W and A from X .

Originally developed to reduce document representations to low-dimensional latent semantic spaces, topic modeling has been successfully deployed for the analysis of count data in a number of applications, ranging from image processing (Tu et al., 2016; Zheng et al., 2015) and image annotation (Feng and Lapata, 2010; Shao et al., 2009), to biochemistry (Reder et al., 2021), genetics (Dey et al., 2017; Kho et al., 2017; Liu et al., 2016; Yang et al., 2019) or microbiome studies (Sankaran and Holmes, 2019; Symul et al., 2023).

A notable extension of topic modeling occurs when additional document-level data is available. Although original topic modeling approaches rely solely on the analysis of the empirical frequency matrix X , this additional information has the potential to significantly improve the estimation of the *word-topic* matrix A and the *document-topic* mixture matrix W , particularly in difficult inference settings, such as when the number of words per document is small. Examples include:

1. *Analyzing tumor microenvironments*: In this context, slices of tumor samples are partitioned into smaller regions known as “tumor microenvironments,” where the frequency of specific immune cell types is recorded (Chen et al., 2020). Here, documents correspond to tumor microenvironments, and words to cell types. The objective is to identify communities of co-abundant cells—the “topics”, taken here as a proxy for patterns of tumor-immunecell interactions—to evaluate whether some can be associated with specific outcomes such as survival rates. In this setting, a reasonable hypothesis consists in assuming that neighboring microenvironments share similar topic proportions. Since these microenvironments are inherently small, leveraging the spatial smoothness of the mixture matrix W can significantly improve inference (Chen et al., 2020). We develop this example in further detail in Section 4.1.
2. *Microbiome studies*: Topic models have also been proven to be extremely useful in microbiome analysis (Sankaran and Holmes, 2019; Symul et al., 2023). In this setting, the data consists of a microbiome count matrix recording the amount of different types of bacteria found in each sample. In this case, microbiome samples are identified to documents, with bacteria playing the roles of the vocabulary, and the goal becomes to identify communities of co-abundant bacteria (Sankaran and Holmes, 2019). When additional covariate information is available (such as age, gender, and other demographic details), we can expect similar samples (documents) to exhibit similar community compositions (topic proportions).

3. *The analysis of short documents*, such as a collection of scientific abstracts or recipes: In this case, while recipes might be short, information on the origin of the recipe can help determine the topics and mixture matrix more accurately by leveraging the assumption that recipes wof neighboring countries will typically share similar topic proportions. We elaborate on this example in greater detail in Section 4.2.

Prior works. To the best of our knowledge, previous attempts to incorporate metadata to improve topic estimation have focused on Bayesian approaches to topic modeling, usually extending the latent Dirichlet allocation (LDA) model of Blei et al. (2001). We defer the detailed description of these methods to Section 5, and only briefly summarize their main characteristics here. By and large, these methods typically incorporate the metadata — often in the form of a covariate matrix—within a prior distribution (Blei and Lafferty, 2006a,b; Roberts et al., 2014; Mcauliffe and Blei, 2007). However, these models (a) are difficult to adapt to different types of covariates or information encoded as a graph, and (b) typically lack theoretical guarantees. Recent work by Chen et al. (2020) proposes extending LDA to analyze documents with known similarities by smoothing the topic proportion hyperparameters along the edges of the graph. However, this method does not empirically yield spatially smooth structures (see Sections 3.4 and 4), and significantly increases the algorithm’s running time.

In the frequentist realm, probabilistic latent semantic indexing (pLSI) has benefited from renewed interest over the past five years. Like LDA, pLSI is built around the data generation mechanism explicated in (1), effectively modeling documents as bags of words. Unlike LDA, pLSI assumes that the matrices A and W are fixed parameters, instead of random variables. In particular, new work by Ke and Wang (2017) and Klopp et al. (2021) suggest procedures to reliably estimate the topic matrix A and mixture matrix W , respectively, and rigorously characterize the consistency and efficiency of their estimators through high-probability error bounds. Although recent work has begun investigating the use of structures to improve estimation in pLSI-based topic models, most approaches have limited this to considering various versions of sparsity (Bing et al., 2020; Wu et al., 2023) or weak sparsity (Tran et al., 2023) for the topic matrix A . To the best of our knowledge, however, no pLSI approach has yet been proposed that effectively leverages similarities between documents nor characterizes the consistency of these estimators.

Contributions

In this paper, we propose the first pLSI method that can be made amenable to the inclusion of additional information on the similarity between documents, as encoded by a known graph. More specifically:

- a. We propose a scalable algorithm based on a graph-aligned singular decomposition of the empirical frequency matrix X to provide estimates of W and A (Section 2). Additionally, we develop a new cross-validation procedure for our graph-based penalty that allows us to choose the optimal regularization parameter adaptively (Section 2.3).
- b. We prove the benefits of the graph alignment procedure by deriving high probability upper bounds for both W and A (Section 3), which we verify through extensive simulations (Section 3.4).

- c. We showcase the advantage of our method over LDA-based methods and non-structured pLSI techniques on three real-world datasets: two spatial transcriptomics examples (Section 4.1) and a recipe dataset (Section 4.2).

Notations

Throughout this paper, we use the following notations. For any $t \in \mathbb{Z}_+$, $[t]$ denotes the set $\{1, 2, \dots, t\}$. For any $a, b \in \mathbb{R}$, we write $a \vee b = \max(a, b)$ and $a \wedge b = \min(a, b)$. We use $\mathbf{1}_d \in \mathbb{R}^d$ to denote the vector with all entries equal to 1 and $\mathbf{e}_k \in \mathbb{R}^d$ to denote the vector with k^{th} element set to 1 and 0 otherwise. For any vector u , its ℓ_2 , ℓ_1 and ℓ_0 norms are defined respectively as $\|u\|_2 = \sqrt{\sum_i u_i^2}$, $\|u\|_1 = \sum_i |u_i|$, and $\|u\|_0 = \sum_i \{u_i \neq 0\}$. Let I_m denote the $m \times m$ identity matrix. For any matrix $A = (a_{ij}) \in \mathbb{R}^{n \times p}$, $A(i, j)$ denote the (i, j) -entry of A , $A_{i\cdot}$ and $A_{\cdot j}$ denote the i^{th} row and j^{th} column of A respectively. Throughout this paper, $\lambda_i(A)$ stands for the i^{th} largest singular value of the matrix A with $\lambda_{\max}(A) = \lambda_1(A)$, $\lambda_{\min}(A) = \lambda_{p \wedge \text{rank}(A)}(A)$. We also denote as $U_K(A)$ and $V_K(A)$ the left and right singular matrix from the rank- K SVD of A . The frobenius, entry-wise ℓ_1 norm and the operator norms of A are denoted as $\|A\|_F = \sqrt{\sum_{i,j} a_{ij}^2}$, $\|A\|_{11} = \sum_{i,j} |a_{ij}|$, and $\|A\|_{op} = \lambda_1(A)$, respectively. The ℓ_{21} norm is denoted as $\|A\|_{21} = \sum_{i \in [n]} \|A_{i\cdot}\|_2$. For any positive semi-definite matrix A , $A^{1/2}$ denotes its principal square root that is positive semi-definite and satisfies $A^{1/2}A^{1/2} = A$. The trace inner product of two matrices $A, B \in \mathbb{R}^{n \times p}$ is denoted by $\langle A, B \rangle = \text{Tr}(A^\top B)$. A^\dagger denotes the pseudo-inverse of the matrix A and P_A denotes the projection matrix onto the subspace spanned by columns of A .

2 Graph-Aligned pLSI

In this section, we introduce graph-aligned pLSI (GpLSI), an extension of the standard pLSI framework that leverages known similarities between documents to improve inference in topic modeling using a graph formalism. We begin by introducing a set of additional notations and model assumptions, before introducing the algorithm in Section 2.3.

2.1 Assumptions

Let $\mathcal{G} = (\mathcal{D}, \mathcal{E})$ denote an undirected graph induced by a known adjacency matrix on the n documents in the corpus. The documents are represented as nodes \mathcal{D} , and \mathcal{E} denotes the edge set of size $|\mathcal{E}| = m$. Throughout this paper, for simplicity, we will assume that \mathcal{G} is binary, but our approach—as discussed in Section 2.3—can be in principle extended to weighted graphs. We denote the graph’s incidence matrix as $\Gamma \in \mathbb{R}^{m \times n}$ where, for the d^{th} edge $e = (i, j), i < j$ between nodes i and j in the graph:

$$\Gamma_{dg} = \begin{cases} 1 & \text{if } g = i \\ -1 & \text{if } g = j \\ 0 & \text{otherwise} \end{cases}$$

It is easy to show that the Laplacian of the graph can be expressed in terms of the incidence matrix as $L = \Gamma^\top \Gamma$ (Hütter and Rigollet, 2016). Let Γ^\dagger be the pseudo-inverse of Γ , and

denote by $\mathbf{s}_i, i = 1 \cdots m$ its columns, so that $\Gamma^\dagger = [\mathbf{s}_1, \cdots, \mathbf{s}_m]$. We also define the *inverse scaling factor* of the incidence matrix Γ (Hütter and Rigollet, 2016), a quantity necessary for assessing the performance of GpLSI:

$$\rho(\Gamma) := \max_{l \in [m]} \|\mathbf{s}_l\|_2 \tag{3}$$

We focus on the estimation of the topic mixture matrix under the assumption that neighboring documents have similar mixture proportions: $W_i \approx W_j$ if $i \sim j$. This implies that the rows of W are assumed to be smooth with respect to the graph \mathcal{G} . Noting that the difference of mixture proportions between neighboring nodes i and j ($e = (i, j) \in \mathcal{E}$) can be written as $(\Gamma W)_l = W_i - W_j$, this smoothness assumption effectively implies sparsity on the rows of the matrix ΓW .

Assumption 1 (Graph-Aligned mixture matrix) *The support (i.e., the number of non-zero rows) of the matrix ΓW is small:*

$$|\text{supp}(\Gamma W)| \leq s, \tag{4}$$

where $s \ll |\mathcal{E}|, n$.

The previous assumption is akin to assuming that the underlying mixture matrix W is piecewise-continuous with respect to the graph \mathcal{G} , or more generally, can be well approximated by a piecewise-continuous function.

Our setting is not limited to connected document graphs. Denote $n_{\mathcal{C}}$ as the number of connected subgraphs of \mathcal{G} and $n_{\mathcal{C}_l}$ as the number of nodes in the l^{th} connected subgraph. Denote

$$n_{\mathcal{C}_{\min}} = \min_{l \in [n_{\mathcal{C}}]} n_{\mathcal{C}_l} \tag{5}$$

The error bound of our estimators will depend on the two quantities $n_{\mathcal{C}}$ and $n_{\mathcal{C}_{\min}}$. In the rest of this paper, we will assume that all connected components have roughly the same size: $n_{\mathcal{C}_1} \asymp \cdots \asymp n_{\mathcal{C}_{n_{\mathcal{C}}}}$.

Assumption 2 (Anchor document) *For each topic $k = 1, \dots, K$, there exists at least one document i (called an anchor document) such that $W_{ik} = 1$ and $W_{il} = 0$ for all $l \neq k$.*

Remark 1 *Assumption 2 is standard in the topic modeling community, as it is a sufficient condition for the identifiability of the topic and mixture matrices A and W (Donoho and Stodden, 2003). Beyond identifiability, we argue here that this could be interpreted as much as a definition as an assumption: Topics are interpretable only when associated with archetypes—that is, “extreme” representations (in our case, anchor documents) — that illustrate the topic more expressively.*

Assumption 3 (Equal Document Sizes) *In this paper, for ease of presentation, we will also assume that the documents have equal sizes: $N_1 = \cdots = N_n = N$. More generally, our results also hold if we assume that the document lengths satisfy $\max_{i \in [n]} N_i \leq C^* \min_{i \in [n]} N_i$ ($N_1 \asymp \cdots \asymp N_n$), in which case $N = \frac{1}{n} \sum_{i=1}^n N_i$ denotes the average document length.*

Assumption 4 (Condition number of M and W) *There exist two constants $c > 1$ and $c^* > 0$ such that*

$$\lambda_K(M) \geq c\lambda_1(W) \quad \text{and} \quad \max\{\kappa(M), \kappa(W)\} \leq c^*.$$

Assumption 5 (Assumption on the minimum word frequency) *We assume that the expected word frequencies h_j defined as: $\forall j \in [p], h_j = \sum_{i=1}^n A_{ij}$ are bounded below by:*

$$\min_{j \in [p]} h_j \geq c_{\min} \frac{\log(n)}{N}$$

where c_{\min} is a constant that does not depend on parameters n, p, N or K .

Remark 2 *Assumption 5 is a relatively strong assumption that essentially restricts the scope of this paper’s analysis to small vocabulary sizes (thereafter referred to as the “low- p ” regime). Indeed, since $\sum_{j=1}^p \sum_{k=1}^K A_{jk} = K$, under assumption 5, it immediately follows that:*

$$pc_{\min} \frac{\log(n)}{N} \leq K \implies p \leq \frac{KN}{\log(n)c_{\min}}$$

This assumption might not reflect the large vocabulary sizes found in many practical problems, where we could expect p to grow with n . A solution to this potential limitation is to assume weak sparsity on the matrix A and to threshold away rare terms using the thresholding procedure proposed in Tran et al. (2023), selecting a subset J of words with large enough frequency. In this case, the rest of our analysis should follow, replacing simply the data matrix X by its subset, $X_{.J}$.

2.2 Estimation procedure: pLSI

Since the smoothness assumption (Assumption 1) pertains to the rows of the topic mixture matrix W , we build on the methodology introduced by Klopp et al. (2021). To the best of our knowledge, their approach achieves the best error bound to date on the matrix W . In this subsection, we provide a brief overview of their method.

When working in the oracle setting—that is, assuming we directly observe the true expected frequency matrix M defined in Equation (2)—Klopp et al. (2021) propose a straightforward three-step procedure to recover the mixture matrix W . Specifically, let U and V be the left and right singular vectors obtained from the singular value decomposition of M , so that $M = U\Lambda V^T$. A critical insight from their work is that U can be decomposed as

$$U = WH, \tag{6}$$

where H is a full-rank $K \times K$ matrix. From this decomposition, it follows that the rows of U —which can be viewed as K -dimensional embeddings of the documents—lie on the K -dimensional simplex Δ_{K-1} . The simplex’s vertices, represented by the rows of H , correspond to the anchor documents (Assumption 2). Thus, identifying these vertices through any standard vertex-finding algorithm applied to the rows of U will enable the estimation of W .

The procedure of Klopp et al. (2021) is summarized as follows:

Step 1: Compute the singular value decomposition of the matrix M , reduced to rank K , to obtain: $M = U\Lambda V^T$.

Step 2: Vertex-Hunting Step: Consider the rows of $U \in \mathbb{R}^{n \times K}$ as points in \mathbb{R}^K on the K -dimensional simplex Δ_{K-1} . To identify its vertices, Klopp et al. (2021) propose to use a vertex-hunting algorithm called the successive projection algorithm (SPA) (Araújo et al., 2001) on the rows of U . This algorithm returns the indices of the selected “anchor documents,” $J \subseteq [n]$ with $|J| = K$. Define $\widehat{H} = U_J$, where each row corresponds to one of the K vertices of the simplex Δ_{K-1} .

Step 3: Recovery of W : W can simply be recovered from U and \widehat{H} as:

$$\widehat{W} = U\widehat{H}^{-1} \tag{7}$$

Step 4: Recovery of A : Finally, A can subsequently be estimated as: $\widehat{A} = \widehat{H}\Lambda V^T$.

In the non-oracle case—that is, when we observe X in Equation (2) instead of M —the procedure is adapted by plugging X instead of M in Step 1 and getting estimates of the singular vectors: $X = \widehat{U}\widehat{\Lambda}\widehat{V}^T$. Klopp et al. (2021) prove the consistency of their estimator of W under a similar set of assumptions as ours (Assumptions 2-4). The following corollary is significant because, to our knowledge, it offers one of the best error bounds on the estimation of the topic mixture matrix W for pLSI.

Corollary 1 (Upper bound in the balanced case, from Klopp et al. (2021)) *Let Assumptions 2-4 hold and let*

$$N \geq CK^5 \log(n + p)$$

for some $C > 0$ large enough. Then, with probability at least $1 - o((n + p)^{-1})$, the matrix \widehat{H} is non-degenerate and the output \widehat{W} of the preconditioned SPOC algorithm (a version of the SPA algorithm) satisfies, for some constant $C_0 > 0$,

$$\min_{P \in \mathcal{P}} \|\widehat{W} - WP\|_F \leq C_0 K \sqrt{\frac{n \log(n + p)}{N}},$$

where \mathcal{P} denotes the set of all permutation matrices.

However, this approach has two key limitations. First, *the consistency of the estimator relies on having a sufficiently large number of words per document.* The authors establish minimax error bounds, showing that the rate of any estimator’s error for W is bounded below by a term on the order of $C\sqrt{\frac{n}{N}}$ (Theorem 3, Klopp et al. (2021)). In other words, the accurate estimation of W requires that each document contains enough words. In many practical scenarios — such as the tumor microenvironment example mentioned earlier — this condition may not hold. However, we might still have access to additional information indicating that certain documents are more similar to one another.

Second, *the method is relatively rigid and does not easily accommodate additional structural information*, such as document-level similarities. Indeed, this method does not rely on convex optimization formulation to which we can add a regularization term, and the vertex-hunting algorithm does not readily incorporate metadata of the documents.

2.3 Estimation procedure: GpLSI

Theoretical insights from Klopp et al. (2021) help explain why topic modeling deteriorates in low- N regimes. When the number of words per document is too small, the observed frequency matrix X can be viewed as a highly noisy approximation of M , causing the estimated singular vectors \hat{U} to deviate significantly from the true underlying point cloud U . To mitigate this issue, Klopp et al. (2021) suggest a preconditioning step that improves the estimation of the singular vectors in noisy settings.

In this paper, we take a different approach by exploiting the graph structure associated with the documents to reduce the noise in X . Rather than preconditioning the empirical frequency matrix, we propose an additional denoising step that leverages the graph structure to produce more accurate estimates of U , V , and Λ .

We aim to accurately estimate the topic mixture matrix W under Assumption 1 by adapting the procedure of Klopp et al. (2021). Specifically, we consider a four-step algorithm for estimating both W and A . Compared to the original approach described in Section 2.2, our adaptation modifies Step 1 and Step 4:

Step 1: Iterative Graph-Aligned SVD of X : We replace the first step of Section 2.2 with a graph-aligned SVD of the empirical word-frequency matrix X . More specifically, in the graph-aligned setting, we assume that the underlying frequency matrix M belongs to the set:

$$\begin{aligned} \mathcal{F}(n, p, K, s) = \{ & M = U\Lambda V^\top \in \mathbb{R}^{n \times p}, \text{rank}(M) = K : \\ & U \in \mathbb{R}^{n \times K}, V \in \mathbb{R}^{p \times K}, \Lambda = \text{diag}(\lambda_1, \lambda_2, \dots, \lambda_K), \\ & |\text{supp}(\Gamma U)| \leq s, \lambda_K > 0\}. \end{aligned} \quad (8)$$

Throughout the paper, we shall allow s, p, N , and n to vary. We will assume the number of topics K to be fixed.

Step 2, 3 Same as Step 2,3 in Section 2.2.

Step 4: Recovery of A : A can subsequently be estimated by solving a constrained regression problem of X on \widehat{W} :

$$\begin{aligned} \widehat{A} = \operatorname{argmin}_{A \in \mathbb{R}^{K \times p}} & \|X - \widehat{W}A\|_F^2, \\ \text{such that } \forall k \in [K], & \sum_{j=1}^p A_{kj} = 1, A_{kj} \geq 0 \end{aligned} \quad (9)$$

2.3.0.1 Iterative Graph-Aligned SVD We propose a method based on power-iterations for Step 1 that iteratively updates the left and right singular vectors while constraining the left singular vector to be aligned with the graph (Algorithm 1). A similar approach has already been studied under Gaussian noise in Yang et al. (2016) where sparsity constraints were imposed on the left and right singular vectors.

Drawing inspiration from this method and adapting it to the multinomial noise setting, Algorithm 1 iterates between three steps. The first consists of denoising the left singular

subspace by leveraging the graph-smoothness assumption (Assumption 1). At iteration t , we define:

$$\bar{U}^t = \arg \min_{U \in \mathbb{R}^{n \times K}} \|U - X\hat{V}^{t-1}\|_F^2 + \hat{\rho}^t \|\Gamma U\|_{21} \quad (10)$$

Here, \bar{U}^t is a denoised version of the projection $X\hat{V}^{t-1}$ that leverages the graph structure to yield an estimate closer to the true U . We then take a rank- K SVD of \bar{U}^t to extract \hat{U}^t (an estimate of U) with orthogonal columns.

$$\text{SVD}(\bar{U}^t) = \hat{U}^t$$

Finally, we update \hat{V}^t . Since we are not assuming any particular structure on the right singular subspace, we simply apply a rank- K SVD on the projection $X^\top \hat{U}^t$. Denoting the projections onto the columns of the estimates as $P_u^t = \hat{U}^t (\hat{U}^t)^\top$ and $P_v^t = \hat{V}^t (\hat{V}^t)^\top$, we iterate the procedure until $\|P_u^t X P_v^t - P_u^{t-1} X P_v^{t-1}\|_F \leq \epsilon$ for a fixed threshold ϵ .

As shown in the next subsection, this algorithm can be proven to considerably improve upon the original SVD estimates. Denoting the final estimates after t_{\max} iterations as \hat{U}, \hat{V} , these estimates can then be plugged into Steps 2-4 to estimate W and A . The improved estimation of \hat{U}, \hat{V} can then be shown to translate subsequently into a more accurate estimation of the matrices W and A (Theorems 3 and 4 presented in the next section).

Although our theoretical results depend on choosing an appropriate level of regularization $\hat{\rho}^t$, the theoretical value of $\hat{\rho}^t$ depends on unknown graph quantities. In practice, therefore, we need a cross validation technique to choose the optimal $\hat{\rho}^t$ in each iteration. We devise a novel graph cross-validation method which effectively finds the optimal graph regularization parameter by partitioning nodes into folds based on a natural hierarchy derived from a minimum spanning tree. The procedure is summarized in Algorithm 2.

Remark 3 *While in the rest of the paper, we typically assume that the graph is binary, our method is in principle generalizable to a weighted graph $\mathcal{G} = (\mathcal{D}, \mathcal{W})$ where \mathcal{W} represents the weighted edge set. In this case, we denote weighted incidence matrix as $\tilde{\Gamma} = \mathbf{T}\Gamma$ where $\mathbf{T} \in \mathbb{R}^{m \times m}$ is a diagonal matrix with entry t_{dd} corresponding to the weight of the d^{th} edge. We note that scaling Γ with \mathbf{T} does not change the projection onto the row space of Γ , thus preserving our theoretical results. Without loss of generality, we work with an unweighted incidence matrix Γ .*

Remark 4 *The penalty in Equation (10) is known as the total-variation penalty in the computer vision literature. As noted in Hütter and Rigollet (2016), this type of penalty is usually a good idea whenever the rows of W take similar values, or may at least be well approximated by piecewise-constant functions. In the implementation of our algorithm, we employ the solver of Sun et al. (2021), as it is the most efficient algorithm available for this type of problem.*

2.3.0.2 Optimization of $\hat{\rho}^t$ We propose using a cross validation technique that leverages a minimum spanning tree (MST-CV) to find the optimal $\hat{\rho}^t$ in Equation (10). Conventional cross validation techniques sample either nodes or edges to divide the dataset into folds. However, these approaches can disrupt the graph structure and underestimate the strength

Algorithm 1 Two-way Iterative Graph-Aligned SVD

- 1: **Input:** Observation X , initial matrix \widehat{V}^0 , incidence matrix Γ , number of topics K , tolerance level ϵ
 - 2: **Output:** Denoised singular vectors \widehat{U}, \widehat{V}
 - 3: **repeat**
 - 4: 1. Graph denoising of U : $\bar{U}^t = \arg \min_{U \in \mathbb{R}^{n \times K}} \|U - X\widehat{V}^{t-1}\|_F^2 + \hat{\rho}^t \|\Gamma U\|_{21}$
 - 5: 2. SVD of \bar{U}^t :

$$\widehat{U}^t \leftarrow \text{Left Singular Vectors in } SVD_K(\bar{U}^t)$$
 - 6: 3. SVD of \widehat{V}^t :

$$\widehat{V}^t \leftarrow \text{Left Singular Vectors in } SVD_K(X^\top \widehat{U}^t)$$
 - 7: 4. Calculate score $s = \|\widehat{P}_u^t X \widehat{P}_v^t - \widehat{P}_u^{t-1} X \widehat{P}_v^{t-1}\|$, $\widehat{P}_u = \widehat{U}^t (\widehat{U}^t)^\top$, $\widehat{P}_v = \widehat{V}^t (\widehat{V}^t)^\top$
 - 8: **until** $s < \epsilon$
-

of the connectivity of the graph. We instead devise a new rule for dividing documents into folds using a minimum spanning tree. This technique is an extension of the cross-validation procedure proposed by Tibshirani and Taylor (2012) for the line graph. Given a minimum spanning tree \mathcal{T} of \mathcal{G} , we randomly choose a source document d_s . For each document d_i , we calculate the shortest path distance $d_{\mathcal{T}}(d_i, d_s)$. Note that this distance is always an integer. We divide the documents into b folds based on the modulus of their distance from the source node: $d_{\mathcal{T}}(d_i, d_s) \bmod b$. Through this construction of folds, we can ensure that for every document, at least one of its 1-hop neighbors is in a different fold.

Let X_i be the i^{th} row of X . For each leave-out fold \mathcal{I}_k , $k \in [b]$, we interpolate the corresponding documents $X_i, \forall i \in \mathcal{I}_k$, filling the missing document information with the average of corresponding neighbors in \mathcal{I}_k^C . This prevents us from using any information from the leave-out fold in training when calculating the cross-validation error. For each ρ in the given grid $\rho_{[1:r]} = \{\rho_1, \rho_2, \dots, \rho_r\}$, we use the interpolated observations X^k to solve the optimization problem in Equation (10) and estimate $\widehat{X}_{\mathcal{I}_k}^k$, the submatrix of \widehat{X}^k with rows in index set \mathcal{I}_k , to calculate cross-validation error. The method is described in Algorithm 2.

2.3.0.3 Initialization The success of the procedure heavily depends on having access to good initial values for V . Since, as highlighted in Remark 2, this manuscript assumes a “low- p ” regime, we propose to simply take the rank- K eigendecomposition of the matrix $X^\top X - \frac{n}{N} \widehat{D}_0$ to obtain an initial estimate \widehat{V}^0 :

$$\widehat{V}^0 = U_K(X^\top X - \frac{n}{N} \widehat{D}_0) \tag{11}$$

where \widehat{D}_0 is a diagonal matrix where each entry is defined as: $(\widehat{D}_0)_{jj} = \frac{1}{n} \sum_{i=1}^n X_{ij}$, and where $U_K(X^\top X - \frac{n}{N} \widehat{D}_0)$ denotes the matrix of K leading eigenvectors of $X^\top X - \frac{n}{N} \widehat{D}_0$.

Theorem 1 Suppose $\max(K, p) \leq n$ and $\sqrt{K} \leq p$. Under Assumptions 1 to 5, the eigenvectors of the matrix $X^\top X - \frac{n}{N} \hat{D}_0$ provide a reasonable approximation to the right singular vectors, in that with probability at least $1 - o(n^{-1})$:

$$\|\sin \Theta(V, \hat{V}^0)\|_{op} \leq \|\sin \Theta(V, \hat{V}^0)\|_F \leq \frac{C}{\lambda_K(M)^2} K \sqrt{\frac{n \log(n)}{N}} \leq C^* K^2 \sqrt{\frac{\log(n)}{nN}}$$

for some constants C and $C^* > 0$. The proof of the theorem is provided in Appendix A.

Algorithm 2 Cross Validation using Minimum spanning tree at iteration t

- 1: **Input:** Observation X , incidence matrix Γ , minimum spanning tree \mathcal{T} of \mathcal{G} , previous estimate \hat{V}^{t-1}
 - 2: **Output:** $\hat{\rho}^t$
 - 3: 1. Randomly choose the source document d_s .
 - 4: 2. Divide documents into b folds : $d_i \in \mathcal{I}_k$ if $d_{\mathcal{T}}(d_i, d_s) \bmod b = k - 1$, for $i \in [n]$ and $k \in [b]$.
 - 5: **for** each leave-out fold $\mathcal{I}_k, k \in [b]$ **do**
 - 6: Interpolation of X^k with average of neighbors: $X_i^k = \frac{1}{|\mathcal{N}(i)|} \sum_{j \in \mathcal{N}(i) \setminus \mathcal{I}_k} X_j$ for $i \in \mathcal{I}_k$
 - 7: **for** $\rho \in \{\rho_1, \rho_2, \dots, \rho_r\}$ **do**
 - 8: $\text{CVERR}_k(\rho) = \|X_{\mathcal{I}_k} - \hat{X}_{\mathcal{I}_k}^k\|_F^2$ where
 - 9: $\hat{U}^{\rho, k} = \arg \min_U \|U - X^k \hat{V}^{t-1}\|_F + \rho \|\Gamma U\|_{21}, \quad \hat{X}^k = \hat{U}^{\rho, k} (\hat{V}^{t-1})^\top$
 - 10: **end for**
 - 11: **end for**
 - 12: 4. Choose optimal ρ : $\hat{\rho}^t = \arg \min_\rho \sum_k \text{CVERR}_k(\rho)$
-

3 Theoretical results

In this section, we provide high-probability bounds on the frobenius norm of the errors for \hat{W} and \hat{A} . We begin by characterizing the effect of the denoising on the estimates of the singular values of X , before showing how the improved estimation of the singular vectors translates into improved error bounds for both W and A .

3.1 Denoising the singular vectors

The effect of our iterative denoising procedure is characterized in the following theorem.

Theorem 2 (Error bound of the graph-aligned SVD) *Let Assumption 1 to 5 hold. Assume $\max(K, p) \leq n$ and $\sqrt{K} \leq p$. Denote \hat{U}, \hat{V} as outputs of Algorithm 1 after t_{\max} iterations.*

If N satisfies

$$N \geq c_{\min}^* \left(K^4 \frac{\log(n)}{n} (n_{\mathcal{C}} + \rho^2(\Gamma) s \lambda_{\max}(\Gamma)) \vee \frac{\log(n)}{n_{\mathcal{C}_{\min}}} \right), \quad (12)$$

there exists a constant $C_0 > 0$ such that with probability at least $1 - o(n^{-1})$,

$$\max\left\{ \inf_{O \in \mathbb{O}_K} \|\widehat{U} - UO\|_F, \inf_{O \in \mathbb{O}_K} \|\widehat{V} - VO\|_F \right\} \leq C_0 K \sqrt{\frac{\log(n)}{nN}} \left(\sqrt{n_{\mathcal{C}}} + \rho(\Gamma) \sqrt{s \lambda_{\max}(\Gamma)} \right) \quad (13)$$

The proof of this result is provided in Appendix B.1.2.

Remark 5 *This result is to be compared against the rates of the estimates obtained without any regularization. In this case, the results of Klopp et al. (2021) show that with probability at least $1 - o((n+p)^{-1})$:*

$$\begin{aligned} \max\{\sin \Theta(U, \widehat{U}), \sin \Theta(V, \widehat{V})\} &\leq \max\left\{ \min_{O \in \mathbb{O}_K} \|\widehat{U} - UO\|_{op}, \min_{O \in \mathbb{O}_K} \|\widehat{V} - VO\|_{op} \right\} \\ &\leq \frac{5\sqrt{2}\lambda_1(M)\|X - M\|_{op}}{\lambda_K^2(M)} \leq \frac{20\sqrt{2}\lambda_1(M)\sqrt{n \log(n)}}{\lambda_K^2(M)\sqrt{N}} \\ &\leq \frac{20\sqrt{2}\sqrt{n}K\sqrt{n \log(n)}}{cn\sqrt{N}} \\ &\leq CK\sqrt{\frac{\log(n)}{N}} \end{aligned} \quad (14)$$

for some constant $C > 0$. In particular, this rate shares with the rate provided in Theorem 2 a factor $K\sqrt{\frac{\log(n)}{N}}$. However, the spatial regularization in our setting allows us to introduce a factor $\frac{1}{\sqrt{n}}(\sqrt{n_{\mathcal{C}}} + \rho(\Gamma)\sqrt{s\lambda_{\max}(\Gamma)})$, which decreases with n .

3.2 Estimation of W and A

Theorem 3 *Let Assumptions 1 to 5 hold. Let $\rho(\Gamma)$, s , $n_{\mathcal{C}}$, and $n_{\mathcal{C}_{\min}}$ be given as (3)-(5). Assume $\max(K, p) \leq n$ and $\sqrt{K} \leq p$. If N satisfies the condition stated in (12), then there exists a constant $C > 0$ such that with probability at least $1 - o(n^{-1})$,*

$$\min_{P \in \mathcal{P}} \|\widehat{W} - WP\|_F \leq CK \sqrt{\frac{\log(n)}{N}} \left(\sqrt{n_{\mathcal{C}}} + \rho(\Gamma) \sqrt{s \lambda_{\max}(\Gamma)} \right) \quad (15)$$

where \mathcal{P} denotes the set of all permutations.

The full proof of the result is provided in Appendix B.2.1. The frobenius norm error of the document-topic mixture matrix W is of the order $O\left(K\sqrt{\frac{\log(n)}{N}}\right)$, demonstrating that the estimator is highly accurate if the document lengths are large enough, as defined by $N \gtrsim (\sqrt{n_{\mathcal{C}}} + \rho(\Gamma)\sqrt{s\lambda_{\max}(\Gamma)}) \log(n)$. This requirement is more relaxed than the condition $N \gtrsim n \log(n+p)$ for pLSI, as stated in Corollary 1. This indicates that GpLSI can produce

accurate estimates even for smaller N , by sharing information among neighboring documents on the graph. The shrinkage of error due to graph-alignment is characterized by the term $\frac{1}{\sqrt{n}}(\sqrt{n\bar{c}} + \rho(\Gamma)\sqrt{s\lambda_{\max}(\Gamma)})$, which is 1, when no nodes are connected. Furthermore, using the inequality $\|\widehat{W} - WP\|_{1,1} \leq \sqrt{Kn}\|\widehat{W} - WP\|_F$, it immediately follows that:

Corollary 2 *Let the conditions of Theorem 3 hold. If N satisfies the condition stated in (12), then there exists a constant $C > 0$ such that with probability at least $1 - o(n^{-1})$,*

$$\min_{P \in \mathcal{P}} \|\widehat{W} - WP\|_{1,1} \leq CK^{3/2} \sqrt{\frac{n \log(n)}{N}} \left(\sqrt{n\bar{c}} + \rho(\Gamma)\sqrt{s\lambda_{\max}(\Gamma)} \right). \quad (16)$$

Theorem 4 *Let the conditions of Theorem 3 hold. If N satisfies the condition stated in (12), then there exists a constant $C > 0$ such that with probability at least $1 - o(n^{-1})$,*

$$\|\widehat{A} - \tilde{P}A\|_F \leq CK^{3/2} \sqrt{\frac{\log(n)}{N}} \left(\sqrt{n\bar{c}} + \rho(\Gamma)\sqrt{s\lambda_{\max}(\Gamma)} \right). \quad (17)$$

where P denotes the same permutation matrix in (15) and $\tilde{P} = P^{-1}$.

Remark 6 *The previous error bound of A demonstrates that the accuracy of \widehat{A} primarily relies on the accuracy of \widehat{W} , which is to be expected of, as we estimate A by regressing X on the estimator \widehat{W} . Our method prioritizes the accurate estimation of W . While the error rate may not achieve the minimax-optimal rate $C\sqrt{\frac{p}{nN}}$ derived in Ke and Wang (2017), it is more accurate than \widehat{A} proposed in Klopp et al. (2021), as confirmed by synthetic experiments in Section 4.*

3.3 Refinements for special graph structures

We now analyze the behavior of the error bound provided in (15) for different graph structures, further explicating the dependency of our bounds on properties of the graph.

3.3.0.1 Erdős-Rényi random graphs We first assume that the graph \mathcal{G} is Erdős-Rényi random graph where each pair of nodes is connected with probability $p = p_0 \frac{\log(n)}{n}$ for a constant $p_0 > 1$.

If there exists a lower bound on the second smallest eigenvalue of the graph Laplacian, that is $\lambda_{n-1}(L) \geq c_1$ ($c_1 > 0$), then $\rho(\Gamma) \leq \sqrt{2}/c_1$ (Hütter and Rigollet, 2016). The quantity $\lambda_{n-1}(L)$, also known as *algebraic connectivity*, provides insights into the properties of the graph, such as its connectivity. In the ER case, with high probability, the algebraic connectivity c_1 has order $O(\log(n))$ and the graph is almost surely connected. Under this setting, we obtain,

$$\min_{P \in \mathcal{P}} \|\widehat{W} - WP\|_F \leq C_1 K \sqrt{\frac{\log(n)}{N}} \left(1 + \frac{\sqrt{s\sqrt{d_{\max}}}}{\log(n)} \right). \quad (18)$$

Here, we exploit the known upper bound of the eigenvalue of the adjacency matrix A and the relationship between A and incidence matrix Γ , $A = \text{diag}(A\mathbf{1}_n) - \Gamma^\top \Gamma$. Since $\lambda_1(A) \leq d_{\max}$, where d_{\max} denotes the maximum degree of the nodes in the graph, we can

deduce that $\lambda_{\max}(\Gamma) = \sqrt{\lambda_{\max}(\Gamma^\top \Gamma)} \leq \sqrt{2d_{\max}}$. In the regime where $\log(n) \gtrsim s^{1/2}d_{\max}^{1/4}$, we arrive at the order $O(K\sqrt{\frac{\log(n)}{N}})$ in (18).

3.3.0.2 1D and 2D Grid graphs We also derive error bounds for grid graphs, which are amenable to the analysis of time series data and for applications in image processing.

1D grid graphs Hütter and Rigollet (2016) show that $\rho(\Gamma) = \sqrt{n}$ and,

$$\min_{P \in \mathcal{P}} \|\widehat{W} - WP\|_F \leq CK\sqrt{\frac{\log(n)}{N}}(1 + \sqrt{sn}) \leq C_2K\sqrt{\frac{sn \log(n)}{N}}. \quad (19)$$

2D grid graphs Next, we expand this to a $L \times L$ 2D grid graph with $n = L^2$.

(Hütter and Rigollet, 2016) show that, in that case, the inverse scaling factor is such that $\rho(\Gamma) \lesssim \sqrt{\log(n)}$. Similar to the 1D case, we obtain

$$\min_{P \in \mathcal{P}} \|\widehat{W} - WP\|_F \leq CK\sqrt{\frac{\log(n)}{N}}(1 + \sqrt{s \log(n)}) \leq C_3K \log(n)\sqrt{\frac{s}{N}}. \quad (20)$$

3.4 Synthetic Experiments

We evaluate the performance of our method using synthetic datasets where W is aligned with respect to a known graph.

3.4.0.1 Experimental Protocol To generate documents, we sample n points uniformly on unit square $[0, 1]^2$, and cluster them into $n_{grp} = 30$ groups using a simple k-means algorithm. Each cluster is randomly assigned to a topic and the mixture W_i for each document is generated by sampling from Dirichlet distribution with $\alpha \sim \text{Dirichlet}(\mathbf{u})$ where $u_k \sim \text{Unif}(0.1, 0.5)$ ($k \in [K]$). Small random noise $N(0, 0.03)$ is then added to the vector α , and α is permuted so that the biggest element of α is assigned to the cluster’s predominant topic.

To create anchor documents, we sample K rows of W and set their weight as \mathbf{e}_k , where \mathbf{e}_k denotes the indicator vector such that $\mathbf{e}_k(k) = 1$, and $\mathbf{e}_k(k') = 0, \forall k \neq k'$. Finally, the matrix A is generated by sampling each entry A_{kj} from a uniform distribution, normalizing each row to ensure that A is a stochastic matrix. A detailed description of the data generating process is provided in Appendix D, and an example of the ground truth topic matrix is shown in Figure 11.

To assess the performance of GpLSI, we compare it against several established methods, including the original pLSI algorithm proposed by Klopp et al. (2021), TopicSCORE (Ke and Wang, 2017), LDA (Blei et al., 2001), and the Spatial LDA (SLDA) approach of Chen et al. (2020). In addition, to highlight the efficiency of our iterative algorithm, we present results from a baseline variant that employs only a single denoising step. This one-step method is described in greater detail in Appendix B.4. To implement these algorithms, we use the R package `TopicScore` and the LDA implementation of the Python library `sklearn`. For SLDA, we use of the Python package `spatial_lda` provided by the authors with the default settings of the algorithm. We run 50 simulations and record the ℓ_1 error, ℓ_2 error of W and A , and the computation time across various parameter settings (p, N, n, K) , reporting medians

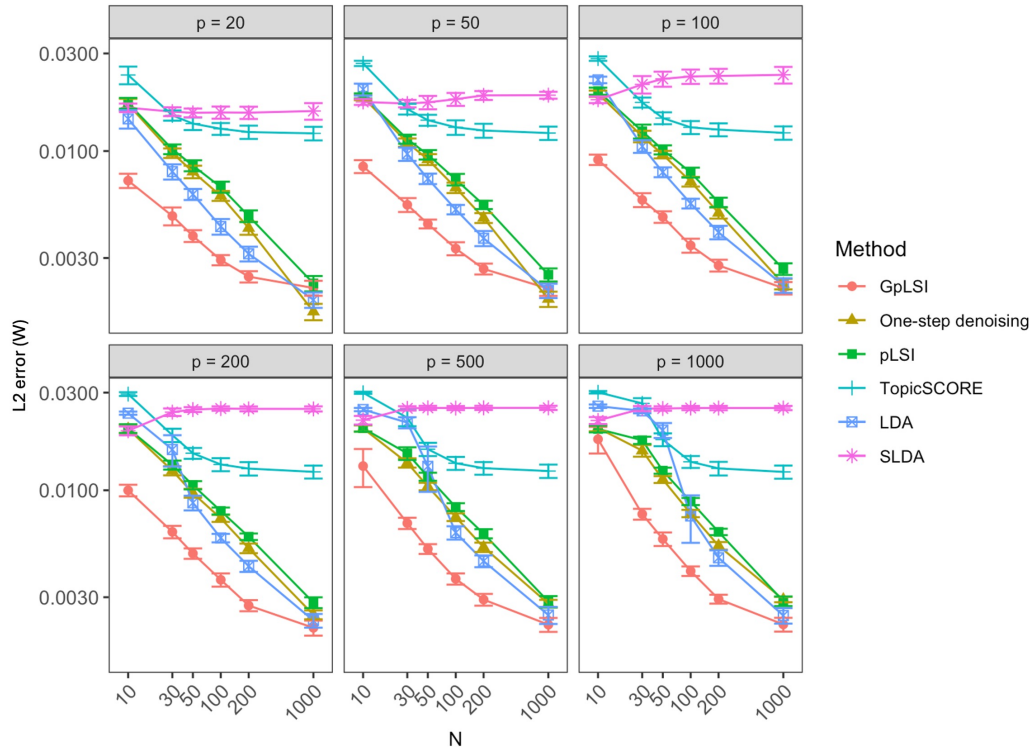


Figure 1: ℓ_2 error for the estimator \widehat{W} (defined as $\min_{P \in \mathcal{P}} \frac{1}{n} \|\widehat{W} - WP\|_F$) for different combinations of document length N and vocabulary size p . Here, $n = 1000$ and $K = 3$.

and interquartile ranges. To evaluate the performance of methods in difficult scenarios where document length N is small compared to vocabulary size p , we check the errors for different combinations of $N = 10, 30, 50, 100, 200, 1000$ and $p = 20, 30, 50, 100, 200, 500$.

3.4.0.2 Results Figure 1 demonstrates that GpLSI achieves the lowest ℓ_2 error for W , even in scenarios with very small N . This shows that sharing information across similar documents on a graph improves the estimation of topic mixture matrix. Notably, while LDA and pLSI exhibit modest performance, they fail in regimes where $N < 100$ and $p \geq 200$. We also confirm that the one-step denoising variant of our method achieves a lower error estimation error than pLSI and LDA in settings where $N \ll p$. For A , we observe similar performance of GpLSI and LDA, both achieving the lowest ℓ_2 error in most settings as shown in Figure 2.

We also examine how the estimation errors scale with the corpus size n and the number of topics K , as shown in Figure 3. The errors in that figure are normalized by n . We observe that GpLSI achieves a rapid decrease in both A and W estimation errors as n grows, substantially outperforming other methods, particularly for the estimation of W . For the estimation of A , as highlighted in Remark 6, our rates and procedure is not optimal compared with existing results (see in particular Ke and Wang (2017), which achieves similar results to ours in Figure 3). However, compared to the procedure proposed by Klopp

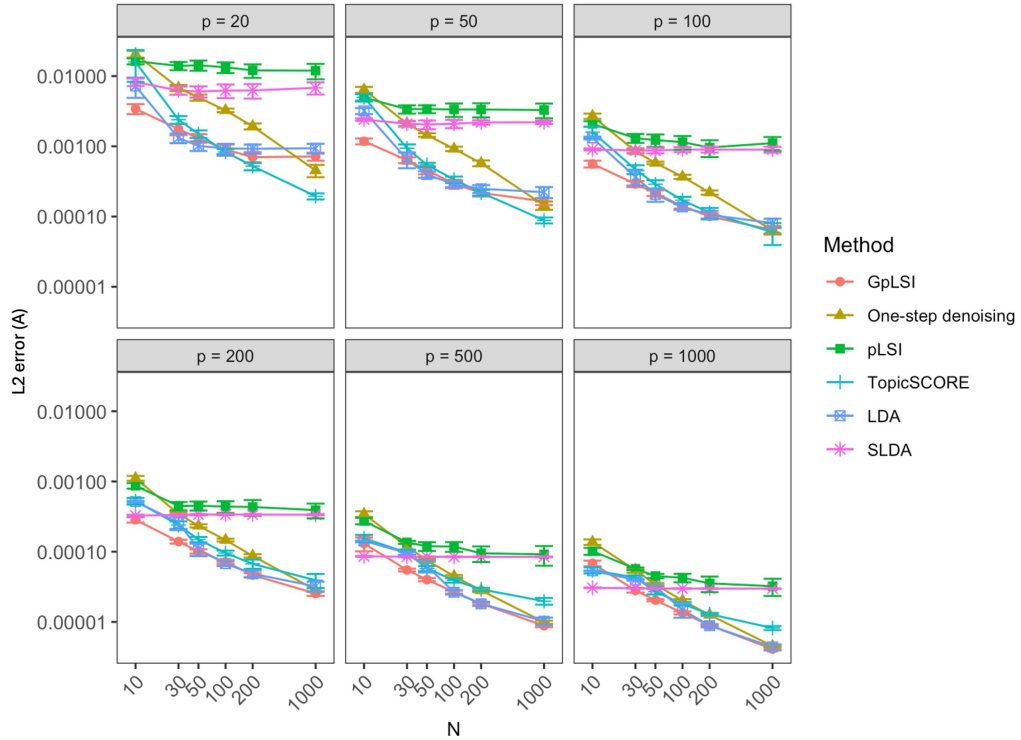


Figure 2: ℓ_2 error for the estimator \hat{A} (defined as $\min_{P \in \mathcal{P}} \frac{1}{p} \|\hat{A} - PA\|_F$) for different combinations of document length N and vocabulary size p . Here, $n = 1000$ and $K = 3$.

et al. (2021), the estimation error is considerably improved. We also show that the behavior of the ℓ_1 errors is similar to that of the ℓ_2 errors in Appendix D.

Finally, we demonstrate how GpLSI leverages the graph information in Figure 4. As N increases, GpLSI chooses smaller graph regularization parameter $\hat{\rho}_{MST-CV}$, since the need to share information across neighbors diminishes as documents become longer and more informative. Additionally, when W is more heterogeneous over the graph—meaning neighboring documents exhibit more heterogeneous topic mixture weights—the ℓ_2 error of W increases. Here, graph heterogeneity is characterized by our simulation parameter n_{grp} (the number of patches that we create). As n_{grp} increases, the unit square is divided into finer patches, and the generated documents within the same topic become more dispersed. Our result indicates that GpLSI works well in settings where the mixture weights are smoother over the document graph and the performance of GpLSI and pLSI become similar as neighboring documents become more heterogeneous.

4 Real-World Experiments

To highlight the applicability of our method, we deploy it on three real-life examples. All the code for the experiments is openly accessible at <https://github.com/yeojin-jung/GpLSI>.

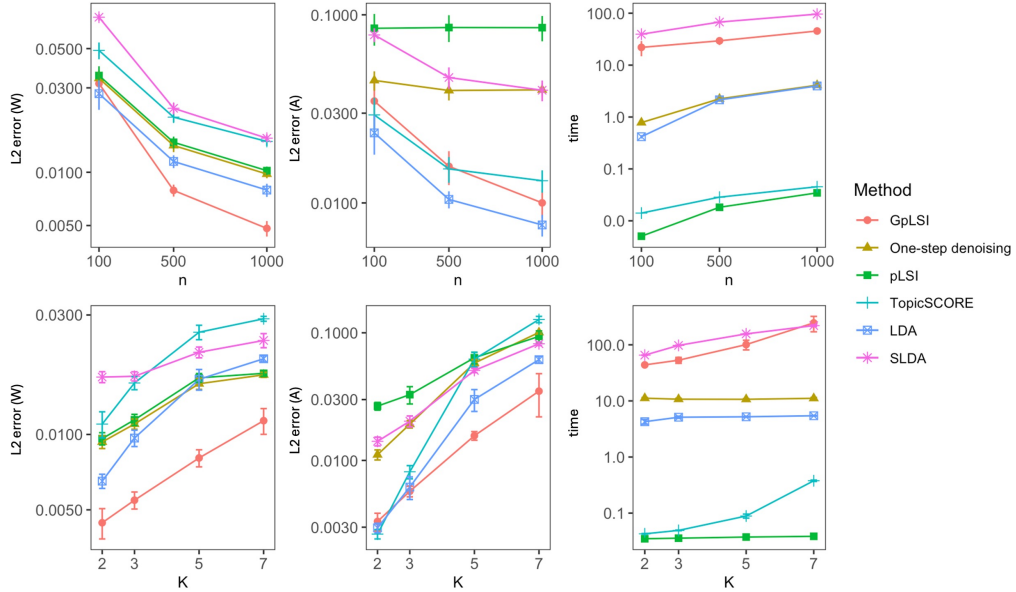


Figure 3: ℓ_2 error of W (left) and A (middle) and computation time (right) for different corpus size n and number of topics K . Here, $N = 30$ and $p = 30$.

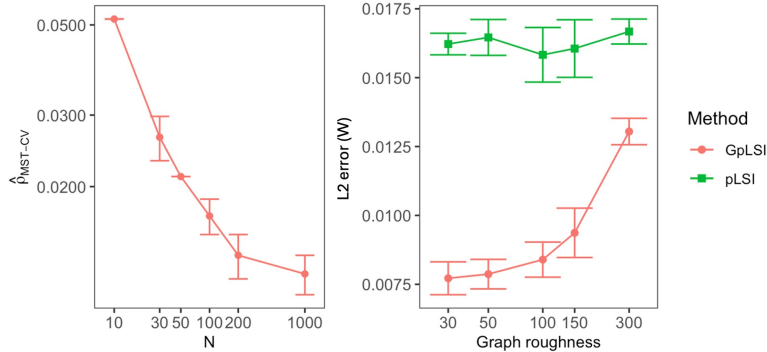


Figure 4: Behavior of $\hat{\rho}_{MST-CV}$ as N increases (left) where $\hat{\rho}_{MST-CV}$ is estimated by Algorithm 2. Behavior of ℓ_2 error over graph heterogeneity (right). Graph heterogeneity is characterized by n_{grp} , the number of patches of documents across the unit square. Each patch is assigned similar topic mixture weights.

4.1 Cellular microenvironments

We first consider the analysis of CODEX data, a recent technology that allows the identification of individual cells in tissue samples. This technology holds important promise in the discovery of different profiles of cell interactions, particularly in cancer samples, where the interactions between cells are hypothesized to be predictive of the capacity of the im-

immune system to cope with the tumor. In recent years, there has been increased interest in the discovery of interesting types of immune cell interaction. Since cellular interactions are hypothesized to be local, these patterns are often referred to as “tumor microenvironments”. Recent work by Chen et al. (2020) proposes using an adaptation of topic modeling to identify communities of cells, or patterns in tumor microenvironments. In this context, tissue samples are partitioned into smaller regions that contain around 20 different cells (our “documents”). Each of these cells corresponds to a known cell type (the “vocabulary”), which, depending on the type of CODEX data used, can yield a vocabulary of 10 to 30 different words. In classifying tumor-immune microenvironments, we can regard a tumor microenvironment as a *document*, immune cell types as *words*, and latent characteristics of a microenvironment as a *topic*. However, due to the small number of words per document, the recovery of the topic mixture matrix and the topics themselves can prove challenging.

In cellular biology, it is natural to assume that spatial proximity of individuals greatly influences the biological structure (Chen et al., 2020). Chen et al. (2020) propose using the adjacency of documents to assign similar topic proportions to neighboring tumor cells. The resulting topics can uncover novel tumor cell types based on their interaction with surrounding immune cells.

We apply our method to two clinically annotated CODEX datasets and analyze patterns of cellular microenvironments using the spatial proximity of cells.

4.1.1 STANFORD COLORECTAL CANCER DATASET

The first CODEX dataset is a collection of 292 tissue samples from 161 colorectal cancer patients collected at Stanford University (Wu et al., 2022). The locations of the cells were retrieved using a Voronoi partitioning of the sample, and the corresponding spatial graphs were constructed encoding the distance between microenvironments. More specifically, we define a tumor microenvironment as the 3-hop neighborhood of each cell, following the definition originally used by Wu et al. (2022). Each microenvironment contains 10 to 30 immune cells of 8 possible types. This aligns with the setting where the document length $N < 30$ is small compared to the vocabulary size $p = 8$. For each tissue sample, we obtain a tumor cellular graph and a tumor microenvironment-by-immune cell frequency matrix. Each sample is annotated with cancer recurrence, a binary variable that denotes whether cancer has recurred after immunotherapy, and survival length.

We aggregate frequency matrices and tumor cellular graphs of all samples and fit three methods: our proposed GpLSI, the original pLSI approach of Klopp et al. (2021), and LDA (Blei et al., 2001) to estimate immune topics. The estimated topic weights of $K = 6$ are illustrated in Figure 5(A). We observe more similar immune topics (Topic 1, 2, 3) in GpLSI and LDA while pLSI has distinct topics. We also provide the estimated topic weights for $K = 1$ to 6 in Appendix E.

To determine the optimal number of topics K , we propose using the method proposed by Fukuyama et al. (2023). In this work, the authors construct “topic paths” to track how individual topics evolve, split or merged, as the number of topics K , increases. They then propose selecting a value of K that achieves both high refinement, reflected in a smaller number of ancestral topics for each current topic, and strong coherence, indicated by the consistent reemergence of each topic in all values of K . We use the R package `topicpaths` to provided

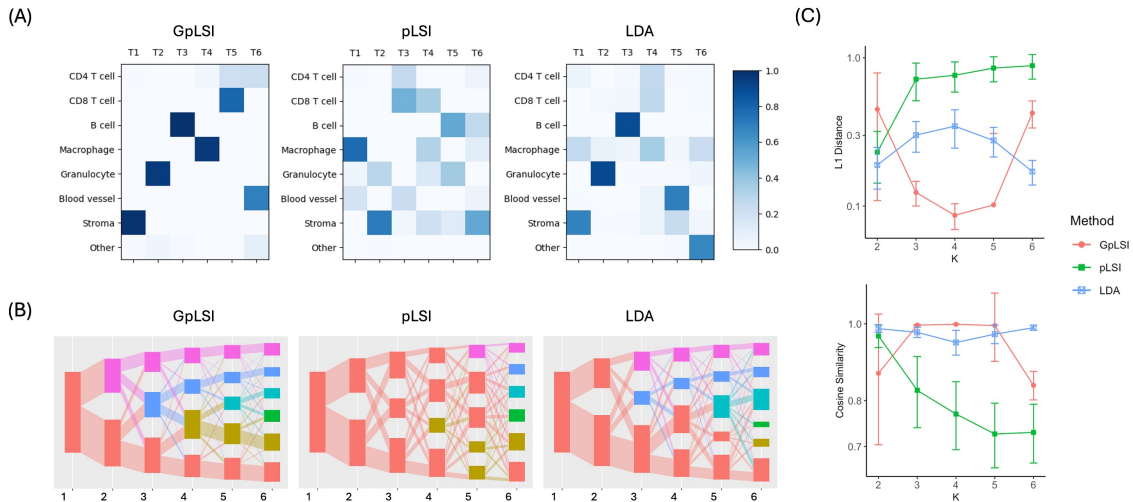


Figure 5: (A) Estimated topic weights \hat{A} of GpLSI, pLSI, and LDA. Topic weights are aligned across methods using cosine similarity. (B) Topic alignment paths of GpLSI, pLSI, and LDA using R package `alto`. (C) Pairwise ℓ_1 distance and cosine similarity of topic weights from different batches of patients.

by the same authors to visualize the alignment paths of the topics, shown in Figure 5(B). We observe that while the GpLSI path has distinct topics up to $K = 6$, other methods fail to provide consistent, well-separated topics.

To evaluate the quality and stability of the recovered topics, we also measure the coherence of the estimated topic weights in several samples, as suggested in Tran et al. (2023). We divide 292 samples into five batches and estimate the topic weights A^b for $b \in [5]$. For every pair of batches (b, b') , we align A^b and $A^{b'}$ (we permute $A^{b'}$ with P where $P = \arg \min_{P \in \mathcal{P}} \|A^b - PA^{b'}\|$) and measure:

- The entry-wise ℓ_1 distance between estimated topics: $d = \|A^b - A^{b'}\|_{1,1}$
- The cosine similarity between topics: $\eta = \frac{1}{K} \sum_{k=1}^K \frac{\langle A_{*k}^b, A_{*k}^{b'} \rangle}{\|A_{*k}^b\|_2 \|A_{*k}^{b'}\|_2}$

These metrics can be used to evaluate the consistency of topics as well as to determine the optimal K . We repeat this procedure five times and plot the scores in Figure 5(C). We notice that GpLSI provides the most coherent topics across batches for $K = 3, 4, 5$, scoring the lowest ℓ_1 distance and highest cosine similarity at $K = 4$. We also observe that the estimated topics in the original pLSI method of Klopp et al. (2021) exhibit greater variability compared to the other two methods. This highlights the benefits of leveraging the spatial structure in the estimation of the topic mixture matrix.

Next, we conduct survival analysis to identify the immune topics associated with higher risk of cancer recurrence. We consider two logistic models with different covariates to predict cancer recurrence and calculate the area under the curve (AUC) of the receiver-operating

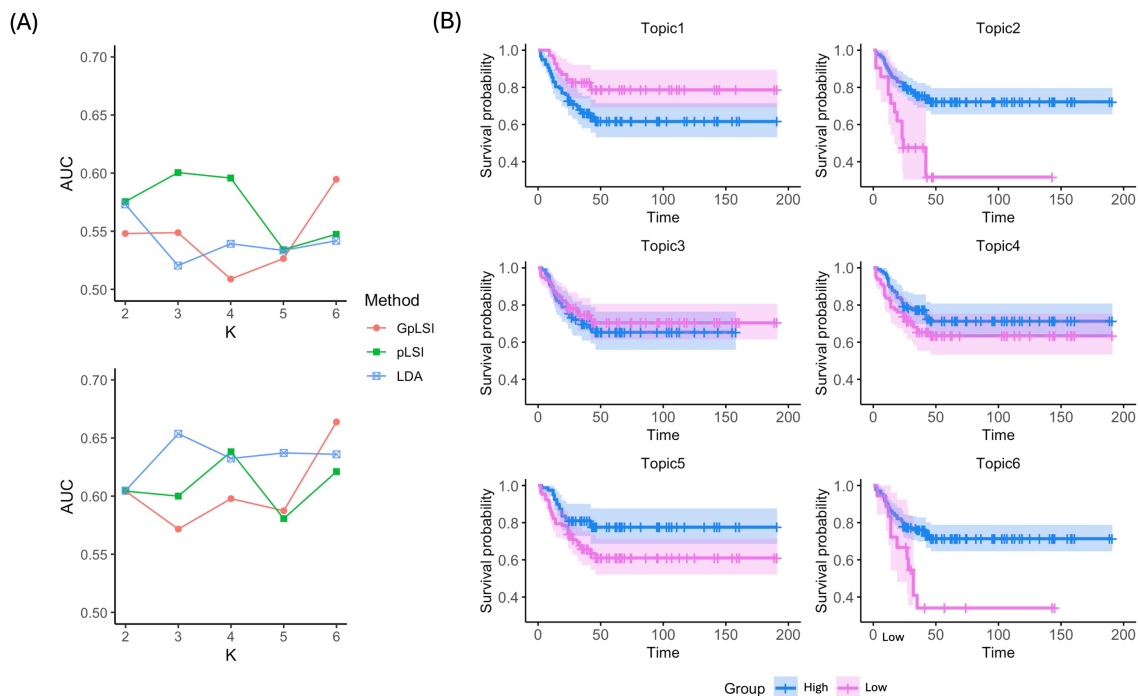


Figure 6: (A) AUC for GpLSI, pLSI, and LDA using isometric log-ratio transformed topic proportions (top) and dichotomized topic proportions (bottom) as covariates. (B) Kaplan-Meier curves of dichotomized topic proportions using GpLSI.

characteristic (ROC) curves to evaluate model performance. In the first model, we use the proportion of each microenvironment topic as covariates for each sample. Since the K covariates sum up to one, we apply isometric log-ratio transformation to represent it with $K - 1$ orthonormal basis vectors (Egozcue et al., 2003). In the second model, we dichotomize each topic proportion to low and high proportion groups. The cutoffs are determined using the maximally selected rank statistics. The AUC for each number of topics is shown in Figure 6(A). GpLSI achieves the highest area under the curve (AUC) at $K = 6$ in both models. We also plot Kaplan Meier curves for each topic using the same dichotomized topic proportions. The result for GpLSI is illustrated in Figure 6(B). We observe that Topic 2, which is characterized by a high prevalence of granulocytes, and Topic 6, a mixture of CD4 T cells and blood vessels, are associated with lower cancer recurrence. Positive effect of granulocytes on cancer prognosis was also reported by Wu et al. (2022), who found out that a microenvironment with clustered granulocyte and tumor cells is associated with better patient outcomes. We observe the same association of granulocyte with lower risk in LDA in Appendix E.

4.1.2 MOUSE SPLEEN DATASET

We also apply our method to identify immune topics in mouse spleen. In this setting, each document is anchored to a B cell (Chen et al., 2020). A previous study has processed the original CODEX images from Goltsev et al. (2018) to obtain the frequencies of non-B cells in

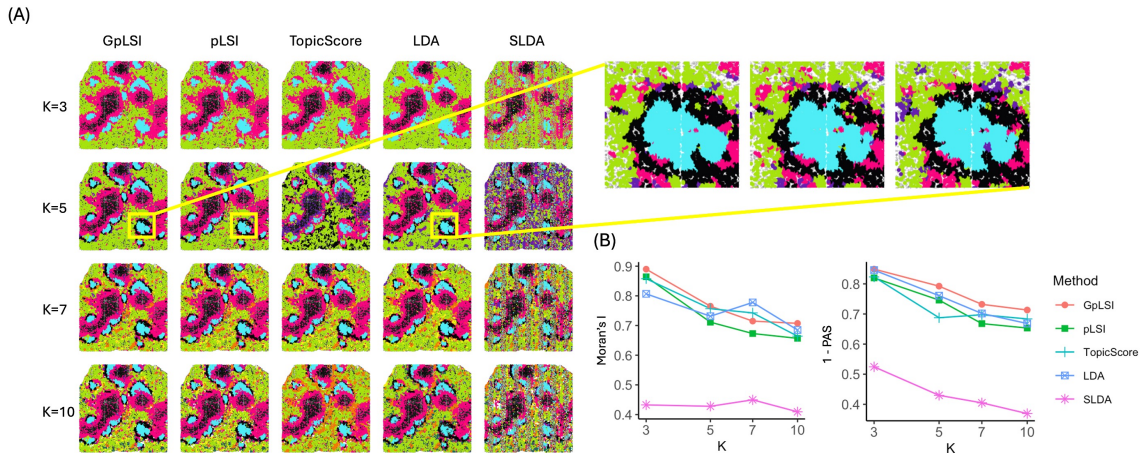


Figure 7: (A) Estimated topics of all methods with $K = 3, 5, 7, 10$ (B) Comparison of clustering performance using Moran’s I and PAS score. We plot 1-PAS for better interpretation.

the 100 pixel neighborhood of each B cell (Chen et al., 2020). The final input for the topic models consists of a 35,271 B cell microenvironments by 24 cell types frequency matrix, along with the positional data of B cells.

In this example, we evaluate GpLSI by examining whether the introduction of our graph-based regularization term in the estimation of topic mixture matrices enhances document clustering. Figure 7(A) presents the estimated topics for all models at $K = 3, 5, 7, 10$. Notably, the topics derived from GpLSI, pLSI, and LDA more clearly demarcate distinct B cell microenvironment domains compared to those estimated by TopicSCORE and LDA. Among these three methods, GpLSI yields the least noisy cellular clustering, as evidenced by the magnified view of a selected subdomain.

We also evaluate the quality of clusters with two metrics, Moran’s I and the percentage of abnormal spots (PAS) (Shang and Zhou, 2022). Moran’s I is a classical measure of spatial autocorrelation that assesses the degree to how values are clustered or dispersed across a spatial domain. PAS score measures the percentage of B cells for which more than 60% of its neighboring B cells have different topics. Higher Moran’s I and lower PAS score indicate more spatial smoothness of the estimated topics. From Figure 7(B), we conclude that GpLSI has the highest Moran I, and the lowest PAS scores, demonstrating improved spatial smoothness of the topics.

4.2 What’s Cooking dataset

This dataset contains recipes from 20 different cuisines across Europe, Asia, and South America. Each recipe is represented as a list of raw ingredients. Ingredients that appear fewer than 10 times across all recipes are excluded. The processed ingredient lists allow us to convert each list into an ingredient-count vector. This results in a count matrix with 13,597 recipes (documents) and 1,019 unique ingredients (words). Our goal is to identify general cooking styles that are prevalent across various countries worldwide.

Under the assumption that neighboring countries would have similar cuisine styles, we construct a graph of recipes based on the geographical proximity of the countries. Specifically, for each recipe, we select the five closest recipes from neighboring countries (including its own country) based on the ℓ_1 distance of the ingredient count vectors and define them as neighboring nodes on the graph. The resulting graph naturally partitions into three distinct subgraphs, each corresponding to Asian, Western European, and Southern American cuisines. Notably, certain recipes from different countries remain connected within this graph, showing that culinary similarities can transcend geographic boundaries. By incorporating this graph structure into the topic estimation process, we introduce an additional layer of regularization that aligns closely related recipes. For instance, it ensures that a Japanese beef broth dish is placed nearer to a Korean beef broth dish, rather than a French one, thereby producing topic mixtures that better reflect the true cultural and gastronomic relationships among recipes.

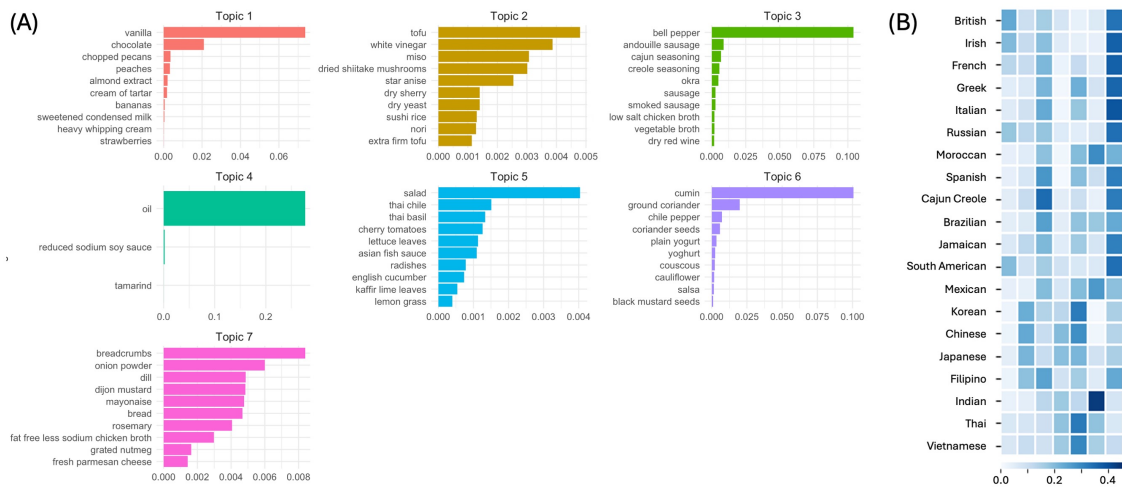


Figure 8: (A) Estimated anchor ingredients for each topic using GpLSI. (B) Proportion of topics for each cuisine. Each recipe was assigned to a topic with the highest document-topic mixture weight. For each cuisine, we count the number of recipes for each topic and divide by the total number of recipes in the cuisine.

We run GpLSI, pLSI, and LDA with $K = 5, 7, 10, 15, 20$ topics. We illustrate the estimated topics of GpLSI in Figure 8. With this approach, Topic 1 is clearly a baking topic and Topic 6 is defined by strong spices and sauces common in Mexican or parts of Southeast Asian cuisines. We also observe a general topic for Asian cuisines (Topic 2) and another for Western countries (Topic 7).

To evaluate the estimated topics, we compare each topic’s characteristics with the the cuisine-by-topic proportion (Figure 8 (C)). Indeed, the style of each topic defined by the anchor ingredients aligns with the cuisines that have a high proportion of that topic. For example, the baking topic (Topic 1) is prevalent in British, Irish, French, Russian, and South American cuisines. In contrast, for pLSI, it is difficult to analyze the characteristics for each topic because Topics 1-4 have one or no identified anchor ingredients. Even examining the most frequent ingredients in Figure 21, the topics are hardly identifiable as there are

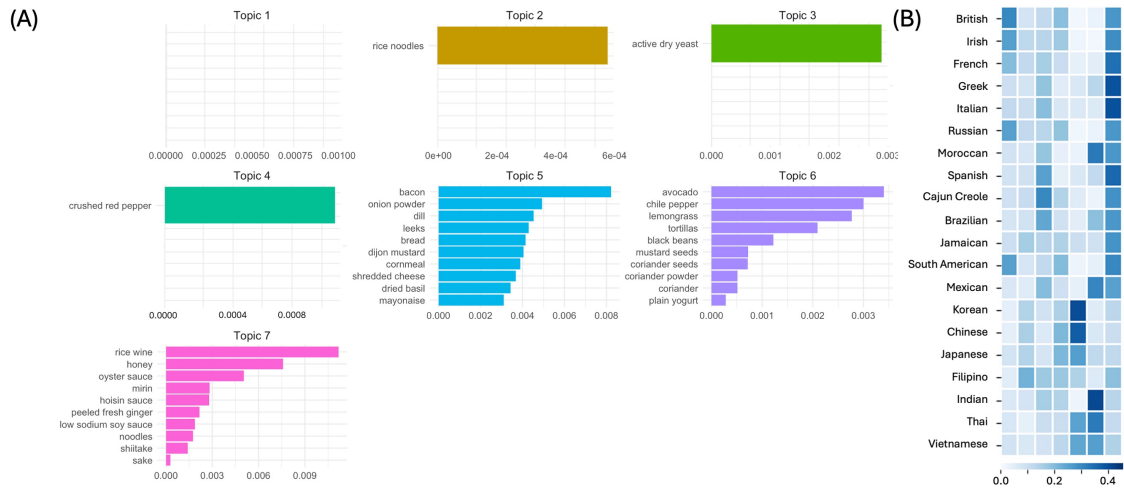


Figure 9: (A) Estimated anchor ingredients for each topic using pLSI. (B) Proportion of topics for each cuisine.

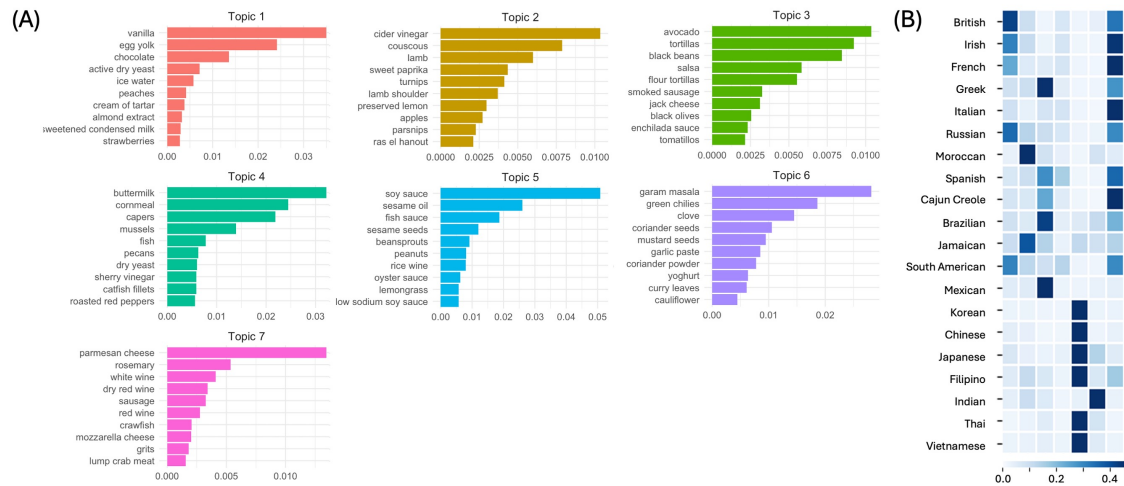


Figure 10: (A) Estimated anchor ingredients for each topic using LDA. (B) Proportion of topics for each cuisine.

many overlapping ingredients such as onion, salt, and olive oil. The ambiguity of the topics recovered by the original pLSI approach are even more evident when grouping cuisines by continent. In that case, applying a classification algorithm to assign recipes to one of 5 groups based on the estimated topic proportions (with $K=5$) yields an accuracy of 61% for plsi, vs 65.5% for our method.

Comparing the cuisine-by-topic proportions of GpLSI and LDA ((C) of Figure 8 and Figure 10), we observe that GpLSI reveals many cuisines as mixtures of different cooking styles. In contrast, for LDA, many cuisines such as Moroccan, Mexican, Korean, Chinese, Thai have their recipes predominantly classified to a single topic. GpLSI provides estimates

of topic mixture and topic weights that are more relevant to our goal of discovering global cooking styles.

5 Related Works

5.0.0.1 Bayesian approaches Existing efforts to incorporate additional information into topic modeling have primarily worked with the Bayesian formulation of topic modeling, known as Latent Dirichlet Allocation (LDA) (Blei et al., 2001). Traditional LDA frames the recovery of W and A as finding appropriate posteriors given the observed data D . In this setting, both W and A are considered to be random variables and endowed with prior probabilities, typically Dirichlet distributions. Letting $T_{im} \in \mathbb{R}^p$ be a one-hot vector representing the m^{th} term of document i (so that $D_i = \sum_{m=1}^{N_i} T_{im}$), the document corpus is assumed to be sampled from the following generative mechanism:

Topic Generation:

$$\forall k \in [K], \quad A_k \sim \text{Dirichlet}(\theta) \quad \text{with } \theta \in \mathbb{R}^p \text{ a hyperparameter} \quad (\text{LDA 1})$$

Document Generation:

$$\forall i \in [n], \quad W_i \sim \text{Dirichlet}(\alpha) \quad \text{with } \alpha \in \mathbb{R}^K \text{ a hyperparameter} \quad (\text{LDA 2})$$

$$\forall m \in [N_i], \quad Z_{im} \sim \text{Multinomial}(1, W_i) \quad (\text{sampling of a topic for the } m^{\text{th}} \text{ word})$$

$$\forall m \in [N_i], \quad T_{im} \sim \text{Multinomial}(1, A_{Z_{im}}) \quad (\text{sampling of a specific word}) \quad (\text{LDA 3})$$

Efforts to incorporate metadata have largely focused on adding additional information at the beginning of this generative model by appropriately modifying the Dirichlet priors. For instance, the dynamic topic modeling approach of Blei and Lafferty (2006b) assumes that documents are observed sequentially, and that consecutive documents have similar topic mixture weights. To accommodate this prior, the authors suggest an autoregressive structure on W , replacing the Dirichlet sampling in equation (LDA 2) by a sequential sampling mechanism of the form $W_{i+1} = \text{softmax}(\eta_{i+1})$, with $\eta_{i+1} \sim N(\eta_i, \sigma^2 I)$. Roberts et al. (2014) extends this approach by using document-level covariates X_i , namely $W_i = \text{softmax}(\eta_i)$, with $\eta_i \sim N(X_i \beta, \Sigma)$. By contrast, the work of McAuliffe and Blei (2007) incorporates metadata into LDA by adding a final step to the generating mechanism, explicitly regressing the document-level covariate $y \in \mathbb{R}$ on topic mixture weights: $y \sim N(W_i \eta, \sigma^2)$.

While these methods allow the flexible incorporation of additional information to the original LDA framework, the metadata is usually assumed to come as a matrix of additional covariates. These approaches thus need to be appropriately tailored depending on the nature of the covariates considered (e.g. changing the normal prior of McAuliffe and Blei (2007) to a Bernoulli or multinomial in the case of categorical covariates, etc). Such changes might introduce additional complexity in the updates, and in cases where certain covariates have no obvious prior, applicability becomes restricted. Most notably, these methods are difficult to adapt to the case where the metadata comes under the form of a graph, which provides a flexible way of encoding complex covariate structures or spatial information. For example, in our corpus of recipes (Section 4.2), the origin of recipes is more easily modeled as a graph, rather than a matrix of covariates. Working with a document-similarity graph bypasses the

need to adapt the method to different types of covariates, as long as the metadata can be mapped into a similarity metric between two documents.

To the best of our knowledge, the only extension of LDA amenable to the graph setting is that of Chen et al. (2020). There, the authors leverage the presumed similarity between connected documents by regularizing the α_i 's in equation (LDA 2) with respect to a known document graph \mathcal{G} , so that $\alpha_i \approx \alpha_j$ if documents i and j are connected in the graph. However, this approach is computationally intensive and, as we find, does not necessarily improve topic accuracy (see Section 3.4). This LDA-based approach also inherits the limitations of Bayesian methods, such as their potentially slow convergence and lack of theoretical guarantees.

5.0.0.2 Probabilistic Latent Semantic Indexing Another popular approach to topic modeling is probabilistic Latent Semantic Indexing (pLSI). In a general sense, pLSI can be broadly described as a non-negative matrix factorization technique. In the oracle setting, assuming we have access to the expected frequency matrix M , pLSI can be understood as solving a constrained rank K decomposition of the form:

$$\widehat{W}, \widehat{A} = \operatorname{argmin}_{W \in \mathbb{R}^{n \times K}, A \in \mathbb{R}^{K \times p}} \|M - WA\|_F^2$$

$$\text{such that } \forall i \in [n], \sum_{k=1}^K W_{ik} = 1, \quad \forall j \in [p], \sum_{k=1}^K A_{kj} = 1$$

pLSI has a rich history in the statistics literature, and offers a robust and scalable alternative to LDA. There has been extensive work on the estimation of topic-word matrix A (Ke and Wang, 2017). Ke and Wang (2017) has established rigorous bounds on the estimation of the topic-word matrix A . For the estimation of document-topic matrix W , Klopp et al. (2021) exploited the simplex structure of its singular vectors to hunt for K vertices, also endowing their estimates with high-probability upper bounds on ℓ_1 and ℓ_2 error. However, as explained in Section 2, these methods are not likelihood-based methods and are characterized by a rigid estimation framework, within which the incorporation of covariates or known correlations within the documents is not trivial. Recent work Bing et al. (2020); Wu et al. (2023); Tran et al. (2023) have just begun considering the addition of more structure to the standard pLSI model, focusing for the most part on leveraging the supposed sparsity of A . To the best of our knowledge, the addition of correlation or similarity between documents remains an open question.

6 Conclusion

In this paper, we present Graph-Aligned pLSI (GpLSI), a topic model that leverages document-level metadata to improve estimation of the topic mixture matrix. We incorporate metadata by translating it into document similarity, which is then represented as edges connecting two documents on a graph. GpLSI is a powerful tool that integrates two complementary sources of information: word frequencies that traditional topic models use, and the document graph induced from metadata, which encodes which documents should share similar topic mixture proportions. To the best of our knowledge, this is the first framework to incorporate document-level metadata into topic models with theoretical guarantees.

At the core of GpLSI is an iterative graph-aligned singular value decomposition applied to the observed document-word matrix X . This procedure projects word frequencies to low-dimensional topic spaces, while ensuring that neighboring documents on the graph share similar topic mixtures. Our SVD approach can also be applied to other works that require dimension reduction with structural constraints on the samples. Additionally, we propose a novel cross validation technique to optimize the level of graph regularization by using the hierarchy of minimum spanning trees to define folds.

Our theoretical analysis and synthetic experiments confirm that GpLSI outperforms existing methods, particularly in “short-document” cases, where the scarcity of words is mitigated by smoothing mixture proportions along neighboring documents. Overall, GpLSI is a fast, highly effective topic model when there is a known structure in the relationship of documents.

We believe that our work offers valuable insights into structural topic models and opens up several avenues for further exploration. A promising direction is to incorporate structure to the topic matrix A while jointly optimizing structural constraints on W . While our work focuses on low- p regime, real world applications, such as genomics data with large p , could benefit from introducing sparsity to the word composition of each topic. Furthermore, there is a significant lack of literature exploring estimators for W and A that simultaneously achieve optimal error rates. We anticipate that future work will develop methods that enforce structure on both matrices while achieving optimal error rates.

Acknowledgments

C.D. and Y.J.J thank Daniel Li for his help implementing a python version of the algorithm of Sun et al. (2021). C.D. gratefully acknowledges support from NSF Award Number RI:2238616, as well as the resources provided by the University of Chicago’s Research Computing Center.

References

- M. C. U. Araújo, T. C. B. Saldanha, R. K. H. Galvao, T. Yoneyama, H. C. Chame, and V. Visani. The successive projections algorithm for variable selection in spectroscopic multicomponent analysis. *Chemometrics and intelligent laboratory systems*, 57(2):65–73, 2001.
- X. Bing, F. Bunea, and M. Wegkamp. Optimal estimation of sparse topic models. *Journal of machine learning research*, 21(177):1–45, 2020.
- D. Blei and J. Lafferty. Correlated topic models. *Advances in neural information processing systems*, 18:147, 2006a.
- D. Blei, A. Ng, and M. Jordan. Latent dirichlet allocation. *Advances in neural information processing systems*, 14, 2001.
- D. M. Blei and J. D. Lafferty. Dynamic topic models. In *Proceedings of the 23rd international conference on Machine learning*, pages 113–120, 2006b.
- S. Boucheron, G. Lugosi, and P. Massart. Concentration inequalities: A nonasymptotic theory of independence oxford, uk: Oxford univ, 2013.
- T. T. Cai and A. Zhang. Rate-optimal perturbation bounds for singular subspaces with applications to high-dimensional statistics. 2018.
- Z. Chen, I. Soifer, H. Hilton, L. Keren, and V. Jovic. Modeling multiplexed images with spatial-lda reveals novel tissue microenvironments. *Journal of Computational Biology*, 27(8):1204–1218, 2020.
- K. K. Dey, C. J. Hsiao, and M. Stephens. Visualizing the structure of rna-seq expression data using grade of membership models. *PLoS genetics*, 13(3):e1006599, 2017.
- D. Donoho and V. Stodden. When does non-negative matrix factorization give a correct decomposition into parts? *Advances in neural information processing systems*, 16, 2003.
- J. J. Egozcue, V. Pawlowsky-Glahn, G. Mateu-Figueras, and C. Barcelo-Vidal. Isometric logratio transformations for compositional data analysis. *Mathematical geology*, 35(3):279–300, 2003.
- Y. Feng and M. Lapata. Topic models for image annotation and text illustration. In *Human Language Technologies: The 2010 Annual Conference of the North American Chapter of the ACL*, pages 831–839. Association for Computational Linguistics, 2010.
- J. Fukuyama, K. Sankaran, and L. Symul. Multiscale analysis of count data through topic alignment. *Biostatistics*, 24(4):1045–1065, 2023.
- N. Gillis and S. A. Vavasis. Semidefinite programming based preconditioning for more robust near-separable nonnegative matrix factorization. *SIAM Journal on Optimization*, 25(1):677–698, 2015.
- C. Giraud. *Introduction to high-dimensional statistics*. Chapman and Hall/CRC, 2021.

- Y. Goltsev, N. Samusik, J. Kennedy-Darling, S. Bhate, M. Hale, G. Vazquez, S. Black, and G. P. Nolan. Deep profiling of mouse splenic architecture with codex multiplexed imaging. *Cell*, 174(4):968–981, 2018.
- J.-C. Hütter and P. Rigollet. Optimal rates for total variation denoising. In *Conference on Learning Theory*, pages 1115–1146. PMLR, 2016.
- Z. T. Ke and M. Wang. A new svd approach to optimal topic estimation. *arXiv preprint arXiv:1704.07016*, 2(4):6, 2017.
- S. J. Kho, H. B. Yalamanchili, M. L. Raymer, and A. P. Sheth. A novel approach for classifying gene expression data using topic modeling. In *Proceedings of the 8th ACM international conference on bioinformatics, computational biology, and health informatics*, pages 388–393, 2017.
- O. Klopp, M. Panov, S. Sigalla, and A. Tsybakov. Assigning topics to documents by successive projections, 2021.
- L. Liu, L. Tang, W. Dong, S. Yao, and W. Zhou. An overview of topic modeling and its current applications in bioinformatics. *SpringerPlus*, 5:1–22, 2016.
- J. McAuliffe and D. Blei. Supervised topic models. *Advances in neural information processing systems*, 20, 2007.
- G. K. Reder, A. Young, J. Altosaar, J. Rajniak, N. Elhadad, M. Fischbach, and S. Holmes. Supervised topic modeling for predicting molecular substructure from mass spectrometry. *F1000Research*, 10:Chem–Inf, 2021.
- M. E. Roberts, B. M. Stewart, D. Tingley, C. Lucas, J. Leder-Luis, S. K. Gadarian, B. Albertson, and D. G. Rand. Structural topic models for open-ended survey responses. *American journal of political science*, 58(4):1064–1082, 2014.
- K. Sankaran and S. P. Holmes. Latent variable modeling for the microbiome. *Biostatistics*, 20(4):599–614, 2019.
- L. Shang and X. Zhou. Spatially aware dimension reduction for spatial transcriptomics. *Nature communications*, 13(1):7203, 2022.
- Y. Shao, Y. Zhou, X. He, D. Cai, and H. Bao. Semi-supervised topic modeling for image annotation. In *Proceedings of the 17th ACM international conference on Multimedia*, pages 521–524, 2009.
- D. Sun, K.-C. Toh, and Y. Yuan. Convex clustering: Model, theoretical guarantee and efficient algorithm. *The Journal of Machine Learning Research*, 22(1):427–458, 2021.
- L. Symul, P. Jeganathan, E. K. Costello, M. France, S. M. Bloom, D. S. Kwon, J. Ravel, D. A. Relman, and S. Holmes. Sub-communities of the vaginal microbiota in pregnant and non-pregnant women. *Proceedings of the Royal Society B*, 290(2011):20231461, 2023.
- R. J. Tibshirani and J. Taylor. Degrees of freedom in lasso problems. 2012.

- H. Tran, Y. Liu, and C. Donnat. Sparse topic modeling via spectral decomposition and thresholding. *arXiv preprint arXiv:2310.06730*, 2023.
- N. A. Tu, D.-L. Dinh, M. K. Rasel, and Y.-K. Lee. Topic modeling and improvement of image representation for large-scale image retrieval. *Information Sciences*, 366:99–120, 2016.
- R. Vershynin. *High-dimensional probability: An introduction with applications in data science*, volume 47. Cambridge university press, 2018.
- P.-Å. Wedin. Perturbation bounds in connection with singular value decomposition. *BIT Numerical Mathematics*, 12:99–111, 1972.
- R. Wu, L. Zhang, and T. Tony Cai. Sparse topic modeling: Computational efficiency, near-optimal algorithms, and statistical inference. *Journal of the American Statistical Association*, 118(543):1849–1861, 2023.
- Z. Wu, A. E. Trevino, E. Wu, K. Swanson, H. J. Kim, H. B. D’Angio, R. Preska, G. W. Charville, P. D. Dalerba, A. M. Egloff, R. Uppaluri, U. Duvvuri, A. T. Mayer, and J. Zou. Space-gm: geometric deep learning of disease-associated microenvironments from multiplex spatial protein profiles. *bioRxiv*, 2022. doi: 10.1101/2022.05.12.491707. URL <https://www.biorxiv.org/content/early/2022/05/13/2022.05.12.491707>.
- D. Yang, Z. Ma, and A. Buja. Rate optimal denoising of simultaneously sparse and low rank matrices. *The Journal of Machine Learning Research*, 17(1):3163–3189, 2016.
- J. Yang, X. Feng, A. F. Laine, and E. D. Angelini. Characterizing alzheimer’s disease with image and genetic biomarkers using supervised topic models. *IEEE journal of biomedical and health informatics*, 24(4):1180–1187, 2019.
- Y. Zheng, Y.-J. Zhang, and H. Larochelle. A deep and autoregressive approach for topic modeling of multimodal data. *IEEE transactions on pattern analysis and machine intelligence*, 38(6):1056–1069, 2015.

Appendix A. Analysis of the initialization step

In this section, we show that the initialization in Algorithm 3 provides reasonable estimators of U and V .

Proof of Theorem 1

Proof We have, by definition of the initialization procedure:

$$\widehat{V}_0 = U_K(X^\top X - \frac{n}{N}\widehat{D}_0).$$

Let D_0 denote the diagonal matrix where each entry $(D_0)_{jj}$ is defined as: $(D_0)_{jj} = \frac{1}{n} \sum_{i=1}^n M_{ij}$. Let \widehat{D}_0 denote its empirical counterpart, that is, the diagonal matrix defined as: $\widehat{D}_0 = \text{diag}(\frac{1}{n} \{\sum_{i=1}^n X_{ij}\}_{j \in [p]})$, so that $\mathbb{E}[\widehat{D}_0] = D_0$.

We have:

$$\begin{aligned} Z^\top Z &= \sum_{i=1}^n Z_i^\top Z_i. \\ \implies \mathbb{E}[Z^\top Z] &= \sum_{i=1}^n \text{Cov}(Z_i) = \sum_{i=1}^n \text{Cov}(X_i) \end{aligned} \quad (21)$$

as Z is a centered version of X . Since each row X_i is distributed as a Multinomial($1, M_i$):

$$(\text{Cov}(X_i))_{jj'} = \begin{cases} \frac{M_{ij}(1-M_{ij})}{N} & \text{if } j = j' \\ -\frac{M_{ij}M_{ij'}}{N} & \text{if } j \neq j' \end{cases} \implies \sum_{i=1}^n (\text{Cov}(X_i))_{jj'} = \begin{cases} \sum_i \frac{M_{ij}(1-M_{ij})}{N} & \text{if } j = j' \\ -\sum_{i=1}^n \frac{M_{ij}M_{ij'}}{N} & \text{if } j \neq j' \end{cases}$$

Thus:

$$\begin{aligned} \mathbb{E}[Z^\top Z] &= \frac{n}{N} D_0 - \frac{M^\top M}{N} \\ &= \frac{n}{N} D_0 - \frac{V^\top \Lambda^2 V}{N}. \end{aligned} \quad (22)$$

Therefore:

$$X^\top X - \frac{n}{N} \widehat{D}_0 - (1 - \frac{1}{N}) M^\top M = Z^\top Z + Z^\top M + M^\top Z - \frac{n}{N} \widehat{D}_0 - \mathbb{E}[Z^\top Z] + \frac{n}{N} \mathbb{E}[\widehat{D}_0] \quad (23)$$

Thus $\mathbb{E}[X^\top X - \frac{n}{N} \widehat{D}_0] = (1 - \frac{1}{N}) M^\top M$. We further note that $(1 - \frac{1}{N}) M^\top M = V \tilde{\Lambda}^2 V$ with $\tilde{\Lambda} = (1 - \frac{1}{N}) \Lambda$, so the eigenvectors of the matrix $X^\top X - \frac{n}{N} \widehat{D}_0$ can be considered as estimators of those of the matrix $M^\top M$.

By the Davis-Kahan theorem (Giraud, 2021):

$$\begin{aligned} \|\sin \Theta(V, \widehat{V}^0)\|_F &\leq 2 \frac{\|X^\top X - \frac{n \widehat{D}_0}{N} - (1 - \frac{1}{N}) M^\top M\|_F}{(1 - \frac{1}{N}) \lambda_K(M)^2} \\ &\leq 2 \frac{\|Z^\top Z - \mathbb{E}[Z^\top Z]\|_F + \frac{n}{N} \|\widehat{D}_0 - \mathbb{E}[\widehat{D}_0]\|_F + \|Z^\top M\|_F + \|M^\top Z\|_F}{(1 - \frac{1}{N}) \lambda_K(M)^2} \end{aligned} \quad (24)$$

By Lemma 10, we have with probability at least $1 - o(n^{-1})$:

$$\begin{aligned} \|Z^\top Z - \mathbb{E}[Z^\top Z]\|_F &\leq C_1 K \sqrt{\frac{n \log(n)}{N}}, \\ \|Z^\top M\|_F = \|M^\top Z\|_F &\leq C_2 K \sqrt{\frac{n \log(n)}{N}}, \end{aligned}$$

and

$$\frac{n}{N} \|\widehat{D}_0 - \mathbb{E}[\widehat{D}_0]\|_F \leq \frac{C_3}{N} \sqrt{\frac{K n \log(n)}{N}}.$$

Thus, assuming $N > 1$, so $\frac{1}{1-\frac{1}{N}} < 2$ and $\frac{1}{N} \leq \frac{1}{2}$:

$$\|\sin \Theta(V, \widehat{V}^0)\|_F \leq \frac{14C}{\lambda_K(M)^2} K \sqrt{\frac{n \log(n)}{N}}$$

with $C = C_1 \vee C_2 \vee C_3$. Under Assumption 4, we have $\lambda_K(M) \geq c\lambda_1(W) \geq c\sqrt{n/K}$ (see Lemma 5), therefore:

$$\|\sin \Theta(V, \widehat{V}^0)\|_F \leq \frac{14C}{c^2} K^2 \sqrt{\frac{\log(n)}{nN}}$$

Note that the condition of N defined in (12) in Theorem 2 ensures that $\|\sin \Theta(V, \widehat{V}^0)\|_F < \frac{1}{2}$. ■

Appendix B. Analysis of iterative graph-aligned denoising

Our proof is organized along the following outline:

1. We begin by showing that our graph-total variation penalty yields better estimates of the left and right singular vectors. To this end, we must show that, provided that the initialization is good enough, the estimation error of the singular vectors decreases with the number of iterations.
2. We show that, by a simple readaptation of the proof by Klopp et al. (2021), our estimator—which simply plugs in our singular vector estimates in the procedure of Klopp et al. (2021)—yields a better estimate of the mixture matrix W .
3. Finally, we show that our estimator of the topic matrix A yields a better error.

B.1 Analysis of the graph-regularized SVD procedure

In this section, we derive high-probability error bounds for the estimates \widehat{U} and \widehat{V} that we obtain in Algorithm 1. For each $t > 0$, we define the error L_t at iteration t as:

$$L_t = \max\{\|\sin(\Theta(V, \widehat{V}^t))\|_F, \|\sin(\Theta(U, \widehat{U}^t))\|_F\}. \quad (25)$$

Our proof is a proof by recursion. We explicit the dependency of L_t on the error at the previous iteration L_{t-1} , and show that $\{L_t\}_{t=1, \dots, t_{\max}}$ forms a geometric series. To this end, we begin by analyzing the error of the denoised matrix \bar{U}^t , of which we later take an SVD to extract \widehat{U}^t .

B.1.1 EFFECT OF THE GRAPH-DENOISING STEP

At each iteration t , the first step of Algorithm 1 is to consider the following optimization problem:

$$\bar{U}^t \in \arg \min_{U \in \mathbb{R}^{n \times K}} \|U - X\widehat{V}^{t-1}\|_F^2 + \rho \|U\|_{2,1} \quad (26)$$

Fix $t > 0$. To simplify notations, we let

$$\tilde{Y} = X\hat{V}^{t-1}, \quad \tilde{U} = M\hat{V}^{t-1}, \quad \tilde{Z} = Z\hat{V}^{t-1} \quad (27)$$

Note that with these notations, \tilde{Y} can be written as:

$$\tilde{Y} = \tilde{U} + \tilde{Z} \quad (28)$$

Lemma 1 (Error bound of Graph-aligned Denoising) *Let Assumption 1 to 5 hold and let $L_t, \bar{U}^t, \tilde{Y}, \tilde{U}, \rho$ be given as (25)-(28). Assume $\max(K, p) \leq n$ and $\sqrt{K} \leq p$. Then, for a choice of $\rho = 4C^* \rho(\Gamma) \sqrt{\frac{Kp_n}{N}} (1 + L_{t-1})$ with a constant $C^* > 0$, there exists a constant $C > 0$ such that with probability at least $1 - o(n^{-1})$, for any $t > 0$,*

$$\|\bar{U}^t - \tilde{U}\|_F \leq C \sqrt{\frac{K \log(n)}{N}} \left(\sqrt{nc} + \rho(\Gamma) \sqrt{s} \sqrt{\lambda_{\max}} (1 + L_{t-1}) \right) \quad (29)$$

Proof By the KKT conditions:

$$2(\bar{U}^t - \tilde{Y}) + \rho \Gamma^\top D \Gamma \bar{U}^t = 0 \quad \text{with } D = \text{diag}\left\{\frac{1}{\|(\Gamma U^t)_e\|_2}\right\}_{e \in \mathcal{E}}$$

This implies:

$$\begin{aligned} \langle \tilde{Y} - \bar{U}^t, \bar{U}^t \rangle &= \frac{\rho}{2} \langle \Gamma \bar{U}^t, D \Gamma \bar{U}^t \rangle = \frac{\rho}{2} \|\Gamma \bar{U}^t\|_{21} \\ \text{and } \forall U \in \mathbb{R}^{n \times p}, \quad \langle \tilde{Y} - \bar{U}^t, U \rangle &= \frac{\rho}{2} \langle \Gamma U, D \Gamma \bar{U}^t \rangle \leq \frac{\rho}{2} \|\Gamma U\|_{21} \end{aligned}$$

Therefore:

$$\begin{aligned} \langle \tilde{Y} - \bar{U}^t, U - \bar{U}^t \rangle &\leq \frac{\rho}{2} (\|\Gamma U\|_{21} - \|\Gamma \bar{U}^t\|_{21}) \\ \langle \tilde{U} - \bar{U}^t, U - \bar{U}^t \rangle &\leq \langle \tilde{Z}, \bar{U}^t - U \rangle + \frac{\rho}{2} (\|\Gamma U\|_{21} - \|\Gamma \bar{U}^t\|_{21}) \end{aligned}$$

Using the polarization inequality:

$$\|U - \bar{U}^t\|_F^2 + \|\tilde{U} - \bar{U}^t\|_F^2 \leq \|U - \tilde{U}\|_F^2 + 2\langle \tilde{Z}, \bar{U}^t - U \rangle + \rho (\|\Gamma U\|_{21} - \|\Gamma \bar{U}^t\|_{21})$$

and, choosing $U = \tilde{U}$:

$$\|\tilde{U} - \bar{U}^t\|_F^2 \leq \langle \tilde{Z}, \bar{U}^t - \tilde{U} \rangle + \frac{\rho}{2} (\|\Gamma \tilde{U}\|_{21} - \|\Gamma \bar{U}^t\|_{21})$$

Let $\Delta = \tilde{U} - \bar{U}^t$. By the triangle inequality, the right-most term in the above inequality can be rewritten as:

$$\begin{aligned} \|\Gamma \tilde{U}\|_{21} - \|\Gamma \bar{U}^t\|_{21} &= \|(\Gamma \tilde{U})_{\mathcal{S}}\|_{21} + \|(\Gamma \tilde{U})_{\mathcal{S}^c}\|_{21} - \|(\Gamma \tilde{U} + \Gamma \Delta)_{\mathcal{S}}\|_{21} - \|(\Gamma \tilde{U} + \Gamma \Delta)_{\mathcal{S}^c}\|_{21} \\ &\leq \|(\Gamma \Delta)_{\mathcal{S}}\|_{21} - \|(\Gamma \Delta)_{\mathcal{S}^c}\|_{21}, \end{aligned}$$

since by assumption, $\|(\Gamma \tilde{U})_{\mathcal{S}^c}\|_{21} = 0$.

We turn to the control of the error term $\langle \tilde{Z}, \bar{U}^t - \tilde{U} \rangle$. Using the decomposition of $I_n = \Pi \oplus^\perp \Gamma^\dagger \Gamma$, we have:

$$\begin{aligned} \langle \tilde{Z}, \bar{U}^t - \tilde{U} \rangle &= \langle \tilde{Z}, \Pi(\bar{U}^t - \tilde{U}) \rangle + \langle \tilde{Z}, \Gamma^\dagger \Gamma(\bar{U}^t - \tilde{U}) \rangle \\ &= \underbrace{\langle \Pi \tilde{Z}, \Pi \Delta \rangle}_{(A)} + \underbrace{\langle (\Gamma^\dagger)^\top \tilde{Z}, \Gamma \Delta \rangle}_{(B)}. \end{aligned} \quad (30)$$

B.1.1.1 Bound on (A) in (30) By Cauchy-Schwarz:

$$\langle \Pi \tilde{Z}, \Pi \Delta \rangle \leq \|\Pi \tilde{Z}\|_F \|\Pi \Delta\|_F$$

We know that $\Pi_{[C_i]} = \frac{1}{n_{C_i}} \mathbf{1}_{C_i} \mathbf{1}_{C_i}^\top$. Using Lemma 14, with probability at least $1 - o(n^{-1})$:

$$\|\Pi \tilde{Z}\|_F^2 \leq C_1 n_C K \frac{\log(n)}{N}$$

B.1.1.2 Bound on (B) in (30).

$$\begin{aligned} \langle (\Gamma^\dagger)^\top \tilde{Z}, \Gamma \Delta \rangle &= \sum_{e \in [m]} \langle ((\Gamma^\dagger)^\top \tilde{Z})_e, (\Gamma \Delta)_e \rangle \\ &\leq \sum_{e \in [m]} \|((\Gamma^\dagger)^\top \tilde{Z})_e\|_2 \|(\Gamma \Delta)_e\|_2 \quad \text{by Cauchy-Schwarz} \\ &\leq \max_{e \in [m]} \|((\Gamma^\dagger)^\top \tilde{Z})_e\|_2 \sum_{e \in [m]} \|(\Gamma \Delta)_e\|_2 \\ &= \max_{e \in [m]} \|((\Gamma^\dagger)^\top \tilde{Z})_e\|_2 \|\Gamma \Delta\|_{21} \end{aligned}$$

Thus, on the event $\mathcal{A} = \{\rho \geq 4 \max_{e \in [m]} \|((\Gamma^\dagger)^\top \tilde{Z})_e\|_2\}$, we have:

$$\langle (\Gamma^\dagger)^\top \tilde{Z}, \Gamma \Delta \rangle \leq \frac{\rho}{4} \|\Gamma \Delta\|_{21}.$$

To derive $\mathbb{P}(\mathcal{A})$, we first establish the relationship between \tilde{Z} and L_{t-1} ,

$$\tilde{Z} = Z(P_V + P_{V_\perp}) \hat{V}^{t-1} = ZV V^\top \hat{V}^{t-1} + ZV_\perp V_\perp^\top \hat{V}^{t-1}$$

Then,

$$\begin{aligned} \max_{e \in [m]} \|((\Gamma^\dagger)^\top \tilde{Z})_e\|_2 &= \max_{e \in [m]} \|((\Gamma^\dagger)^\top (ZV V^\top \hat{V}^{t-1} + ZV_\perp V_\perp^\top \hat{V}^{t-1}))_e\|_2 \\ &\leq \max_{e \in [m]} \|((\Gamma^\dagger)^\top Z)_e\|_2 \|V^\top \hat{V}^{t-1}\|_{op} + \max_{e \in [m]} \|((\Gamma^\dagger)^\top Z)_e\|_2 \|V_\perp^\top \hat{V}^{t-1}\|_{op} \\ &\leq \max_{e \in [m]} \|((\Gamma^\dagger)^\top Z)_e\|_2 (1 + L_{t-1}) \end{aligned}$$

where we used the fact $\|\sin \Theta(V, \hat{V}^{t-1})\|_F = \|V_\perp^\top \hat{V}^{t-1}\|_F \geq \|V_\perp^\top \hat{V}^{t-1}\|_{op}$. From Lemma 11, for a choice of $\rho = 4C^* \rho(\Gamma) \sqrt{\frac{K \log(n)}{N}} (1 + L_{t-1})$, then $\mathbb{P}[\mathcal{A}] \geq 1 - o(n^{-1})$.

Therefore:

$$\begin{aligned} \|\Delta\|_F^2 &\leq \|\Pi \tilde{Z}\|_F \|\Delta\|_F + \frac{3\rho}{4} \|\Gamma \Delta\|_{21} \\ &\leq \|\Pi \tilde{Z}\|_F \|\Delta\|_F + \frac{3\rho}{4} \sqrt{s} \|\Gamma \Delta\|_F \\ &\leq \|\Pi \tilde{Z}\|_F \|\Delta\|_F + \frac{3\rho}{4} \sqrt{s} \sqrt{\lambda_{\max}(\Gamma)} \|\Delta\|_F \end{aligned} \tag{31}$$

and thus:

$$\begin{aligned} \|\tilde{U} - \bar{U}^t\|_F &\leq C_1 \sqrt{\frac{n_c K \log(n)}{N}} + 3C_2 \rho(\Gamma) \sqrt{s} \sqrt{\lambda_{\max}(\Gamma)} \sqrt{\frac{K \log(n)}{N}} (1 + L_{t-1}) \\ &\leq C \sqrt{\frac{K \log(n)}{N}} (\sqrt{n_c} + \rho(\Gamma) \sqrt{s} \sqrt{\lambda_{\max}(\Gamma)} (1 + L_{t-1})) \end{aligned}$$

■

B.1.2 PROOF OF THEOREM 2

Proof Let L_t be the error at each iteration t :

$$L_t = \max\{\|\sin(\Theta(V, \hat{V}^t))\|_F, \|\sin(\Theta(U, \hat{U}^t))\|_F\}. \quad (32)$$

B.1.2.1 Bound on $\|\sin(\Theta(U, \hat{U}^t))\|_F$. We start by deriving a bound for $\|\sin \Theta(U, \hat{U}^t)\|_F$. Let U_\perp denote the orthogonal complement of U , so that:

$$I_n = UU^\top + U_\perp U_\perp^\top.$$

Noting that \hat{U}^t is the matrix corresponding to the top K left singular vectors of the matrix $\tilde{U}^t = (\tilde{U}^t - MV) + MV = (\tilde{U}^t - M\hat{V}^t + M\hat{V}^t - MV) + MV$, by Theorem 1 of Cai and Zhang (2018) (Lemma 6 in the appendix):

$$\begin{aligned} \|\sin \Theta(U, \hat{U}^t)\|_F &\leq \frac{\|P_{U_\perp}(\tilde{U}^t - M\hat{V}^t + M\hat{V}^t - MV)\|_F}{\lambda_{\min}(U^\top \tilde{U}^t)} \\ &= \frac{\|P_{U_\perp}(\tilde{U}^t - M\hat{V}^t)\|_F}{\lambda_{\min}(U^\top \tilde{U}^t)} \end{aligned}$$

where the second line follows from noting that $P_{U_\perp}(M\hat{V}^t - MV) = 0$.

Since Λ is a diagonal matrix, we have:

$$\begin{aligned} \lambda_{\min}(U^\top M\hat{V}^{t-1}) &= \lambda_{\min}(\Lambda V^\top \hat{V}^{t-1}) = \min_{u \in \mathbb{R}^K, v \in \mathbb{R}^p: \|u\|=\|v\|=1} u^\top \Lambda V^\top \hat{V}^{t-1} v \\ &= \lambda_K(M) \min_{u \in \mathbb{R}^K, v \in \mathbb{R}^p: \|u\|=\|v\|=1} u^\top V^\top \hat{V}^{t-1} v \\ &= \lambda_K(M) \lambda_{\min}(V^\top \hat{V}^{t-1}) \end{aligned}$$

Thus, by Weyl's inequality:

$$\begin{aligned} \lambda_{\min}(U^\top \tilde{U}^t) &= \lambda_{\min}(U^\top (\tilde{U}^t - M\hat{V}^{t-1} + M\hat{V}^{t-1})) \\ &\geq -\lambda_{\max}(U^\top (\tilde{U}^t - M\hat{V}^{t-1})) + \lambda_{\min}(U^\top M\hat{V}^{t-1}) \\ &\geq \lambda_{\min}(\Lambda V^\top \hat{V}^{t-1}) - \|\tilde{U}^t - M\hat{V}^{t-1}\|_F = \lambda_K(M) \sqrt{1 - L_{t-1}^2} - \|\Delta\|_F \end{aligned}$$

where $\Delta = \tilde{U}^t - M\hat{V}^{t-1}$. By Lemma 1, we know that:

$$\|\Delta\|_F \leq C \sqrt{\frac{K \log(n)}{N}} (\sqrt{n_c} + \rho(\Gamma) \sqrt{s} \sqrt{\lambda_{\max}(\Gamma)} (1 + L_{t-1})) = \eta_n + \delta_n L_{t-1}$$

with $\eta_n = C\sqrt{\frac{K\log(n)}{N}}\left(\sqrt{n_{\mathcal{C}}} + \rho(\Gamma)\sqrt{s}\sqrt{\lambda_{\max}(\Gamma)}\right)$ and $\delta_n = C\rho(\Gamma)\sqrt{s\lambda_{\max}(\Gamma)\frac{K\log(n)}{N}}$. Thus:

$$\begin{aligned}\|\sin\Theta(U, \hat{U}^t)\|_F &\leq \frac{\|\Delta\|_F}{\lambda_K(M)\sqrt{1-L_{t-1}^2} - \|\Delta\|_F} \\ &\leq \frac{\eta_n + \delta_n L_{t-1}}{\lambda_K(M)\sqrt{1-L_{t-1}^2} - (\eta_n + \delta_n L_{t-1})} \\ &\leq \frac{\eta_n + \delta_n L_{t-1}}{\lambda_K(M)/2 - (\eta_n + \delta_n L_{t-1})}\end{aligned}$$

where the last line follows by assuming that $L_{t-1} \leq \frac{1}{2} \quad \forall t \geq 0$ (we will show that this indeed holds). By using a first-order Taylor expansion around 0 for the function $f(x) = \frac{a+bx}{c-a-bx}$ for $x \in (0, 1/2)$, we obtain:

$$f(x) < \frac{a}{c-a} + \frac{bc}{(c-a-b/2)^2}x, \quad \text{for } x \in (0, 1/2).$$

Therefore, seeing that we have $\eta_n \geq \delta_n$ and letting $u = \frac{\eta_n}{\lambda_K(M)/2 - \eta_n} = \frac{2\eta_n}{\lambda_K(M) - 2\eta_n}$ and $r = \frac{\lambda_K(M)/2\delta_n}{(\lambda_K(M)/2 - \eta_n - \delta_n/2)^2} = \frac{2\lambda_K(M)\delta_n}{(\lambda_K(M) - 2\eta_n - \delta_n)^2} \leq \frac{2\lambda_K(M)\eta_n}{(\lambda_K(M) - 3\eta_n)^2}$, we have:

$$\|\sin\Theta(U, \hat{U}^t)\|_F \leq u + rL_{t-1}$$

By Assumption 4, we have $\lambda_K(M) \geq c\sqrt{\frac{n}{K}}$. Therefore, $\lambda_K(M) \geq 10\eta_n$ as soon as:

$$\begin{aligned}n &\geq \frac{100C^2}{c^2} \frac{K^2 \log(n)}{N} (n_{\mathcal{C}} + \rho^2(\Gamma)s\lambda_{\max}(\Gamma)) \\ \implies N &\geq \frac{100C^2}{c^2} \frac{K^2 \log(n)}{n} (n_{\mathcal{C}} + \rho^2(\Gamma)s\lambda_{\max}(\Gamma))\end{aligned}\tag{33}$$

Thus, in this setting:

$$r \leq \frac{2\lambda_K(M)\eta_n}{(\lambda_K(M) - 3\eta_n)^2} \leq \frac{2\lambda_K(M)\eta_n}{(\frac{7}{10}\lambda_K(M))^2} \leq \frac{200/49\eta_n}{\lambda_K(M)} \leq \frac{20}{49} \leq \frac{1}{2}.\tag{34}$$

and

$$u \leq \frac{2\eta_n}{\lambda_K(M) - 2\eta_n} \leq \frac{5/2\eta_n}{\lambda_K(M)} \leq \frac{5}{20} = \frac{1}{4}$$

Also given that $L_{t-1} \leq \frac{1}{2}$,

$$\|\sin\Theta(U, \hat{U}^t)\|_F \leq u + rL_{t-1} \leq \frac{5/2\eta_n + 100/49\eta_n}{\lambda_K(M)} \leq \frac{1}{2}.$$

B.1.2.2 Bound on $\|\sin\Theta(V, \hat{V}^t)\|_F$ By definition of the second step:

$$\hat{V}^t = SVD_K(X^\top \hat{U}^t).$$

By Theorem 1 of Cai and Zhang (2018) (summarized for our use case in Lemma 6 in Appendix C):

$$\begin{aligned} \|\sin \Theta(V, \widehat{V}^t)\|_F &\leq \frac{\|P_{V_\perp}(M^\top(\widehat{U}^t - U) + Z^\top \widehat{U}^t)\|_F}{\lambda_{\min}(V^\top X^\top \widehat{U}^t)} \\ &= \frac{\|P_{V_\perp}(Z^\top \widehat{U}^t)\|_F}{\lambda_{\min}(V^\top X^\top \widehat{U}^t)} \quad \text{since } P_{V_\perp} M^\top(\widehat{U}^t - U) = 0 \end{aligned}$$

We have:

$$\begin{aligned} \lambda_{\min}(V^\top X^\top \widehat{U}^t) &= \lambda_{\min}(V^\top M^\top \widehat{U}^t + V^\top Z^\top \widehat{U}^t) \\ &\geq \lambda_{\min}(\Lambda U^\top \widehat{U}^t) - \lambda_{\max}(V^\top Z^\top \widehat{U}^t) \quad (\text{Weyl's inequality}) \\ &= \lambda_{\min}(\Lambda) \underbrace{\lambda_{\min}(U^\top \widehat{U}^t)}_{=\sqrt{1-L_t^2}} - \|V^\top Z^\top \widehat{U}^t\|_F \\ &\geq \lambda_{\min}(\Lambda) \sqrt{1-L_t^2} - \|V^\top Z^\top \widehat{U}^t\|_F \end{aligned}$$

Thus, assuming that $L_t \leq \frac{1}{2}, \forall t$:

$$\|\sin \Theta(V, \widehat{V}^t)\|_F \leq \frac{\|V_\perp^\top Z^\top \widehat{U}^t\|_F}{\frac{1}{2} \lambda_K(M) - \|V^\top Z^\top \widehat{U}^t\|_F}.$$

Furthermore:

$$\begin{aligned} \|V^\top Z^\top \widehat{U}^t\|_F &\leq \|V^\top Z^\top U U^\top \widehat{U}^t\|_F + \|V^\top Z^\top U_\perp U_\perp^\top \widehat{U}^t\|_F \\ &\leq \|V^\top Z^\top U\|_F \|U^\top \widehat{U}^t\|_{op} + \|V^\top Z^\top U_\perp\|_{op} \|U_\perp^\top \widehat{U}^t\|_F \\ &\leq CK \sqrt{\frac{\log(n)}{N}} + C \sqrt{\frac{Kn \log(n)}{N}} \|\sin \Theta(U, \widehat{U}^t)\|_F \end{aligned}$$

where the last inequality follows by noting that $\|U^\top \widehat{U}^t\|_F \leq 1$ and from Lemma 13, which show that with probability at least $1 - o(\frac{1}{n})$:

$$\|Z^\top U\|_F \leq CK \sqrt{\frac{\log(n)}{N}}$$

and since $U_\perp \in \mathbb{R}^{n \times (n-K)}$:

$$\|Z^\top U_\perp\|_{op} \leq C \sqrt{Kn \frac{\log(n)}{N}}.$$

Therefore, using the same arguments as in the previous paragraph, using $\tilde{\eta}_n = CK \sqrt{\frac{\log(n)}{N}}$ and $\tilde{\delta}_n = C \sqrt{\frac{Kn \log(n)}{N}}$, we have:

$$f(x) < \frac{a}{c-a} + \frac{bc}{(c-a-b/2)^2} x, \quad \text{for } x \in (0, 1/2).$$

Therefore, we have $\tilde{\eta}_n \leq \tilde{\delta}_n$, and letting $\tilde{u} = \frac{\tilde{\eta}_n}{\lambda_K(M)/2 - \tilde{\eta}_n}$ and $\tilde{r} = \frac{\lambda_K(M)/2\tilde{\delta}_n}{(\lambda_K(M)/2 - \tilde{\eta}_n - \tilde{\delta}_n/2)^2} = \frac{2\lambda_K(M)\tilde{\delta}_n}{(\lambda_K(M) - 2\tilde{\eta}_n - \tilde{\delta}_n)^2} \leq \frac{2\lambda_K(M)\tilde{\delta}_n}{(\lambda_K(M) - 3\tilde{\delta}_n)^2}$,

$$\|\sin \Theta(V, \hat{V}^t)\|_F \leq \tilde{u} + \tilde{r} \|\sin \Theta(U, \hat{U}^t)\|_F \leq \tilde{u} + \tilde{r} L_{t-1}$$

when L_t decreases with each iteration. Again, we note that $\lambda_K(M) \geq 10\tilde{\delta}_n$ as soon as:

$$\begin{aligned} n &\geq \frac{100C^2}{c^2} \frac{K^2 n \log(n)}{N} \\ \implies N &\geq \frac{100C^2}{nc^2} K^2 \log(n) \end{aligned} \quad (35)$$

Then we can show that,

$$\tilde{r} \leq \frac{2\lambda_K(M)\tilde{\delta}_n}{(\lambda_K(M) - 3\tilde{\delta}_n)^2} \leq \frac{2\lambda_K(M)\tilde{\delta}_n}{(\frac{7}{10}\lambda_K(M))^2} \leq \frac{200/49\tilde{\delta}_n}{\lambda_K(M)} \leq \frac{1}{2} \quad (36)$$

and

$$\tilde{u} \leq \frac{2\tilde{\delta}_n}{\lambda_K(M) - 2\tilde{\delta}_n} \leq \frac{5/2\tilde{\delta}_n}{\lambda_K(M)} \leq \frac{5}{20} = \frac{1}{4}$$

Also given that $L_{t-1} \leq \frac{1}{2}$,

$$\|\sin \Theta(V, \hat{V}^t)\|_F \leq \tilde{u} + \tilde{r} L_{t-1} \leq \frac{5/2\tilde{\delta}_n + 100/49\tilde{\delta}_n}{\lambda_K(M)} \leq \frac{1}{2}$$

and

$$\frac{\tilde{u}}{1 - \tilde{r}} \leq \frac{3\tilde{\delta}_n}{\lambda_K(M)} \times \frac{\lambda_K(M)}{\lambda_K(M) - 4\tilde{\delta}_n} \leq \frac{1}{2}.$$

Therefore, for all t ,

$$L_t \leq \frac{1}{2}.$$

B.1.2.3 Behavior of L_t L_t is a decreasing function of t for $t \geq 1$, and by Theorem 1, $L_0 \leq \frac{1}{2}$ (We later show in (46)). From the previous sections,

$$\begin{aligned} \|\sin \Theta(U, \hat{U}^t)\|_F &\leq \frac{5/2C}{\lambda_K(M)} \sqrt{\frac{K \log(n)}{N}} \left(\sqrt{nc} + \rho(\Gamma) \sqrt{s\lambda_{\max}(\Gamma)} \right) \\ &\quad + \frac{200/49C}{\lambda_K(M)} \sqrt{\frac{K \log(n)}{N}} \rho(\Gamma) \sqrt{s\lambda_{\max}(\Gamma)} L_{t-1} \\ \|\sin \Theta(V, \hat{V}^t)\|_F &\leq \frac{5/2C}{\lambda_K(M)} K \sqrt{\frac{\log(n)}{N}} + \frac{200/49C}{\lambda_K(M)} \sqrt{\frac{Kn \log(n)}{N}} L_{t-1} \end{aligned}$$

Thus,

$$\begin{aligned}
 L_t &\leq u + rL_{t-1} \\
 &\leq u + r(u + rL_{t-2}) \\
 &\leq r^t L_0 + u(1 + r + r^2 + \dots + r^{t-1}) \\
 &\leq r^t L_0 + u \frac{1 - r^t}{1 - r}
 \end{aligned} \tag{37}$$

where

$$\begin{aligned}
 u &= \frac{5/2C}{\lambda_K(M)} \sqrt{\frac{K \log(n)}{N}} \left(\sqrt{nc} + \rho(\Gamma) \sqrt{s\lambda_{\max}(\Gamma)} \right) \\
 r &= \frac{200/49C}{\lambda_K(M)} K \sqrt{\frac{\log(n)}{N}} \left(\rho(\Gamma) \sqrt{s\lambda_{\max}(\Gamma)} \vee \sqrt{n} \right)
 \end{aligned}$$

where $r \leq \frac{1}{2}$. In particular, we want to find t_{\max} such that $r^{t_{\max}} L_0 \leq \frac{u}{1-r}$. Using $r \leq \frac{1}{2}$ (as previously shown) and that $L_0 \leq \frac{1}{2}$,

$$\begin{aligned}
 \frac{r^{t_{\max}}}{2} &\leq \frac{u}{1-r} \\
 \implies t_{\max} &\geq \frac{-\log(2u) + \log(1-r)}{|\log(r)|} \geq \frac{-2\log(2) - \log(u)}{\log(2)}
 \end{aligned}$$

Combining with the previous inequality (and since $\log(2) \leq \frac{1}{4}$) and the fact that under Assumption 4, we have $\lambda_K(M) \geq c\sqrt{n/K}$, we can choose t_{\max} as,

$$t_{\max} = \left(2\log(nN) - 4\log\left(\frac{5/2C}{c}\right) - 4\log(K) - 2\log(\log n) - 4\log(\sqrt{nc} + \rho(\Gamma)\sqrt{s\lambda_{\max}(\Gamma)}) - 2 \right) \vee 1$$

Thus, it is sufficient to choose t_{\max} as,

$$t_{\max} = 2\log\left(\frac{nN}{K^2}\right) \vee 1 \tag{38}$$

Denote $m_1 = \sqrt{nc} + \rho(\Gamma)\sqrt{s\lambda_{\max}(\Gamma)}$ and $m_n = \rho(\Gamma)\sqrt{s\lambda_{\max}(\Gamma)} \vee \sqrt{n}$. Lastly, once t_{\max} is chosen as (38), the bound on $L_{t_{\max}}$ in (37) becomes,

$$\begin{aligned}
 L_{t_{\max}} &\leq \frac{2u}{1-r} \\
 &= \frac{10C}{\lambda_K(M)} \sqrt{\frac{K \log(n)}{N}} \left(\sqrt{nc} + \rho(\Gamma) \sqrt{s\lambda_{\max}(\Gamma)} \right) \\
 &\leq \frac{10C}{c} K \sqrt{\frac{\log(n)}{nN}} \left(\sqrt{nc} + \rho(\Gamma) \sqrt{s\lambda_{\max}(\Gamma)} \right) \leq \frac{1}{c}
 \end{aligned} \tag{39}$$

where $c > 1$ (Assumption 4). This concludes the proof. ■

B.2 Analysis of the Estimation of W

In this section, we adapt the proof of Klopp et al. (2021) that derives a high probability bound for the outcome \widehat{W} after successive projections. We evaluate the vertices \widehat{H} detected by SPA with the rows of \widehat{U} as the input. To accomplish this, we first need to bound the row-wise error of \widehat{U} which is closely related to the upper bound of the estimated vertices $\widehat{H} = \widehat{U}_J$ and ultimately, is linked to $\widehat{W} = \widehat{U}\widehat{H}^{-1}$. Similarly to Klopp et al. (2021), define $\beta(M, X)$ as,

$$\max_{i=1, \dots, n} \|\mathbf{e}_i^T (\widehat{U} - UO)\|_2 \leq \beta(M, X) \quad (40)$$

We first need the following assumption on $\beta(M, X)$.

Assumption 6 For a constant $\bar{C} > 0$, we have

$$\beta(M, X) \leq \frac{\bar{C}}{\lambda_1(W)\kappa(W)K\sqrt{K}}$$

Lemma 2 (Adapted from Corollary 5 of Klopp et al. (2021)) *Let Assumptions 1 to 6 hold. Assume that $M \in \mathbb{R}^{n \times p}$ is a rank- K matrix. Let $U, \widehat{U} \in \mathbb{R}^{n \times K}$ be the left singular vectors corresponding to the top K singular values of M and its perturbed matrix $X \in \mathbb{R}^{n \times p}$, respectively. Let J be the set of indices returned by the SPA with input (\widehat{U}, K) , and $\widehat{H} = \widehat{U}_J$. Let $O \in \mathbb{O}_K$ be the same matrix as (13). Then, for a small enough \bar{C} , there exists a constant $C' > 0$ and a permutation \tilde{P} such that*

$$\|\widehat{H} - \tilde{P}HO\|_F \leq C' \sqrt{K}\kappa(W)\beta(M, X) \quad (41)$$

where $\beta(M, X)$ is defined as (40).

Proof The proof here is a direct combination of Theorem 4 and Corollary 5 of Klopp et al. (2021), for SPA (rather than pre-conditioned SPA). The crux of the argument consists of applying Theorem 2 in (Gillis and Vavasis, 2015) which bounds the error of SPA in the near-separable nonnegative matrix factorization setting,

$$\widehat{U} = UO + N = WHO + N = WQ + N$$

where $Q = HO$ and $N \in \mathbb{R}^{n \times K}$ is the noise matrix. Note that the rows of U lie on a simplex with vertices H and weights W . The theorem states that if the row-wise error of N is bounded by an ϵ such that:

$$\|\mathbf{e}_i^T N\|_2 \leq \epsilon \leq C_* \frac{\lambda_{\min}(Q)}{K\sqrt{K}} \quad (42)$$

for some small constant $C_* > 0$, we can bound the column-wise error of \widehat{U} for columns in the set J under permutation π ,

$$\|\widehat{U}_j - q_{\pi(j)}\|_2 \leq C' \kappa(Q)\epsilon$$

Applying this result to our setting, under Assumption 4,6 and Lemma 5, our bound on $\|\mathbf{e}_i^\top N\|_2 = \|\mathbf{e}_i^\top (\hat{U} - UO)\|_2$ satisfies (42),

$$\|\mathbf{e}_i^\top (\hat{U} - UO)\|_2 \leq \frac{\bar{C}}{\lambda_1(W)\kappa(W)K\sqrt{K}} \leq \frac{\bar{C}}{\lambda_1(W)K\sqrt{K}} \leq \frac{C_*\lambda_{\min}(HO)}{K\sqrt{K}}$$

for a small enough $\bar{C} \leq C_*$. Noting that $\hat{H} = \hat{U}_J$ and $\kappa(H) = \kappa(W)$, with the permutation matrix \tilde{P} corresponding to π , we get

$$\|\hat{H} - \tilde{P}HO\|_F \leq C' \sqrt{K}\kappa(W)\beta(M, X) \quad (43)$$

■

We then readapt the proof of Lemma 2 from Klopp et al. (2021) with our new \hat{U} .

Lemma 3 (Adapted from Lemma 2 of Klopp et al. (2021)) *Let the conditions of Lemma 2 hold. Then \hat{H} is non-degenerate and the estimated topic mixture matrix $\hat{W} = \hat{U}\hat{H}^{-1}$ satisfies,*

$$\min_{P \in \mathcal{P}} \|\hat{W} - WP\|_F \leq 2C' \sqrt{K}\lambda_1^2(W)\kappa(W)\beta(X, \Gamma) + \lambda_1(W)\|\hat{U} - UO\|_F$$

where \mathcal{P} denotes the set of all permutations.

Proof The first part of the proof on the invertibility of \hat{H} is analogous to Lemma 2 in Klopp et al. (2021), where combined with Lemma 5, we obtain the inequality,

$$\lambda_{\min}(\hat{H}) \geq \frac{1}{2\lambda_1(W)}$$

and for the singular values of H^{-1} and \hat{H}^{-1} :

$$\lambda_1(\hat{H}^{-1}) \leq 2\lambda_1(W) = 2\lambda_1(H^{-1})$$

Using the result of Lemma 2, we have

$$\begin{aligned} \|\hat{W} - WP\|_F &= \|\hat{U}\hat{H}^{-1} - UH^{-1}P\|_F \\ &\leq \|\hat{U}(\hat{H}^{-1} - O^\top H^{-1}P)\|_F + \|(\hat{U} - UO)[P^{-1}HO]^{-1}\|_F \\ &\leq \|\hat{H}^{-1}\|_{op}\|H^{-1}\|_{op}\|\hat{H} - \tilde{P}HO\|_F + \|\hat{U} - UO\|_F\|H^{-1}\|_{op} \\ &\leq 2C' \sqrt{K}\lambda_1^2(W)\kappa(W)\beta(X, \Gamma) + \lambda_1(W)\|\hat{U} - UO\|_F \end{aligned}$$

where we used the well known inequality $\|A^{-1} - B^{-1}\|_F \leq \|A^{-1}\|_{op}\|B^{-1}\|_{op}\|A - B\|_F$. ■

B.2.1 PROOF OF THEOREM 3

We are now ready to prove our main result.

Proof Notably, by the property of maximum row norms, $\max_{i=1,\dots,n} \|\mathbf{e}_i^\top (\widehat{U} - UO)\|_2 \geq \|\widehat{U} - UO\|_F / \sqrt{n}$. It is then sufficient to set $\beta(M, X)$ defined in (40),

$$\beta(M, X) = \frac{10C}{\sqrt{n}\lambda_K(M)} \sqrt{\frac{K \log(n)}{N}} \left(\sqrt{nc} + \rho(\Gamma) \sqrt{s\lambda_{\max}(\Gamma)} \right) \quad (44)$$

which is a high probability bound on $\max_{i=1,\dots,n} \|\mathbf{e}_i^\top (\widehat{U} - UO)\|_2$ with probability at least $1 - o(n^{-1})$ (Theorem 2).

We first show that the initialization error in Theorem 1 is upper bounded by $\frac{1}{2}$. Combining Assumption 4 and Lemma 5, we have

$$\lambda_k(M) \geq c\lambda_1(W) \geq c\sqrt{n/K} \quad (45)$$

Then using the condition on N , (12),

$$\begin{aligned} \|\sin \Theta(V, \widehat{V}^0)\|_F &\leq \frac{C}{\lambda_K(M)^2} K \sqrt{\frac{n \log(n)}{N}} \\ &\leq \frac{CK^2}{c^2 n} \sqrt{\frac{n \log(n)}{N}} \\ &\leq \frac{C}{c^2 (\sqrt{nc} + \rho^2(\Gamma) s \lambda_{\max}(\Gamma))} \leq \frac{1}{2} \end{aligned} \quad (46)$$

for large enough $c > 0$.

Next from (12), (44), and (45),

$$\beta(M, X) \leq \frac{1}{\sqrt{c_{\min}^*} K \sqrt{K} \lambda_K(M)} \leq \frac{\bar{C}}{\lambda_1(W) \kappa(W) K \sqrt{K}} \quad (47)$$

which proves Assumption 6. Thus, we are ready to use Theorem 2 and Lemma 3. We can now plug in $\beta(M, X)$ (44) and the error bound of graph-regularized SVD (13) in the bound of $\min_{P \in \mathcal{P}} \|\widehat{W} - WP\|_F$ in Lemma 3.

$$\begin{aligned} \|\widehat{W} - WP\|_F &\leq 2C' \sqrt{K} \lambda_1^2(W) \kappa(W) \beta(X, \Gamma) + \lambda_1(W) \|\widehat{U} - UO\|_F \\ &\leq \frac{20C' C}{\sqrt{n}} \left(\frac{\lambda_1(W)}{\lambda_K(M)} \right)^2 \lambda_K(M) \kappa(W) K \sqrt{\frac{\log(n)}{N}} \left(\sqrt{nc} + \rho(\Gamma) \sqrt{s\lambda_{\max}(\Gamma)} \right) \\ &\quad + 10C \frac{\lambda_1(W)}{\lambda_K(M)} \sqrt{\frac{K \log(n)}{N}} \left(\sqrt{nc} + \rho(\Gamma) \sqrt{s\lambda_{\max}(\Gamma)} \right) \\ &\leq \frac{20c^* C' C}{\sqrt{nc^2}} \lambda_K(M) K \sqrt{\frac{\log(n)}{N}} \left(\sqrt{nc} + \rho(\Gamma) \sqrt{s\lambda_{\max}(\Gamma)} \right) \\ &\quad + \frac{10C}{c} \sqrt{\frac{K \log(n)}{N}} \left(\sqrt{nc} + \rho(\Gamma) \sqrt{s\lambda_{\max}(\Gamma)} \right) \\ &\leq \frac{20C}{c} K \sqrt{\frac{\log(n)}{N}} \left(\sqrt{nc} + \rho(\Gamma) \sqrt{s\lambda_{\max}(\Gamma)} \right) \end{aligned} \quad (48)$$

Here, we used the bounds on condition numbers in Assumption 4 and $\lambda_K(M) \leq \sqrt{n}$ in Lemma 4. ■

B.3 Analysis of the Estimation of A

Using the result of Theorem 3, we now proceed to bound the error of \widehat{A} in Step 4 (9).

Proof By the simple basic inequality, letting $P = \arg \min_{O \in \mathcal{F}} \|\widehat{W} - WO\|_F$:

$$\begin{aligned}
 \|X - \widehat{W}\widehat{A}\|_F^2 &\leq \|X - \widehat{W}P^{-1}A\|_F^2 \\
 \|WA + Z - \widehat{W}\widehat{A}\|_F^2 &\leq \|WA + Z - \widehat{W}P^{-1}A\|_F^2 \\
 \|(W - \widehat{W}P^{-1})A + \widehat{W}(P^{-1}A - \widehat{A}) + Z\|_F^2 &\leq \|(W - \widehat{W}P^{-1})A + Z\|_F^2 \\
 \|\widehat{W}(P^{-1}A - \widehat{A})\|_F^2 &\leq 2\langle \widehat{W}(\widehat{A} - P^{-1}A), (W - \widehat{W}P^{-1})A + Z \rangle \\
 &= 2\langle \widehat{W}(\widehat{A} - P^{-1}A), (W - \widehat{W}P^{-1})A \rangle + 2\langle \widehat{W}(\widehat{A} - P^{-1}A), Z \rangle \\
 &\leq 2\|\widehat{W}(\widehat{A} - P^{-1}A)\|_F \|(W - \widehat{W}P^{-1})A\|_F \\
 &\quad + 2\|\widehat{W}(\widehat{A} - P^{-1}A)\|_F \max_{U \in \mathbb{R}^{n \times p}: \|U\|_F=1} \langle U, Z \rangle \\
 \|\widehat{W}(P^{-1}A - \widehat{A})\|_F &\leq 2\|(W - \widehat{W}P^{-1})A\|_F + C_2 \sqrt{\frac{\log(n)}{N}} \\
 &\leq 2\lambda_1(A)\|(W - \widehat{W}P^{-1})\|_F + C_2 \sqrt{\frac{\log(n)}{N}} \\
 \|P^{-1}A - \widehat{A}\|_F &\leq 2\|(W - \widehat{W}P^{-1})A\|_F + C_2 \sqrt{\frac{\log(n)}{N}} \\
 &\leq 2 \frac{\lambda_1(A)}{\lambda_{\min}(\widehat{W})} \|W - \widehat{W}P^{-1}\|_F + C_2 \sqrt{\frac{\log(n)}{N}} \\
 &\leq \frac{\lambda_1(A)\|W - \widehat{W}P^{-1}\|_F}{\lambda_K(W) - \|W - \widehat{W}P^{-1}\|_{op}} + 2C_2 \sqrt{\frac{\log(n)}{N}} \quad (*) \\
 &\leq \frac{\lambda_1(A)}{\lambda_K(W)/\|W - \widehat{W}P^{-1}\|_F - 1} + 2C_2 \sqrt{\frac{\log(n)}{N}} \\
 &\leq C_1 \frac{\lambda_1(A)}{\lambda_K(W)} \|W - \widehat{W}P^{-1}\|_F + 2C_2 \sqrt{\frac{\log(n)}{N}}
 \end{aligned}$$

where in (*) we have used Weyl's inequality to conclude,

$$\lambda_{\min}(\widehat{W}) \geq \lambda_K(W) - \|W - \widehat{W}P^{-1}\|_F.$$

Now, assume that N is large enough so that (12) holds. Combining Lemma 5 and Theorem 3, $\|W - \widehat{W}P^{-1}\|_F$ becomes small enough so that $\|W - \widehat{W}P^{-1}\|_F \leq \frac{2}{c} < 1 \leq \lambda_K(W)$.

By definition, Z represents some centered multinomial noise, with each entry Z_i being independent. Similar to proof of Lemma 13, $\langle U, Z \rangle$ can be represented as a sum of nN centered variables:

$$\begin{aligned} \langle U, Z \rangle &= \text{tr}(U^\top Z) = \sum_{j=1}^p \sum_{i=1}^n U_{ij} Z_{ij} \\ &= \frac{1}{N} \sum_{j=1}^p \sum_{i=1}^n \sum_{m=1}^N U_{ij} (T_{im}(j) - \mathbb{E}[T_{im}(j)]) \\ &= \frac{1}{N} \sum_{i=1}^n \sum_{m=1}^N \eta_{im} \quad \text{with } \eta_{im} = \sum_{j=1}^p U_{ij} (T_{im}(j) - \mathbb{E}[T_{im}(j)]) \end{aligned}$$

We have:

$$\text{Var}\left(\sum_{i=1}^n \eta_{im}\right) = \sum_{i=1}^n \text{Var}\left(\sum_{j=1}^p U_{ij} T_{im}(j)\right) = \sum_{i=1}^n \left(\sum_{j=1}^p U_{ij}^2 M_{ij} - \left(\sum_{j=1}^p U_{ij} M_{ij}\right)^2 \right) \leq 1,$$

since $\sum_{i=1}^n \sum_{j=1}^p U_{ij}^2 = 1$ and thus:

$$\sum_{m=1}^N \text{Var}\left(\sum_{i=1}^n \eta_{im}\right) \leq N.$$

Moreover, for each i, m ,

$$\begin{aligned} \sum_{m=1}^N \left| \sum_{i=1}^n \eta_{im} \right|^q &= N \left| \sum_{i=1}^n \sum_{j=1}^p U_{ij} (T_{im}(j) - \mathbb{E}[T_{im}(j)]) \right|^q \\ &\leq N \left(\sum_{i=1}^n \sum_{j=1}^p U_{ij}^2 \times \sum_{i=1}^n \sum_{j=1}^p (T_{im}(j) - M_{ij})^2 \right)^{\frac{q}{2}} \\ &\leq N \left(\sum_{i=1}^n \sum_{j=1}^p (T_{im}(j)^2 + M_{ij}^2 - 2M_{ij}T_{im}(j)) \right)^{\frac{q}{2}} \\ &\leq N 2^{\frac{q}{2}} \\ &= 2N 2^{(q-2)/2} \\ &< \frac{q!}{2} (4N) \left(\frac{2^{1/2}}{3}\right)^{q-2} \end{aligned}$$

Thus, by Bernstein's inequality (Lemma 7 with $v = 4N$ and $c = \frac{\sqrt{2}}{3}$):

$$\mathbb{P}\left[\left|\frac{1}{N} \sum_{m=1}^N \sum_{i=1}^n \eta_{im}\right| > t\right] \leq 2e^{-\frac{N^2 t^2 / 2}{4N + \sqrt{2} N t / 3}} = 2e^{-\frac{N t^2 / 2}{4 + \sqrt{2} t / 3}} \quad (49)$$

Choosing $t = C^* \sqrt{\frac{\log(n)}{N}}$:

$$\mathbb{P}\left[\frac{1}{N} \sum_{m=1}^N \sum_{i=1}^n \eta_{im} > t\right] \leq 2e^{-\frac{(C^*)^2 \log(n)/2}{4 + \frac{C^* \sqrt{2}}{3} \sqrt{\frac{\log(n)}{N}}}} \quad (50)$$

Thus, with probability at least $1 - o(n^{-1})$, $|\langle U, Z \rangle| \leq C^* \sqrt{\frac{\log(n)}{N}}$.

Lastly, we use the fact, $\lambda_1(A) \leq \|A\|_F \leq \sqrt{K}$, and $\lambda_K(W) \geq 1$ from Lemma 5 and the result of Theorem 3 to get the final bound of A ,

$$\|\widehat{A} - P^{-1}A\|_F \leq CK^{3/2} \sqrt{\frac{\log(n)}{N}} \left(\sqrt{nc} + \rho(\Gamma) \sqrt{s\lambda_{\max}(\Gamma)} \right)$$

■

B.4 Comparison with One-step Graph-Aligned denoising

We also propose a fast one-step graph-aligned denoising of the matrix X that could be an alternative of the iterative graph-aligned SVD in Step 1 of 2.3. We denoise the frequency matrix X by the following optimization problem,

$$\widehat{M} = \operatorname{argmin}_{M \in \mathbb{R}^{n \times p}} \|X - M\|_F^2 + \rho \|\Gamma M\|_{21} \quad (51)$$

A SVD on the denoised matrix \widehat{M} yields estimates of the singular values U and V (Algorithm 3). Through extensive experiments with synthetic data detailed in Section 4, we find that one-step graph-aligned denoising provides more accurate estimates than pLSI but still falls short compared to the iterative graph-aligned denoising (GpLSI). We provide a theoretical upper bound on its error as well as its comparison to the error of pLSI where there is no graph-aligned denoising.

Algorithm 3 One-step Graph-aligned denoising

- 1: **Input:** Observation X , incidence matrix Γ
 - 2: **Output:** Denoised singular vectors \widehat{U} and \widehat{V} .
 - 3: 1. Graph denoising on X with MST-CV: $\tilde{M} = \operatorname{argmin}_{M \in \mathbb{R}^{n \times p}} \|X - M\|_F^2 + \hat{\rho} \|\Gamma M\|_{21}$
 - 4: 2. Perform the rank- K SVD of \tilde{M} : $\tilde{M} \approx \widehat{U} \widehat{\Lambda} \widehat{V}$
-

We begin by analyzing the one-step graph-aligned denoising, as proposed in Algorithm 3. We begin by reminding the reader that, in our proposed setting, the observed word frequencies in each document are assumed to follow a “signal + noise” model, as per (2):

$$X = M + Z$$

where the true probability M is assumed to admit the following SVD decomposition:

$$M = \mathbb{E}[X] = U \Lambda V^\top.$$

Theorem 5 (Upper bound on the one-step denoising error) *Let Assumptions 1 to 5 hold. Denote $\rho(\Gamma)$, s , n_C , and $n_{C_{\min}}$ as (3)-(5) and assume $\max(K, p) \leq n$ and $\sqrt{K} \leq p$. Let \widehat{U} and \widehat{V} be given as estimators obtained from Algorithm 3. Then, there exists a constant $C > 0$, such that with probability at least $1 - o(n^{-1})$,*

$$\max\{\|\sin \Theta(U, \widehat{U})\|_F, \|\sin \Theta(V, \widehat{V})\|_F\} \leq CK \sqrt{\frac{\log(n)}{nN}} \left(\sqrt{n_C} + \rho(\Gamma) \sqrt{s} \sqrt{\lambda_{\max}(\Gamma)} \right) \quad (52)$$

where $\lambda_K(M)$ denotes the K^{th} singular value of M .

Proof

Let \widehat{M} be the solution of (51):

$$\widehat{M} = \operatorname{argmin}_{M \in \mathbb{R}^{n \times p}} \|M - X\|_F^2 + \rho \|\Gamma M\|_{21}$$

Let $\Delta = \widehat{M} - M$, and $Z = X - M$. By the basic inequality, we have:

$$\begin{aligned} \|\widehat{M} - X\|_F^2 + \rho \|\Gamma \widehat{M}\|_{21} &\leq \|M - X\|_F^2 + \rho \|\Gamma M\|_{21} \\ \|\widehat{M} - M\|_F^2 &\leq 2\langle X - M, \widehat{M} - M \rangle + \rho \|\Gamma M\|_{21} - \rho \|\Gamma \widehat{M}\|_{21} \\ &= 2\langle Z, (\Pi + \Gamma^\dagger \Gamma) \Delta \rangle + \rho \|\Gamma M\|_{21} - \rho \|\Gamma \Delta + \Gamma M\|_{21} \\ &\leq 2 \underbrace{\langle \Pi Z, \Pi \Delta \rangle}_{(A)} + 2 \underbrace{\langle (\Gamma^\dagger)^T Z, \Gamma \Delta \rangle + \rho(\|\Gamma \Delta\|_{21} - \|\Gamma \Delta\|_{S^c})}_{(B)} \end{aligned} \quad (53)$$

where $S = \operatorname{supp}(\Gamma W)$ and in the penultimate line, we have used the decomposition of \mathbb{R}^n on the two orthogonal subspaces: $\mathbb{R}^n = \operatorname{Im}(\Pi) \oplus^\perp \operatorname{Im}(\Gamma^\dagger \Gamma)$, so that:

$$\forall x \in \mathbb{R}^n, \quad x = \Pi x + \Gamma^\dagger \Gamma x$$

We proceed by characterizing the behavior of each of the terms (A) and (B) in the final line of (53) separately.

B.4.0.1 Concentration of (A). By Cauchy-Schwarz, it is immediate to see that:

$$\langle \Pi Z, \Pi \Delta \rangle \leq \|\Pi Z\|_F \|\Pi \Delta\|_F.$$

By Lemma 12, with probability at least $1 - o(n^{-1})$:

$$(A) \leq 2 \sqrt{C_1 K n_C \frac{\log(n)}{N}} \|\Delta\|_F$$

B.4.0.2 Concentration of (B). We have:

$$\begin{aligned} &2\langle (\Gamma^\dagger)^T Z, \Gamma \Delta \rangle + \rho(\|\Gamma \Delta\|_{21} - \|\Gamma \Delta\|_{S^c}) \\ &\leq 2 \max_{e \in \mathcal{E}} \|[(\Gamma^\dagger)^T Z]_e\|_2 \times \|\Gamma \Delta\|_{21} + \rho(\|\Gamma \Delta\|_{21} - \|\Gamma \Delta\|_{S^c}) \end{aligned}$$

Let \mathcal{A} denote the event: $\mathcal{A} = \{\rho \geq 4 \max_{e \in \mathcal{E}} \|[(\Gamma^\dagger)^T Z]_e\|_2\}$. By Lemma 11, for a choice of $\rho = 4C_2 \rho(\Gamma) \sqrt{\frac{K \log(n)}{N}}$, then $\mathbb{P}[\mathcal{A}] \geq 1 - o(n^{-1})$.

Then, on \mathcal{A} , we have:

$$2\langle (\Gamma^\dagger)^T Z, \Gamma \Delta \rangle + \rho(\|\Gamma \Delta\|_{21} - \|\Gamma \Delta\|_{S^c}) \leq \frac{3\rho}{2} \|\Gamma \Delta\|_{21} - \frac{\rho}{2} \|\Gamma \Delta\|_{S^c} \quad (54)$$

B.4.0.3 Concentration We thus have:

$$\begin{aligned}
 \|\Delta\|_F^2 &\leq 4\sqrt{C_1 K n_C \frac{\log(n)}{N}} \|\Delta\|_F + \frac{3\rho}{2} \|(\Gamma\Delta)_{S^c}\|_{21} \\
 &\leq 4\sqrt{C_1 K n_C \frac{\log(n)}{N}} \|\Delta\|_F + \frac{3\rho}{2} \sqrt{s} \|\Gamma\Delta\|_F \\
 &\leq 4\sqrt{C_1 K n_C \frac{\log(n)}{N}} \|\Delta\|_F + \frac{3\rho}{2} \sqrt{s} \sqrt{\lambda_{\max}(\Gamma)} \|\Delta\|_F \\
 \|\Delta\|_F &\leq 4\sqrt{C_1 K n_C \frac{\log(n)}{N}} + \frac{3\rho}{2} \sqrt{s} \sqrt{\lambda_{\max}(\Gamma)} \\
 \|\Delta\|_F &\leq 4\sqrt{C_1 K n_C \frac{\log(n)}{N}} + 6\rho(\Gamma) C_2 \sqrt{\frac{K \log(n)}{N}} \sqrt{s} \sqrt{\lambda_{\max}(\Gamma)} \\
 &\leq C \left(\sqrt{n_C} + \rho(\Gamma) \sqrt{s} \sqrt{\lambda_{\max}(\Gamma)} \right) \sqrt{\frac{K \log(n)}{N}}
 \end{aligned}$$

Then by applying Wedin's $\sin\Theta$ theorem (Wedin, 1972),

$$\begin{aligned}
 \|\sin\Theta(U, \widehat{U})\|_F &\leq \frac{\max\{\|(M - \widehat{M})V\|_F, \|U^\top(M - \widehat{M})\|_F\}}{\lambda_K(M)} \\
 &\leq \frac{C}{\lambda_K(M)} \sqrt{\frac{K \log(n)}{N}} \left(\sqrt{n_C} + \rho(\Gamma) \sqrt{s} \sqrt{\lambda_{\max}(\Gamma)} \right)
 \end{aligned}$$

The derivation for \widehat{V} is symmetric, which leads us to the final bound,

$$\max\{\|\sin\Theta(U, \widehat{U})\|_F, \|\sin\Theta(V, \widehat{V})\|_F\} \leq \frac{C}{\lambda_K(M)} \sqrt{\frac{K \log(n)}{N}} \left(\sqrt{n_C} + \rho(\Gamma) \sqrt{s} \sqrt{\lambda_{\max}(\Gamma)} \right)$$

This concludes our proof. ■

We observe first that the error bound for one-step graph-aligned denoising has better rate than the one with no regularization, provided in (14). We also note that the rate of one-step denoising and GpLSI is equivalent up to a constant. Although the dependency of the error on parameters n, p, K , and N is the same for both methods, our empirical studies in Section 3.4 reveal that GpLSI still achieves lower errors compared to one-step denoising.

Appendix C. Auxiliary Lemmas

Let matrices X, M, Z, W , and A be defined as in Equation (2). In this section, we provide inequalities on the singular values of the unobserved quantities W, M , and H , perturbation bounds for singular spaces, as well as concentration bounds on noise terms, which are useful for proving our main results in Section 3.

C.1 Inequalities on Unobserved Quantities

Lemma 4 For the matrix M (Equation 2), the following inequalities hold:

$$\begin{aligned}\lambda_K(M) &\leq \sqrt{n} \times \min_{j \in [p]} \sqrt{h_j} \\ \lambda_1(M) &\leq \sqrt{n}\end{aligned}$$

Proof We observe that for each $j \in [p]$, the variational characterization of the smallest eigenvalue of the matrix $M^\top M/n$ yields:

$$\begin{aligned}\lambda_K\left(\frac{M^\top M}{n}\right) &\leq \left[\frac{M^\top M}{n}\right]_{jj} \\ &= \frac{1}{n} \sum_{i=1}^n M_{ij}^2 \\ &\leq \frac{1}{n} \sum_{i=1}^n M_{ij} \\ &\leq \sqrt{h_j}\end{aligned}$$

since

$$\frac{1}{n} \sum_{i=1}^n M_{ij} = \frac{1}{n} \sum_{i=1}^n \sum_{k=1}^K W_{ik} A_{kj} \leq \left\| \frac{1}{n} \sum_{i=1}^n W_{i \cdot} \right\|_2 \|A_{\cdot j}\|_2 \leq \sqrt{h_j}.$$

Similarly:

$$\begin{aligned}\lambda_1\left(\frac{M^\top M}{n}\right) &\leq \text{Tr}\left(\frac{M^\top M}{n}\right) \\ &= \sum_{j=1}^p \frac{1}{n} \sum_{i=1}^n M_{ij}^2 \\ &\leq \frac{1}{n} \sum_{i=1}^n \sum_{j=1}^p M_{ij} \\ &\leq 1\end{aligned}$$

■

We also add the following lemma from Klopp et al. (2021) to make this manuscript self-contained.

Lemma 5 (Lemma 6 from the supplemental material of Klopp et al. (2021)) *Let Assumption 2 be satisfied. For the matrices W , H , \hat{H} defined in Equations (6) and (7), we have*

$$\lambda_K(W) \geq 1, \quad \lambda_1(W) \geq \sqrt{n/K} \quad (55)$$

and

$$\lambda_1(H) = \frac{1}{\lambda_K(W)}, \quad \lambda_K(H) = \frac{1}{\lambda_1(W)}, \quad \kappa(H) = \kappa(W) \quad (56)$$

C.2 Matrix Perturbation Bounds

In this section, we provide rate-optimal bounds for the left and right singular subspaces. While the original Wedin's perturbation bound (Wedin, 1972) treats the singular subspaces symmetrically, work by Cai and Zhang (2018) provides sharper bounds for each subspace individually. This refinement is particularly relevant in our setting where an additional denoising step of the left singular subspace leads to different perturbation behaviors of left and right singular subspaces as iterations progress.

Consider the SVD of an approximately rank- K matrix $M \in \mathbb{R}^{n \times K}$ ($n > K$),

$$M = \begin{bmatrix} U & U_{\perp} \end{bmatrix} \begin{bmatrix} \Lambda \\ \mathbf{0} \end{bmatrix} V^{\top} \quad (57)$$

where $U \in \mathbb{O}^{n \times K}$, $U_{\perp} \in \mathbb{O}^{n \times (n-K)}$, $\Lambda \in \mathbb{R}^{K \times K}$, and $V \in \mathbb{O}^{K \times K}$.

Let $X = M + Z$ be the perturbed version of M with the perturbation matrix Z . We can write the SVD of X as:

$$X = \begin{bmatrix} \hat{U} & \hat{U}_{\perp} \end{bmatrix} \begin{bmatrix} \hat{\Lambda} \\ \mathbf{0} \end{bmatrix} \hat{V}^{\top} \quad (58)$$

where \hat{U} , \hat{U}_{\perp} , $\hat{\Lambda}$, \hat{V} have the same structures as U , U_{\perp} , Λ , V . We can decompose Z into two parts,

$$Z = Z_1 + Z_2 = P_U Z + P_{U_{\perp}} Z \quad (59)$$

Lemma 6 (Adapted from Theorem 1 of Cai and Zhang (2018)) *Let M , X , and Z be given as in Equations (57)-(59). Then:*

$$\begin{aligned} \|\sin \Theta(U, \hat{U})\|_{op} &\leq \frac{\|Z_2\|_{op}}{\lambda_{\min}(U^{\top} X V)} \wedge 1 \\ \|\sin \Theta(U, \hat{U})\|_F &\leq \frac{\|Z_2\|_F}{\lambda_{\min}(U^{\top} X V)} \wedge \sqrt{p} \end{aligned} \quad (60)$$

$$\begin{aligned} \|\sin \Theta(V, \hat{V})\|_{op} &\leq \frac{\|Z_1\|_{op}}{\lambda_{\min}(U^{\top} X V)} \wedge 1 \\ \|\sin \Theta(V, \hat{V})\|_F &\leq \frac{\|Z_1\|_F}{\lambda_{\min}(U^{\top} X V)} \wedge \sqrt{p} \end{aligned} \quad (61)$$

Proof This result is a simplified version of the original theorem under the setting $\text{rank}(M) = K$. ■

C.3 Concentration Bounds

We first introduce the general Bernstein inequality and its variant which will be used for proving high probability bounds for noise terms in Section C.3.2.

C.3.1 GENERAL INEQUALITIES

Lemma 7 (Bernstein inequality (Corollary 2.11, Boucheron et al. (2013))) *Let X_1, \dots, X_n be independent random variables such that there exists positive numbers v and c such that $\sum_{i=1}^n \mathbb{E}[X_i^2] \leq v$ and*

$$\sum_{i=1}^n \mathbb{E}[(X_i)_+^q] \leq \frac{q!}{2} v c^{q-2} \quad (62)$$

for all integers $q \geq 3$. Then for any $t > 0$,

$$\mathbb{P}\left(\left|\sum_{i=1}^n X_i\right| \geq t\right) \leq 2 \exp\left(-\frac{t^2/2}{v + ct}\right)$$

A special case of the previous lemma occurs when all variables are bounded by a constant b , by taking $v = \sum_{i=1}^n \mathbb{E}[X_i^2]$ and $c = b/3$.

Lemma 8 (Bernstein inequality for bounded variables (Theorem 2.8.4, Vershynin (2018)))

Let X_1, \dots, X_n be independent random variables with $|X_i| \leq b$, $\mathbb{E}[X_i] = 0$ and $\text{Var}[X_i] \leq \sigma_i^2$ for all i . Let $\sigma^2 := n^{-1} \sum_{i=1}^n \sigma_i^2$. Then for any $t > 0$,

$$\mathbb{P}\left(n^{-1} \left|\sum_{i=1}^n X_i\right| \geq t\right) \leq 2 \exp\left(-\frac{nt^2/2}{\sigma^2 + bt/3}\right)$$

C.3.2 TECHNICAL LEMMAS

Lemma 9 (Concentration of the cross-terms $Z_i^\top Z_j$) *Let Assumptions 1-4 hold. With probability at least $1 - o(n^{-1})$:*

$$|Z_j^\top Z_l - \mathbb{E}(Z_j^\top Z_l)| \leq C^* \sqrt{\frac{nh_j h_l \log n}{N}} \quad \text{for all } j, l \in [p] \text{ with } j \neq l \quad (63)$$

$$|Z_j^\top Z_j - \mathbb{E}(Z_j^\top Z_j)| \leq C^* \sqrt{\frac{nh_j^2 \log n}{N}} + \frac{C^*}{N} \sqrt{\frac{nh_j \log n}{N}} \quad \text{for all } j \in [p] \quad (64)$$

where $\forall j \in [p], h_j = \sum_{k=1}^K A_{kj}$.

Proof The proof is a re-adaptation of Lemma C.4 in Tran et al. (2023) for any word j .

Similar to the analysis of Ke and Wang (2017), we rewrite each row X_i as a sum over N word entries $T_{im} \in \mathbb{R}^p$, where T_{im} denotes the m^{th} word in document i , encoded as a one-hot vector:

$$T_{im}(j) = \begin{cases} 1 & \text{if the } m^{\text{th}} \text{ word in document } i \text{ is word } j \\ 0 & \text{otherwise,} \end{cases} \quad (65)$$

where the notation $a(j)$ denotes the j^{th} entry of the vector a . Under this formalism, we rewrite each row of Z as:

$$Z_{i\cdot} = \frac{1}{N} \sum_{m=1}^N (T_{im} - \mathbb{E}[T_{im}]) \in \mathbb{R}^p.$$

In the previous expression, under the pLSI model (Equation 1), the $\{T_{im}\}_{m=1}^N$ are i.i.d. samples from a multinomial distribution with parameter M_i .

We can also express each entry Z_{ij} as:

$$Z_{ij} = \frac{1}{N} \sum_{m=1}^N (T_{im}(j) - \mathbb{E}[T_{im}(j)]) \quad (66)$$

Denote $S_{im}(j) := T_{im}(j) - \mathbb{E}[T_{im}(j)]$.

Fix $j, l \in [p]$. The $\{S_{im}^{(j)}\}_{\substack{i=1, \dots, n \\ m=1, \dots, N}}$ are all independent of one another (for all i and m) and $T_{im}(j) \sim \text{Bernoulli}(M_{ij})$. By (66), we note that

$$\begin{aligned} Z_j^\top Z_l &= \sum_{i=1}^n Z_{ij} Z_{il} = \frac{1}{N^2} \sum_{i=1}^n \sum_{m=1}^N \sum_{s=1}^N S_{im}(j) S_{is}(l) \\ &= \frac{1}{N^2} \sum_{i=1}^n \sum_{m=1}^N S_{im}(j) S_{im}(l) + \frac{1}{N^2} \sum_{i=1}^n \sum_{\substack{1 \leq m, s \leq N \\ m \neq s}} S_{im}(j) S_{is}(l) \\ &= \frac{n}{N} V_1 + \frac{N-1}{N} V_2 \end{aligned}$$

where we define

$$V_1 := \frac{1}{nN} \sum_{i=1}^n \sum_{m=1}^N S_{im}(j) S_{im}(l) \quad (67)$$

$$V_2 := \frac{1}{N(N-1)} \sum_{i=1}^n \sum_{\substack{1 \leq m, s \leq N \\ m \neq s}} S_{im}(j) S_{is}(l) \quad (68)$$

We note that the random variable V_2 is centered ($\mathbb{E}(V_2) = 0$), and we need an upper bound with high probability on $|V_1 - \mathbb{E}(V_1)|$ and $|V_2|$. We deal with each of these variables separately.

C.3.2.1 Upper bound on V_2 . We remind the reader that we have fixed $j, l \in [p]$. Define \mathcal{S}_N as the set of permutations on $\{1, \dots, N\}$ and $N' := \lfloor N/2 \rfloor$. Also define

$$W_i(S_{i1}, \dots, S_{iN}) := \frac{1}{N'} \sum_{m=1}^{N'} S_{i,2m-1}(j) S_{i,2m}(l)$$

Then by symmetry (note that the inner sum over m, s in the definition of V_2 has $N(N-1)$ summands),

$$V_2 = \frac{\sum_{i=1}^n \sum_{\pi \in \mathcal{S}_N} W_i(S_{i,\pi(1)}, \dots, S_{i,\pi(N)})}{N!}$$

Define, for a given $\pi \in \mathcal{S}_N$,

$$Q_\pi := \sum_{i=1}^n N' W_i(S_{\pi(1)}, \dots, S_{\pi(N)})$$

so that $N'V_2 = \frac{1}{N!} \sum_{\pi \in S_N} Q_\pi$. For arbitrary $t, s > 0$, by Markov's inequality and the convexity of the exponential function,

$$\mathbb{P}(N'V_2 \geq t) \leq e^{-st} \mathbb{E}(e^{sN'V_2}) \leq e^{-st} \frac{\sum_{\pi \in S_N} \mathbb{E}(e^{sQ_\pi})}{N!}$$

Also, define $Q = Q_\pi$ for π the identity permutation. Observe that

$$Q = \sum_{i=1}^n \sum_{m=1}^{N'} Q_{im} \quad \text{where } Q_{im} = S_{i,2m-1}(j) S_{i,2m}(l)$$

so Q is a (double) summation of mutually independent variables. We have $|Q_{im}| \leq 1$, $\mathbb{E}(Q_{im}) = 0$ and $\mathbb{E}(Q_{im}^2) \leq h_j h_l$ where $\forall j \in [p], h_j = \sum_{k=1}^K A_{kj}$. The rest of the proof for V_2 is similar to the standard proof for the usual Bernstein's inequality.

Denote $G(x) = \frac{e^x - 1 - x}{x^2}$, $G(x)$ is increasing as a function of x . Hence,

$$\begin{aligned} \mathbb{E}(e^{sQ_{im}}) &= \mathbb{E} \left(1 + sQ_{im} + \frac{s^2 Q_{im}^2}{2} + \dots \right) \\ &= \mathbb{E}[1 + s^2 Q_{im}^2 G(sQ_{im})] \quad \text{since } \mathbb{E}[Q_{im}] = 0 \\ &\leq \mathbb{E}[1 + s^2 Q_{im}^2 G(s)] \\ &\leq 1 + s^2 h_j h_l G(s) \leq e^{s^2 h_j h_l G(s)} \end{aligned}$$

Hence,

$$e^{-st} \mathbb{E}(e^{sQ}) = \exp(-st + N' n h_j h_l s^2 G(s))$$

Since this bound is applicable to all Q_π and not just the identity permutation, we have

$$\mathbb{P}(N'V_2 \geq t) \leq \exp(-st + N' n h_j h_l s^2 G(s)) = \exp(-st + N' n h_j h_l (e^s - 1 - s))$$

Now we choose $s = \log \left(1 + \frac{t}{N' n h_j h_l} \right) > 0$. Then

$$\begin{aligned} \mathbb{P}(N'V_2 \geq t) &\leq \exp \left[-t \log \left(1 + \frac{t}{N' n h_j h_l} \right) + N' n h_j h_l \left(\frac{t}{N' n h_j h_l} - \log \left(1 + \frac{t}{N' n h_j h_l} \right) \right) \right] \\ &= \exp \left[-N' n h_j h_l H \left(\frac{t}{N' n h_j h_l} \right) \right] \end{aligned}$$

where we define the function $H(x) = (1+x) \log(1+x) - x$. Note that we have the inequality

$$H(x) \geq \frac{3x^2}{6+2x}$$

for all $x > 0$. Hence,

$$\mathbb{P}(N'V_2 \geq t) \leq \exp \left(-\frac{t^2/2}{N' n h_j h_l + t/3} \right)$$

or by rescaling,

$$\mathbb{P}(N'V_2 \geq N'nt) \leq \exp \left(-\frac{N'nt^2/2}{h_j h_l + t/3} \right) \quad (69)$$

We can choose $t^2 = \frac{C^* h_j h_l}{N^n} \log n$ and note that $h_j h_l \geq c_{\min}^2 \frac{\log n}{nN}$ by Assumption 5. Hence, with probability $1 - o(n^{-1})$,

$$|V_2| \leq C^* \sqrt{\frac{nh_j h_l \log n}{N}}$$

By a simple union bound, we note that:

$$\begin{aligned} \mathbb{P} \left[\exists(j, l) : |V_2^{(j,l)}| \geq C^* \sqrt{\frac{nh_j h_l \log n}{N}} \right] &\leq \sum_{j,l} \mathbb{P} \left[|V_2^{(j,l)}| \geq C^* \sqrt{\frac{nh_j h_l \log n}{N}} \right] \\ &\leq p^2 e^{-C^* \log(n)} = e^{2 \log(p) - C^* \log(n)} \\ &\leq e^{-C \log(n)} \end{aligned} \quad (70)$$

where the last line follows by Assumption 5 (which implies that p is small), noting that for some large enough constant $\tilde{C} < C^*$ such that $n^{\tilde{C}} \geq p^2$, $2 \log(p) - C^* \log(n) \leq \tilde{C} \log(n) - C^* \log(n) = -(C^* - \tilde{C}) \log(n)$. Thus, for C^* large enough, for any j, l , with probability $1 - e^{-C \log(n)} = 1 - o(n^{-1})$:

$$|V_2| \leq C^* \sqrt{\frac{nh_j h_l \log n}{N}}$$

C.3.2.2 Upper bound on V_1 . As for V_1 , we can just apply the usual Bernstein's inequality. We remind the reader that $M_{ij} = \mathbb{E}[T_{im}(j)]$; we further note that $M_{ij} \leq h_j$. Since $S_{im}(j) = T_{im}(j) - M_{ij}$,

$$S_{im}(j)S_{im}(l) = T_{im}(j)T_{im}(l) - M_{ij}T_{im}(l) - M_{il}T_{im}(j) + M_{ij}M_{il} \quad (71)$$

Case 1: If $j \neq l$: then $T_{im}(j)T_{im}(l) = 0$ and so

$$\begin{aligned} \text{Var}[S_{im}(j)S_{im}(l)] &= \text{Var}[M_{ij}T_{im}(l) + M_{il}T_{im}(j)] \\ &\leq \mathbb{E}[M_{ij}T_{im}(l) + M_{il}T_{im}(j)]^2 \\ &= M_{ij}^2 M_{il} + M_{il}^2 M_{ij} = M_{ij}M_{il}(M_{ij} + M_{il}) \\ &\leq M_{ij}M_{il} \leq h_j h_l \end{aligned}$$

since $M_{ij} + M_{il} \leq 1$. Hence, by Bernstein's inequality,

$$\mathbb{P}(|V_1 - \mathbb{E}(V_1)| \geq t) \leq 2 \exp\left(-\frac{nNt^2/2}{h_j h_l + t/3}\right)$$

which is similar to (69), so picking $t^2 = C^* \frac{h_j h_l \log(n)}{nN}$, we obtain with probability $1 - o(n^{-1})$ that

$$\frac{n}{N}|V_1 - \mathbb{E}(V_1)| \leq \frac{C^*}{N} \sqrt{\frac{nh_j h_l \log n}{N}} \leq C^* \sqrt{\frac{nh_j h_l \log n}{N}}$$

and (63) is proven.

Case 2: If $j = l$ then since $T_{im}^2(j) = T_{im}(j)$, (71) leads to

$$S_{im}^2(j) = T_{im}(j)(1 - 2M_{ij}) + M_{ij}^2 \quad (72)$$

and since $|1 - 2M_{ij}| \leq 1$ and $\text{Var}(T_{im}(j)) = M_{ij}(1 - M_{ij})$,

$$\text{Var}[S_{im}^2(j)] \leq M_{ij} \leq h_j$$

and so we obtain (64) since with probability $1 - o(n^{-1})$

$$\frac{n}{N} |V_1 - \mathbb{E}(V_1)| \leq \frac{C^*}{N} \sqrt{\frac{nh_j \log(n)}{N}}$$

■

Lemma 10 (Concentration of the covariance matrix $X^\top X$) *Let Assumptions 1-5 hold. With probability $1 - o(n^{-1})$, the following statements hold true:*

$$\begin{aligned} \|Z^\top Z - \mathbb{E}[Z^\top Z]\|_F &\leq C^* K \sqrt{\frac{n \log n}{N}} \\ \|MZ^T\|_F &\leq C^* K \sqrt{\frac{n \log n}{N}} \\ \|\widehat{D}_0 - D_0\|_F &\leq C^* \sqrt{\frac{K \log n}{nN}} \end{aligned}$$

Proof

Let $\forall j \in [p]$, $h_j = \sum_{k=1}^K A_{kj}$.

C.3.2.3 Concentration of $\|Z^\top Z - \mathbb{E}[Z^\top Z]\|_F$ We have:

$$\begin{aligned} \|Z^\top Z - \mathbb{E}[Z^\top Z]\|_F^2 &= \sum_{j,j'=1}^p ((Z^\top Z)_{jj'} - \mathbb{E}[(Z^\top Z)_{jj'}])^2 \\ &= \sum_j ((Z^\top Z)_{jj} - \mathbb{E}[(Z^\top Z)_{jj}])^2 + \sum_{j \neq j'} ((Z^\top Z)_{jj'} - \mathbb{E}[(Z^\top Z)_{jj'}])^2 \\ &= \sum_j \left(2(C^*)^2 \frac{nh_j^2 \log(n)}{N} + 2 \frac{(C^*)^2}{N^2} \frac{nh_j \log(n)}{N} \right) + \sum_{j \neq j'} (C^*)^2 \frac{nh_j h_{j'} \log(n)}{N} \\ &\leq C^* \sum_{j,j'} \frac{nh_j h_{j'} \log(n)}{N} \text{ since by Assumption 5, } \min_j h_j \geq c_{\min} \frac{\log(n)}{N} \\ &\leq C^* K^2 \frac{n \log(n)}{N} \text{ since } \sum_j h_j = K \end{aligned}$$

where the third line follows by Lemma 9.

C.3.2.4 Concentration of $\|\widehat{D}_0 - D_0\|_F$ For a fixed $j \in [p]$ we have

$$(\widehat{D}_0)_{j,j} - (D_0)_{j,j} = \frac{1}{n} \sum_{i=1}^n Z_{ij} = \frac{1}{nN} \sum_{i=1}^n \sum_{m=1}^N (T_{im}(j) - \mathbb{E}[T_{im}(j)])$$

Note that since $T_{im}(j) \sim \text{Bernoulli}(M_{ij})$, $|T_{im}(j) - \mathbb{E}[T_{im}(j)]| \leq 1$ and

$$\text{Var}(T_{im}(j)) = M_{ij}(1 - M_{ij}) \leq M_{ij} = \sum_{k=1}^K A_{jk} W_{ki} \leq \sum_{k=1}^K A_{jk} = h_j \quad (73)$$

(and also $\text{Var}(T_{im}(j)) \leq 1$). We apply Bernstein's inequality to conclude for any $t > 0$:

$$\mathbb{P}\left(|(\widehat{D}_0)_{j,j} - (D_0)_{j,j}| \geq t\right) \leq 2 \exp\left(-\frac{nNt^2/2}{h_j + t/3}\right)$$

Choosing $t = C^* \sqrt{\frac{h_j \log n}{nN}}$. Since $h_j \geq c_{\min} \frac{\log(n)}{N}$ (Assumption 5), we obtain that with probability at least $1 - o(n^{-1})$,

$$\begin{aligned} |(\widehat{D}_0)_{j,j} - (D_0)_{j,j}| &\leq C^* \sqrt{\frac{h_j \log n}{nN}} \\ &\leq C^* \sqrt{\frac{h_j \log n}{nN}} \end{aligned}$$

Taking a union bound over $j \in [p]$, we obtain that:

$$\mathbb{P}[\exists j \in [p] : |(\widehat{D}_0)_{j,j} - (D_0)_{j,j}| > C^* \sqrt{\frac{h_j \log n}{nN}}] \leq p e^{-C^* \log(n)} = e^{\log(p) - C^* \log(n)} \leq e^{-(C^* - 1) \log(n)} = o\left(\frac{1}{n}\right)$$

since we assume that $p \ll n$. Therefore, with probability at least $o(n^{-1})$:

$$\|(\widehat{D}_0)_{j,j} - (D_0)_{j,j}\|_F^2 \leq \sum_{j=1}^p (C^*)^2 \frac{h_j \log n}{nN}$$

and since $\sum_j h_j = K$:

$$\|(\widehat{D}_0)_{j,j} - (D_0)_{j,j}\|_F \leq C^* \sqrt{\frac{K \log n}{nN}}$$

C.3.2.5 Concentration of $\|M^\top Z\|_F$ We have:

$$\begin{aligned} \|M^\top Z\|_F &= \|V \Lambda U^\top Z\|_F \\ &\leq \lambda_1(M) \|U^\top Z\|_F \end{aligned}$$

Noting that $\lambda_1(M) \leq \sqrt{n}$ (Lemma 4), by Lemma 13, with probability at least $1 - o(n^{-1})$:

$$\|M^\top Z\|_F \leq C^* K \sqrt{\frac{n \log(n)}{N}}$$

■

Lemma 11 (Concentration of $\|(\Gamma^\dagger Z)_e\|_2, e \in \mathcal{E}$) *Let Assumptions 1-5 hold. With probability at least $1 - o(n^{-1})$, for all edges $e \in \mathcal{E}$:*

$$|(\Gamma^\dagger)_e^\top (Z_{\cdot j} - \mathbb{E}[Z_{\cdot j}])| \leq C^* \rho(\Gamma) \sqrt{\frac{h_j \log(n)}{N}}, \quad (74)$$

$$\|((\Gamma^\dagger)^\top Z)_e\|_2 \leq C^* \rho(\Gamma) \sqrt{\frac{K \log(n)}{N}}. \quad (75)$$

where $\forall j \in [p], h_j = \sum_{k=1}^K A_{kj}$.

Proof

Fix $e \in \mathcal{E}$ and define $T_{im}(j)$ as in (65). Decomposing each $Z_{ij} - \mathbb{E}[Z_{ij}]$ as $Z_{ij} - \mathbb{E}[Z_{ij}] = \frac{1}{N} \sum_{m=1}^N (T_{im}(j) - \mathbb{E}[T_{im}(j)])$, we note that the product $((\Gamma^\dagger)^\top (Z - \mathbb{E}[Z]))_e$ can be written as a sum of nN independent terms:

$$(\Gamma^\dagger)_e^\top (Z_{\cdot j} - \mathbb{E}[Z_{\cdot j}]) = \frac{1}{N} \sum_{m=1}^N \left(\sum_{i=1}^n \Gamma_{ie}^\dagger (T_{im}(j) - \mathbb{E}[T_{im}(j)]) \right) = \frac{1}{N} \sum_{m=1}^N \sum_{i=1}^n \eta_{im},$$

with $\eta_{im} = \Gamma_{ie}^\dagger (T_{im}(j) - \mathbb{E}[T_{im}(j)])$.

1. Each η_{im} verifies Bernstein's condition (Equation (62)): We have:

$$\sum_{i=1}^n \sum_{m=1}^N \mathbb{E}[(\eta_{im})_+^q] = \sum_{i=1}^n \sum_{m=1}^N \mathbb{E}\left[\left(\Gamma_{ie}^\dagger (T_{im}(j) - \mathbb{E}[T_{im}(j)])\right)_+^q\right]$$

We note that: $\forall q \geq 3, \mathbb{E}[(T_{im}(j) - \mathbb{E}[T_{im}(j)])^q] = (1 - M_{ij})(-M_{ij})^q + M_{ij}(1 - M_{ij})^q$. Therefore, if $q = 2k$ for $k \geq 1$, $\mathbb{E}[(T_{im}(j) - \mathbb{E}[T_{im}(j)])^q] \leq M_{ij} = \sum_k W_{ik} A_{kj} \leq \sum_k A_{kj} = h_j$ and:

$$\begin{aligned} \sum_{i=1}^n \sum_{m=1}^N \mathbb{E}[(\eta_{im})_+^{2k}] &\leq \sum_{m=1}^N \sum_{i=1}^n |\Gamma_{ie}^\dagger|^{2k} h_j \\ &\leq N h_j \sum_{i=1}^n (|\Gamma_{ie}^\dagger|^2)^{k-1} |\Gamma_{ie}^\dagger|^2 \\ &\leq N h_j \rho^2(\Gamma) \rho^{2(k-1)}(\Gamma), \end{aligned}$$

where the last line follows by noting that $|\Gamma_{ie}^\dagger|^2 \leq \sum_{i=1}^n |\Gamma_{ie}^\dagger|^2 \leq \rho^2(\Gamma)$, so $|\Gamma_{ie}^\dagger|^{2(k-1)} \leq \rho^{2(k-1)}(\Gamma)$.

For $q = 2k + 1$ odd ($k \geq 1$), we note that:

$$\begin{aligned} \sum_{i=1}^n \sum_{m=1}^N \mathbb{E}[(\eta_{im})_+^{2k+1}] &\leq \sum_{i=1}^n \sum_{m=1}^N \mathbb{E}[|\eta_{im}|^{2k+1}] \\ &\leq \left(\sum_{m=1}^N \sum_{i=1}^n \mathbb{E}[|\eta_{im}|^{2k}] \right)^{\frac{1}{2}} \left(\sum_{m=1}^N \sum_{i=1}^n |\eta_{im}|^{2k+2} \right)^{\frac{1}{2}} \quad (\text{Cauchy Schwartz along } i, m) \\ &\leq N h_j \rho^{2k+1}(\Gamma) \\ &\leq N h_j \rho^2(\Gamma) \rho^{2k-1}(\Gamma) \end{aligned}$$

2. Each of the variance $\text{Var}(S_m) = \sum_{i=1}^n \text{Var}(\eta_{im})$ is also bounded:

$$\text{Var}(\eta_{im}) = (\Gamma^\dagger)_{ie}^2 \text{Var}(T_{im}(j)) \leq (\Gamma^\dagger)_{ie}^2 h_j.$$

Thus:

$$\sum_{m=1}^N \sum_{i=1}^n \text{Var}(\eta_{im}) \leq N \rho^2(\Gamma) h_j.$$

Therefore, by Bernstein's inequality (Lemma 7), plugging in $v = N \rho^2(\Gamma) h_j$ and $c = \frac{\rho(\Gamma)}{3}$:

$$\mathbb{P}\left[\frac{1}{N} \left| \sum_{i=1}^n \sum_{m=1}^N \eta_{im} \right| > t\right] \leq 2e^{-\frac{N^2 t^2 / 2}{N \rho(\Gamma)^2 h_j + \frac{\rho(\Gamma)}{3} \times N t}}.$$

Choosing $t = C^* \rho(\Gamma) \sqrt{\frac{h_j \log(n)}{N}}$, with $C^* > 1$, we have:

$$\mathbb{P}\left[\frac{1}{N} \left| \sum_{i=1}^n \sum_{m=1}^N \eta_{im} \right| > C^* \rho(\Gamma) \sqrt{\frac{h_j \log(n)}{N}}\right] \leq 2e^{-\frac{(C^*)^2 \log(n) / 2}{1 + \frac{C^*}{3} \sqrt{\frac{\log(n)}{h_j N}}}}.$$

Therefore, by Assumption 5, $h_j > c_{\min} \frac{\log(n)}{N}$, then, with probability at least $1 - o(n^{-1})$, $|((\Gamma^\dagger)^\top Z)_{ej}| \leq C^* \rho(\Gamma) \sqrt{\frac{h_j \log(n)}{N}}$.

Therefore, by a simple union bound and following the argument in (70):

$$\mathbb{P}[\exists j : |((\Gamma^\dagger)^\top Z)_{ej}| \geq C^* \rho(\Gamma) \sqrt{\frac{h_j \log(n)}{N}}] \leq p e^{-C^* \log(n)} = e^{\log(p) - C^* \log(n)} \leq e^{-(C^* - 1) \log(n)}.$$

since we assume that $p \ll n$. Writing $\|((\Gamma^\dagger)^\top Z)_e\|_2^2 = \sum_{j=1}^p |((\Gamma^\dagger)^\top Z)_{ej}|^2$, we thus have:

$$\begin{aligned} \mathbb{P}[\|((\Gamma^\dagger)^\top Z)_e\|_2^2 \geq \sum_{j=1}^p (C^*)^2 \rho^2(\Gamma) \frac{h_j \log(n)}{N}] &\leq \mathbb{P}[\exists j : |((\Gamma^\dagger)^\top Z)_{ej}| \geq C^* \rho(\Gamma) \sqrt{\frac{h_j \log(n)}{N}}] \\ \implies \mathbb{P}[\|((\Gamma^\dagger)^\top Z)_e\|_2^2 \leq (C^*)^2 \rho^2(\Gamma) \frac{K \log(n)}{N}] &\geq 1 - o(n^{-1}). \end{aligned} \tag{76}$$

where the last line follows by noting that $\sum_{j=1}^p h_j = K$.

Finally, to show that this holds for any $e \in \mathcal{E}$, it suffices to apply a simple union bound:

$$\begin{aligned} \mathbb{P}[\exists e \in \mathcal{E} : \|((\Gamma^\dagger)^\top Z)_e\|_2^2 \geq C^* \rho^2(\Gamma) \frac{K \log(n)}{N}] &\leq \sum_{e \in \mathcal{E}} \mathbb{P}[\|((\Gamma^\dagger)^\top Z)_e\|_2^2 \geq C^* \rho^2(\Gamma) \frac{K \log(n)}{N}] \\ &\leq |\mathcal{E}| e^{-C \log(n)} \\ &\leq e^{c_0 \log(n) - C^* \log(n)} \end{aligned} \tag{77}$$

with $c_0 < 2$. Therefore, $\mathbb{P}[\exists e \in \mathcal{E} : \|((\Gamma^\dagger)^\top Z)_e\|_2^2 \geq C^* \rho^2(\Gamma) \frac{K \log(n)}{N}] = o(\frac{1}{n})$ for a choice of C^* sufficiently large. \blacksquare

Lemma 12 (Concentration of $\|\Pi Z\|_F$) *Let Assumptions 1-5 hold. With probability at least $1 - o(n^{-1})$:*

$$\|\Pi Z\|_F^2 \leq C^* n_C K \frac{\log(n)}{N} \quad (78)$$

Proof We remind the reader that letting \mathcal{C}_j denote the j^{th} connected component of the graph \mathcal{G} and $n_{\mathcal{C}_l} = |\mathcal{C}_l|$ its cardinality, Π can be arranged as a block diagonal form where each block represents a connected component, $\Pi_{[\mathcal{C}_l]} = \frac{1}{n_{\mathcal{C}_l}} \mathbf{1}_{\mathcal{C}_l} \mathbf{1}_{\mathcal{C}_l}^T$. Since the components \mathcal{C}_l are all disjoint, $\|\Pi Z\|_F$ can be further decomposed as:

$$\begin{aligned} \|\Pi Z\|_F^2 &\leq \sum_{l=1}^{n_C} \left\| \frac{1}{n_{\mathcal{C}_l}} \mathbf{1}_{\mathcal{C}_l} \mathbf{1}_{\mathcal{C}_l}^T Z_{[\mathcal{C}_l]} \right\|_F^2 \\ &= \sum_{l=1}^{n_C} n_{\mathcal{C}_l} \left\| \frac{1}{n_{\mathcal{C}_l}} \mathbf{1}_{\mathcal{C}_l}^T Z_{[\mathcal{C}_l]} \right\|_2^2 \end{aligned}$$

By Assumption 3, $\forall i, N_i = N$. Following Equation (65), we rewrite each row of Z as:

$$Z_{i\cdot} = \frac{1}{N} \sum_{m=1}^N (T_{im} - \mathbb{E}[T_{im}]) \in \mathbb{R}^p.$$

In the previous expression, under the pLSI model, (1), the $\{T_{im}\}_{m=1}^N$ are i.i.d. samples from a multinomial distribution with parameter $M_{i\cdot}$. Thus, for each word j and each connected component \mathcal{C}_l :

$$\frac{1}{n_{\mathcal{C}_l}} \mathbf{1}_{\mathcal{C}_l}^T Z_{[\mathcal{C}_l]j} = \frac{1}{n_{\mathcal{C}_l} N} \sum_{i \in \mathcal{C}_l} \sum_{m=1}^M (T_{im}(j) - \mathbb{E}[T_{im}(j)]).$$

Fixing j and denoting $S_{im}^{(j)} = T_{im}(j) - \mathbb{E}[T_{im}(j)]$, we note that the $\left\{ S_{im}^{(j)} \right\}_{\substack{i=1, \dots, n \\ m=1, \dots, N}}$ are independent of one another (for all i and m), and since $T_{im}(j) \sim \text{Bernoulli}(M_{ij})$, $|S_{im}^{(j)}| \leq 2$. Define $h_j := \sum_{k=1}^K A_{kj}$. Then,

$$\text{Var}(S_{im}^{(j)}) = \mathbb{E}[(T_{im}^{(j)})^2] - M_{ij}^2 = \mathbb{E}[T_{im}^{(j)}] - M_{ij}^2 \leq M_{ij} = \sum_{k=1}^K W_{ik} A_{kj} \leq \sum_{k=1}^K A_{kj} = h_j.$$

Therefore, by the Bernstein inequality (Lemma 8), for the l^{th} connected component \mathcal{C}_l of the graph \mathcal{G} and for any word $j \in [p]$:

$$\forall t > 0, \quad \mathbb{P}\left[\left| \frac{1}{n_{\mathcal{C}_l}} \mathbf{1}_{\mathcal{C}_l}^T Z_{[\mathcal{C}_l]j} \right| > t \right] = \mathbb{P}\left[\frac{1}{n_{\mathcal{C}_l} N} \left| \sum_{i \in \mathcal{C}_l} \sum_{m=1}^N S_{im}^{(j)} \right| > t \right] \leq 2 \exp\left\{ -\frac{n_{\mathcal{C}_l} N t^2 / 2}{h_j + \frac{2}{3}t} \right\}.$$

Choosing $t^2 = C^* \frac{h_j}{n_{\mathcal{C}_l} N} \log(n)$, the previous inequality becomes:

$$\begin{aligned} \mathbb{P}\left[\left|\frac{1}{n_{\mathcal{C}_l}} \mathbf{1}_{\mathcal{C}_l}^T Z_{[\mathcal{C}_l]j}\right| > \sqrt{C^* \frac{h_j}{n_{\mathcal{C}_l} N} \log(n)}\right] &\leq 2 \exp\left\{-\frac{C^* h_j \log(n)}{h_j + \frac{2}{3} \sqrt{C^* \frac{h_j \log(n)}{n_{\mathcal{C}_l} N}}}\right\} = 2 \exp\left\{-\frac{C^* \log(n)}{1 + \frac{2}{3} \sqrt{C^* \frac{\log(n)}{h_j n_{\mathcal{C}_l} N}}}\right\} \\ &\leq 2 \exp\{-C^* \log(n)\}. \end{aligned}$$

as long as $h_j \geq c_{\min} \frac{\log(n)}{n_{\mathcal{C}_l} N}$ (which follows from Assumption 5 since $h_j \geq c_{\min} \frac{\log(n)}{N}$). Therefore, by a simple union bound:

$$\begin{aligned} &\mathbb{P}\left[\exists j \in [p], \exists l \in [n_C] : \frac{1}{n_{\mathcal{C}_l} N} \left| \sum_{i \in \mathcal{C}_l} \sum_{m=1}^N S_{im}^{(j)} \right| > \sqrt{C^* \frac{h_j}{n_{\mathcal{C}_l} N} \log(n)}\right] \\ &\leq 2pn_C \exp\{-C^* \log(n)\} \\ &= \exp\{\log(2) + \log(p) + \log(n_C) - C^* \log(n)\} \\ &\leq \exp\{-C \log(n)\}, \end{aligned}$$

where the last line holds for some large enough constant $\tilde{C} < C^*$ such that $n^{\tilde{C}} \geq 2pn_C$ and $C = C^* - \tilde{C}$. As a consequence of Assumption 5, we know that $p \ll n$ (see remark 2) and under the graph-aligned setting, $n_C \ll n$. Thus with probability $1 - o(n^{-1})$, for all $j \in [p]$ and all $l \in [n_C]$:

$$\left\| \frac{1}{n_l} \mathbf{1}_{\mathcal{C}_l}^T Z_{[n_C]} \right\|_2^2 \leq \sum_{j \in [p]} C^* \frac{h_j}{n_{\mathcal{C}_l} N} \log(n) = C^* \frac{K}{n_{\mathcal{C}_l} N} \log(n).$$

where the last equality follows from the fact that $\sum_{j=1}^p h_j = \sum_{j=1}^p \sum_{k=1}^K A_{kj} = K$. Therefore:

$$\begin{aligned} \|\Pi Z\|_F^2 &= \sum_{l=1}^{n_C} n_{\mathcal{C}_l} \left\| \frac{1}{n_{\mathcal{C}_l}} \mathbf{1}_{\mathcal{C}_l}^T Z_{[n_C]} \right\|_2^2 \\ &\leq \sum_{l=1}^{n_C} C^* n_{\mathcal{C}_l} K \frac{\log(n)}{n_{\mathcal{C}_l} N} \\ &\leq C^* n_C K \frac{\log(n)}{N} \end{aligned}$$

■

Lemma 13 (Concentration of $\|U^\top Z\|_F$) *Let Assumptions 1-5 hold. Let $U \in \mathbb{R}^{n \times r}$ denote a projection matrix: $U^\top U = I_r$, with r a term that does not grow with n or p and $r \leq n$, and let Z denote some centered multinomial noise as in Equation 2. Then with probability at least $1 - o(n^{-1})$:*

$$\|U^\top Z\|_F \leq C \sqrt{\frac{Kr \log(n)}{N}} \quad (79)$$

Proof Let $\tilde{Z} = U^\top Z$. We have:

$$\|\tilde{Z}\|_F^2 = \sum_{j=1}^p \sum_{k=1}^r \tilde{Z}_{kj}^2 \quad (80)$$

We first note that

$$\forall k \in [r], \forall j \in [p], \quad \tilde{Z}_{kj} = \frac{1}{N} \sum_{m=1}^N (U_{\cdot k}^\top T_{\cdot m}(j) - \mathbb{E}[U_{\cdot k}^\top T_{\cdot m}(j)]) \quad (81)$$

$$= \frac{1}{N} \sum_{m=1}^N \sum_{i=1}^n (U_{ik} T_{im}(j) - \mathbb{E}[U_{ik} T_{im}(j)]) \quad (82)$$

$$= \frac{1}{N} \sum_{m=1}^N \sum_{i=1}^n \eta_{im} \quad \text{with } \eta_{im} = U_{ik} T_{im}(j) - \mathbb{E}[U_{ik} T_{im}(j)] \quad (83)$$

Thus, \tilde{Z}_{kj} is a sum of nN centered independent variables.

Fix $k \in [r], j \in [p]$. We have: $\text{Var}(\sum_{i=1}^n \eta_{im}) = \sum_{i=1}^n U_{ik}^2 M_{ij} (1 - M_{ij}) \leq \sum_{i=1}^n U_{ik}^2 h_j$ where $h_j = \sum_{k=1}^K A_{kj}$, since $M_{ij} \leq h_j$. Therefore, as $\sum_{i=1}^n U_{ik}^2 = 1$:

$$\sum_{m=1}^N \sum_{i=1}^n \text{Var}(\eta_{im}) = N h_j.$$

Moreover, for each i, m , $|\eta_{im}| < |U_{ik}| \leq 1$. Thus, by Bernstein's inequality (Lemma 7, with $v = N h_j$ and $c = 1/3$):

$$\mathbb{P}\left[\left|\frac{1}{N} \sum_{m=1}^N \sum_{i=1}^n \eta_{im}\right| > t\right] \leq 2e^{-\frac{Nt^2/2}{h_j + t/3}}$$

Choosing $t = C^* \sqrt{\frac{h_j \log(n)}{N}}$:

$$\mathbb{P}\left[\left|\frac{1}{N} \sum_{m=1}^N \sum_{i=1}^n \eta_{im}\right| > t\right] \leq 2e^{-\frac{(C^*)^2 \log(n)/2}{1 + \frac{C^*}{3} \sqrt{\frac{\log(n)}{h_j N}}}}$$

Therefore, by Assumption 5, $h_j > c_{\min} \frac{\log(n)}{N}$, then, with probability at least $1 - o(n^{-1})$, $|\tilde{Z}_{kj}|^2 \leq C^* \frac{h_j \log(n)}{N}$.

Therefore, by a simple union bound:

$$\begin{aligned} & \mathbb{P}[\exists(j, k) : |\tilde{Z}_{kj}|^2 > C^* \frac{h_j \log(n)}{N}] < rpe^{-C^* \log(n)} \\ \implies & \mathbb{P}[\|\tilde{Z}\|_F^2 > C \frac{Kr \log(n)}{N}] < rpe^{-C^* \log(n)} \quad \text{since } \sum_{j=1}^p h_j = K. \end{aligned} \quad (84)$$

Since we assume that $pr \ll n$, the result follows. \blacksquare

Lemma 14 (Concentration of $\|\Pi ZV\|_F$) *Let Assumptions 1-5 hold. Let V be a orthogonal matrix: $V \in \mathbb{R}^{p \times K}$, $V^\top V = I_K$. Let Π denote the projection matrix unto $\text{Ker}(\Gamma^\dagger \Gamma)$, such that $I_n = \Pi \oplus^\perp \Gamma^\dagger \Gamma$. With probability at least $o(n^{-1})$:*

$$\|\Pi \tilde{Z}\|_F^2 \leq C^* n_C K \frac{\log(n)}{N} \quad (85)$$

where $\tilde{Z} = ZV$.

Proof We follow the same procedure as the proof of Lemma 12. Letting \mathcal{C}_j denote the j^{th} connected component of the graph \mathcal{G} and $n_{\mathcal{C}_l} = |\mathcal{C}_l|$ its cardinality, $\|\Pi \tilde{Z}\|_F$ can be decomposed as:

$$\begin{aligned} \|\Pi \tilde{Z}\|_F^2 &\leq \sum_{l=1}^{n_C} \left\| \frac{1}{n_{\mathcal{C}_l}} \mathbf{1}_{\mathcal{C}_l} \mathbf{1}_{\mathcal{C}_l}^T \tilde{Z}_{[\mathcal{C}_l]} \right\|_F^2 \\ &= \sum_{l=1}^{n_C} n_{\mathcal{C}_l} \left\| \frac{1}{n_{\mathcal{C}_l}} \mathbf{1}_{\mathcal{C}_l}^T \tilde{Z}_{[\mathcal{C}_l]} \right\|_2^2 \end{aligned}$$

By Assumption 3, $\forall i, N_i = N$. Using the definition of T_{im} provided in (65), for each $k \in [K]$, and each connected component \mathcal{C}_l :

$$\frac{1}{n_{\mathcal{C}_l}} \mathbf{1}_{\mathcal{C}_l}^T \tilde{Z}_{[\mathcal{C}_l]k} = \frac{1}{n_{\mathcal{C}_l} N} \sum_{i \in \mathcal{C}_l} \sum_{m=1}^M \sum_{j=1}^p (T_{im}(j) - \mathbb{E}[T_{im}(j)]) V_{jk}.$$

Fix j and denote $\eta_{jm} = (T_{im}(j) - \mathbb{E}[T_{im}(j)]) V_{jk}$. We have $|\sum_{j=1}^p \eta_{jm}| \leq 2$ and

$$\text{Var}\left(\sum_{j=1}^p \eta_{jm}\right) = \sum_{j=1}^p M_{ij} (V_{jk})^2 - \left(\sum_{j=1}^p M_{ij} V_{jk}\right)^2 \leq 1$$

Therefore, by Bernstein's inequality (Lemma 8), for the l^{th} connected component \mathcal{C}_l of the graph \mathcal{G} and for any $k \in [K]$:

$$\forall t > 0, \quad \mathbb{P}\left[\left|\frac{1}{n_{\mathcal{C}_l}} \mathbf{1}_{\mathcal{C}_l}^T \tilde{Z}_{[\mathcal{C}_l]k}\right| > t\right] = \mathbb{P}\left[\frac{1}{n_{\mathcal{C}_l} N} \left|\sum_{i \in \mathcal{C}_l} \sum_{m=1}^M \sum_{j=1}^p \eta_{jm}\right| > t\right] \leq 2 \exp\left\{-\frac{n_{\mathcal{C}_l} N t^2 / 2}{1 + \frac{2}{3}t}\right\}.$$

Choosing $t^2 = C^* \frac{\log(n)}{n_{\mathcal{C}_l} N}$, the previous inequality becomes:

$$\mathbb{P}\left[\left|\frac{1}{n_{\mathcal{C}_l}} \mathbf{1}_{\mathcal{C}_l}^T \tilde{Z}_{[\mathcal{C}_l]k}\right| > \sqrt{C^* \frac{\log(n)}{n_{\mathcal{C}_l} N}}\right] \leq 2 \exp\left\{-\frac{C^* \log(n)}{1 + \frac{2}{3} \sqrt{C^* \frac{\log(n)}{n_{\mathcal{C}_l} N}}}\right\} \leq 2 \exp\{-C \log(n)\}.$$

as long as $n_{\mathcal{C}_l} N \gtrsim \log(n)$. Therefore, by a simple union bound:

$$\begin{aligned} &\mathbb{P}\left[\exists k \in [K], \exists l \in [n_C] : \frac{1}{n_{\mathcal{C}_l} N} \left|\sum_{i \in \mathcal{C}_l} \sum_{m=1}^M \sum_{j=1}^p \eta_{jm}\right| > \sqrt{C^* \frac{\log(n)}{n_{\mathcal{C}_l} N}}\right] \\ &\leq 2K n_C \exp\{-C^* \log(n)\} \\ &= \exp\{\log(2) + \log(K) + \log(n_C) - C^* \log(n)\} \\ &\leq \exp\{-(C-3) \log(n)\}, \end{aligned}$$

where the last line holds for some large enough constant $\tilde{C} < C^*$ such that $n^{\tilde{C}} \geq 2Kn_C$ and $C = C^* - \tilde{C}$. Thus with probability $1 - o(n^{-1})$, for all $k \in [K]$ and all $l \in [n_C]$:

$$\left\| \frac{1}{n_l} \mathbf{1}_{\mathcal{C}_l}^T \tilde{Z}_{[n_C]} \right\|_2^2 \leq \sum_{k \in [K]} \frac{C^* \log(n)}{n_{\mathcal{C}_l} N} = C^* \frac{K}{n_{\mathcal{C}_l} N} \log(n).$$

and

$$\begin{aligned} \|\Pi \tilde{Z}\|_F^2 &= \sum_{l=1}^{n_C} n_{\mathcal{C}_l} \left\| \frac{1}{n_{\mathcal{C}_l}} \mathbf{1}_{\mathcal{C}_l}^T \tilde{Z}_{[n_C]} \right\|_2^2 \\ &\leq \sum_{l=1}^{n_C} C^* n_{\mathcal{C}_l} K \frac{\log(n)}{n_{\mathcal{C}_l} N} \\ &\leq C^* n_C K \frac{\log(n)}{N} \end{aligned}$$

■

Appendix D. Synthetic Experiments

We propose the following procedure for generating synthetic datasets such that the topic mixture matrix W is aligned with respect to a known graph.

1. **Generate spatially coherent documents** Generate n points (documents) over a unit square $[0, 1]^2$. Divide the unit square into $n_{grp} = 30$ equally spaced grids and get the center for each grid. Apply k-means algorithm to the points with these as initial centers. This will divide the unit square into 30 different clusters. Next, randomly assign these clusters to K different topics. In the end, within the same topic, we will observe some clusters of documents that are not necessarily next to each other (see Figure 11). This is a more challenging setting where the algorithm has to leverage between the spatial information and document-word frequencies to estimate the topic mixture matrix. Based on the coordinates of documents, construct a spatial graph where for each document, edges are set for the $m = 5$ closest documents and weights as the inverse of the euclidean distance between two documents.
2. **Generate matrices W and A** For each cluster, we generate a topic mixture weight $\alpha \sim \text{Dirichlet}(\mathbf{u})$ where $u_k \sim \text{Unif}(0.1, 0.5)$ ($k \in [K]$). We order α so that the biggest element of α is assigned to the cluster's dominant topic. We also add small Gaussian noise to α so that in the end, for each document in the cluster, $W_i = \alpha + \epsilon$, $\epsilon_k \sim N(0, 0.03)$. We sample K rows of W as *anchor documents* and set them as \mathbf{e}_k . The elements of A are generated from $\text{Unif}(0, 1)$ and normalized so that each row of A sums up to 1. Similarly to anchor documents, K columns of A are selected as *anchor words* and set to \mathbf{e}_k .

3. **Generate frequency matrix X** We obtain the ground truth $M = WA$ and sample each row of D from $\text{Multinomial}(N, M_{i.})$. Each row of X is obtained by $X_{i.} = D_{i.}/N$.

Figure 11 illustrates the ground truth mixture weights, $W_{.k}$, for each topic generated with parameters $n = 1000, N = 30, p = 30$ and $K = 3$. Here, each dot in the unit square represents a document, with lighter colors indicating higher mixture weights. We observe patches of documents that share similar topic mixture weights.

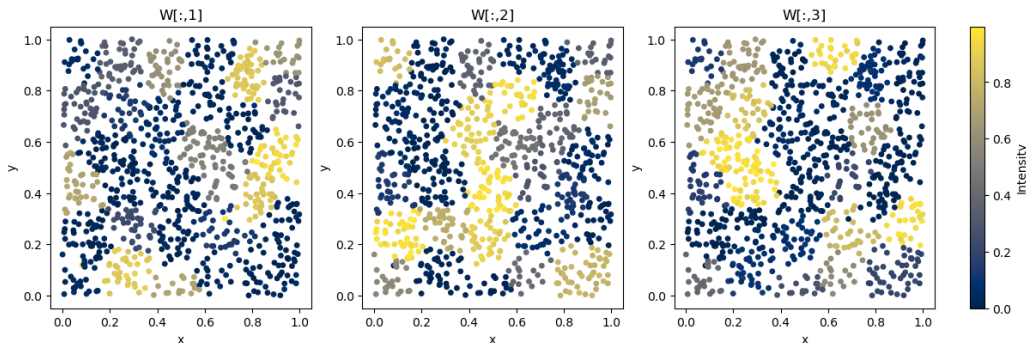


Figure 11: Heatmap of generated ground truth $W_{.1}, W_{.2}, W_{.3}$, representing each topic mixture weight.

We show the ℓ_1 errors of estimated \widehat{W} and \widehat{A} under the same parameter settings as Section 3.4. We observe that the behavior of ℓ_1 error is similar to ℓ_2 error in Section 3.4. GpLSI has the lowest ℓ_1 errors of \widehat{W} , followed by LDA and one-step graph-aligned denoising. We also observe that GpLSI has the lowest ℓ_1 errors of \widehat{A} .

Appendix E. Experiments

In this section, we provide supplementary plots for our analysis on the real datasets discussed in Section 4.

E.1 Estimated tumor-immune microenvironment topic weights in Section 4.1.1

We present the estimated tumor-immune microenvironment topics estimated with GpLSI, pLSI, and LDA for $K = 1$ to 6. The topics are aligned among the methods as well as among different number of topics, K . Topics dominated by stroma, granulocyte, and B cells, recur in both GpLSI and LDA.

E.2 Kaplan-Meier curves of different topic groups in Section 4.1.1

We plot Kaplan-Meier curves for tumor-immune micro-environment topics using the dichotomized topic proportion for each patient. We observe that granulocyte (Topic 2) is associated with lower risk of cancer recurrence across all methods.

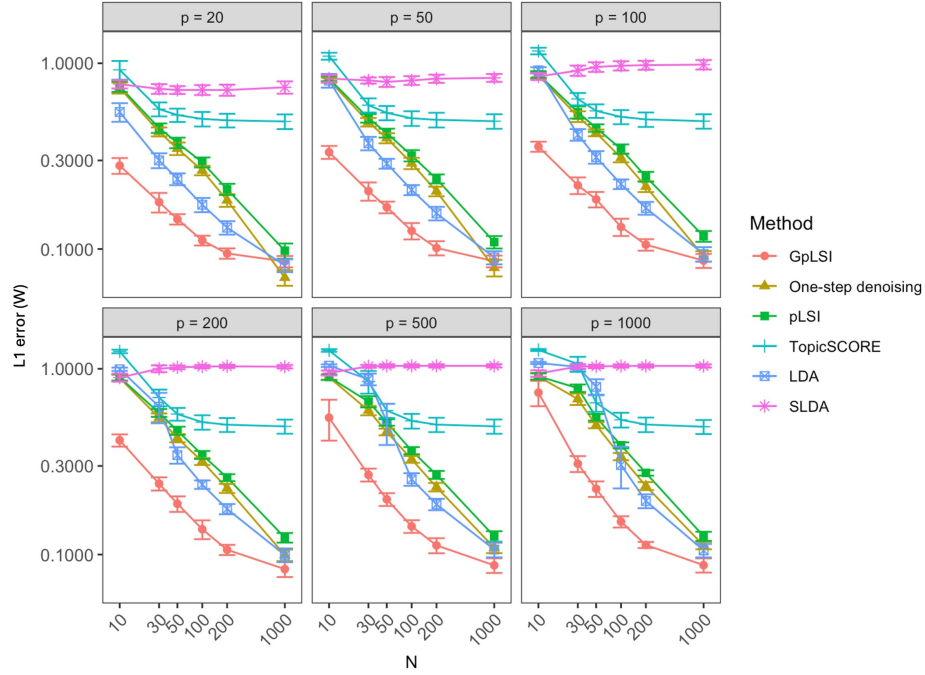


Figure 12: ℓ_1 error for the estimator \widehat{W} (defined as $\min_{P \in \mathcal{P}} \frac{1}{n} \|\widehat{W} - WP\|_F$) for different combinations of document length N and vocabulary size p . Here, $n = 1000$ and $K = 3$.

E.3 Topics by top common ingredients in Section 4.2

We illustrate each topic with the top ten ingredients with the highest estimated weights. Compared to anchor ingredients in Section 4.2, we observe that there are more overlapping ingredients among topics. While the top ten and anchor ingredients for each topic in GpLSI and LDA reflect similar styles, it is difficult to match anchor ingredients to the top ten ingredients in pLSI because the top ten ingredients are too similar across topics.

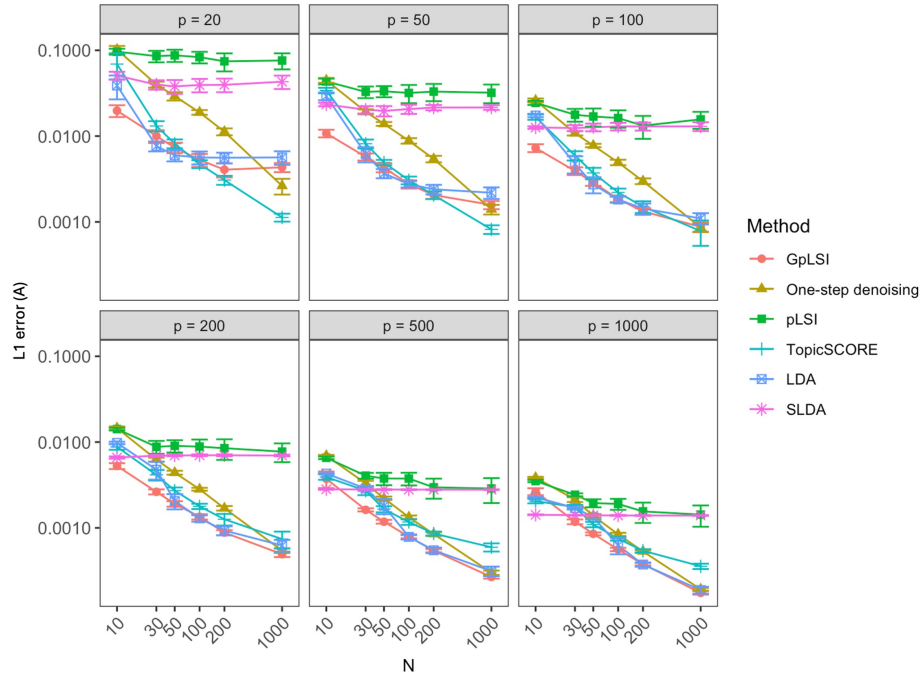


Figure 13: ℓ_1 error for the estimator \hat{A} (defined as $\min_{P \in \mathcal{P}_p} \frac{1}{p} \|\hat{A} - PA\|_F$) for different combinations of document length N and vocabulary size p . Here, $n = 1000$ and $K = 3$.

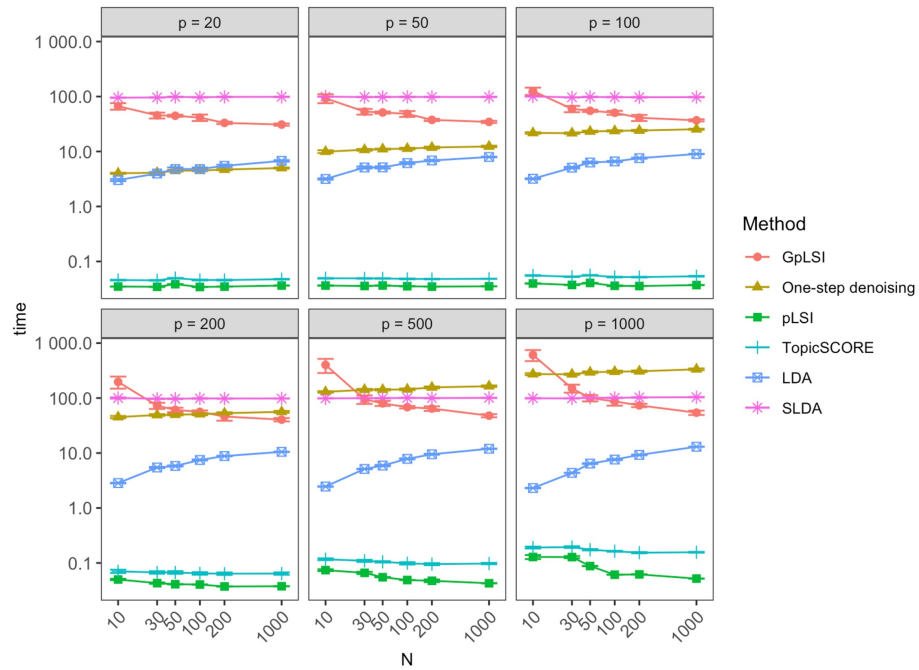


Figure 14: Computation time for different combinations of document length N and vocabulary size p . Here, $n = 1000$ and $K = 3$.

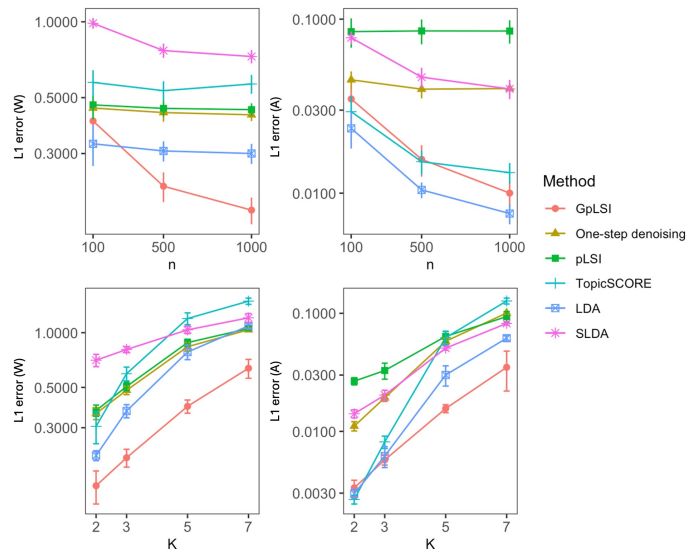


Figure 15: ℓ_1 error of W (left), A (right) for different corpus size n and number of topics K . Here, $N = 30$ and $p = 30$.

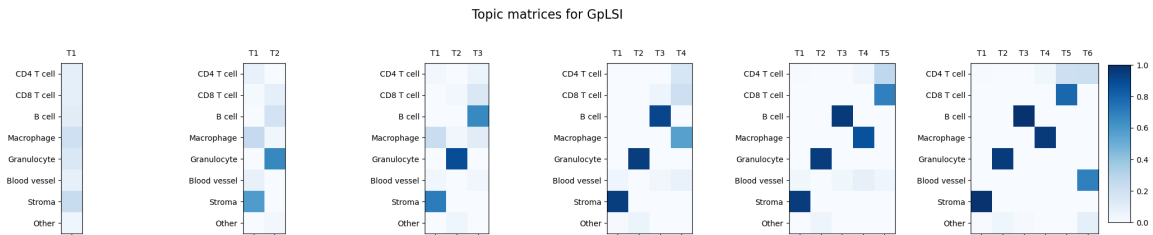


Figure 16: Estimated topic weights of tumor-immune microenvironments using GpLSI.

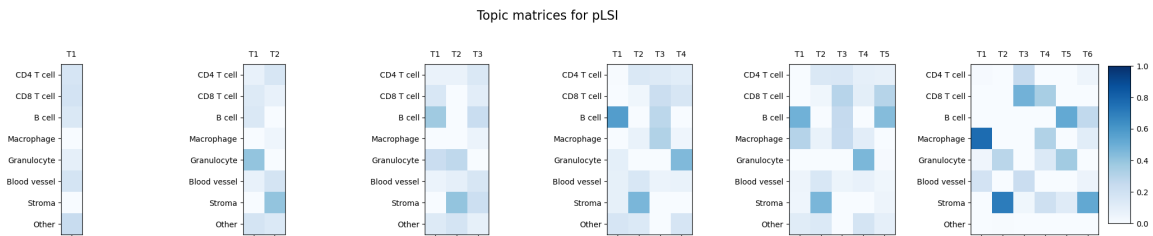


Figure 17: Estimated topic weights of tumor-immune microenvironments using pLSI.

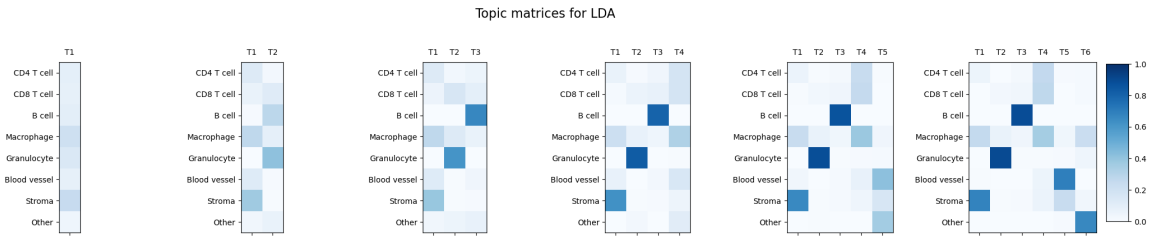


Figure 18: Estimated topic weights of tumor-immune microenvironments using LDA.

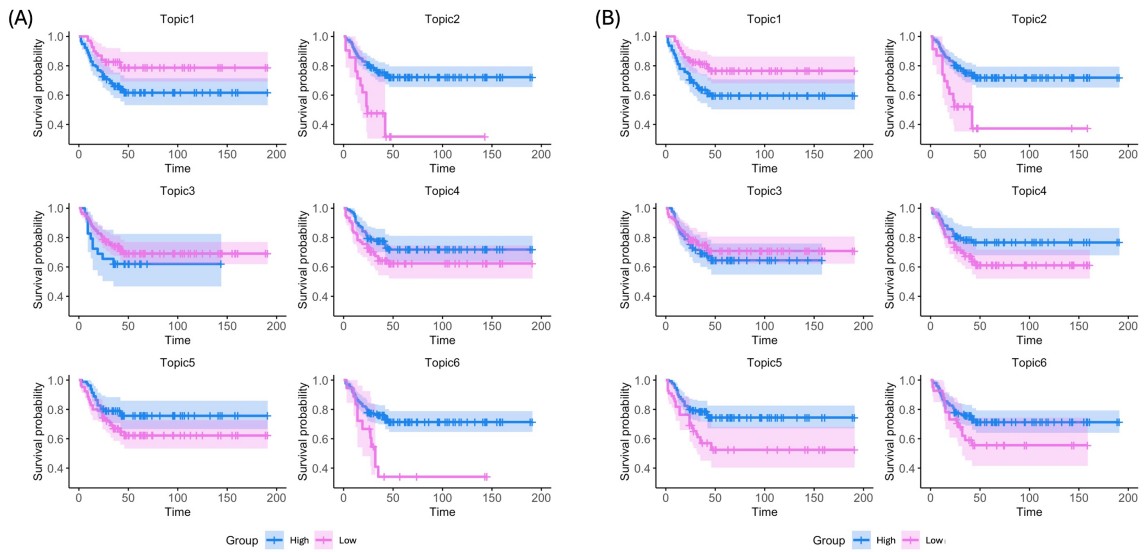


Figure 19: Kaplan-Meier curves of dichotomized topic proportions using pLSI (left) and LDA (right).

GRAPH-STRUCTURED TOPIC MODELING

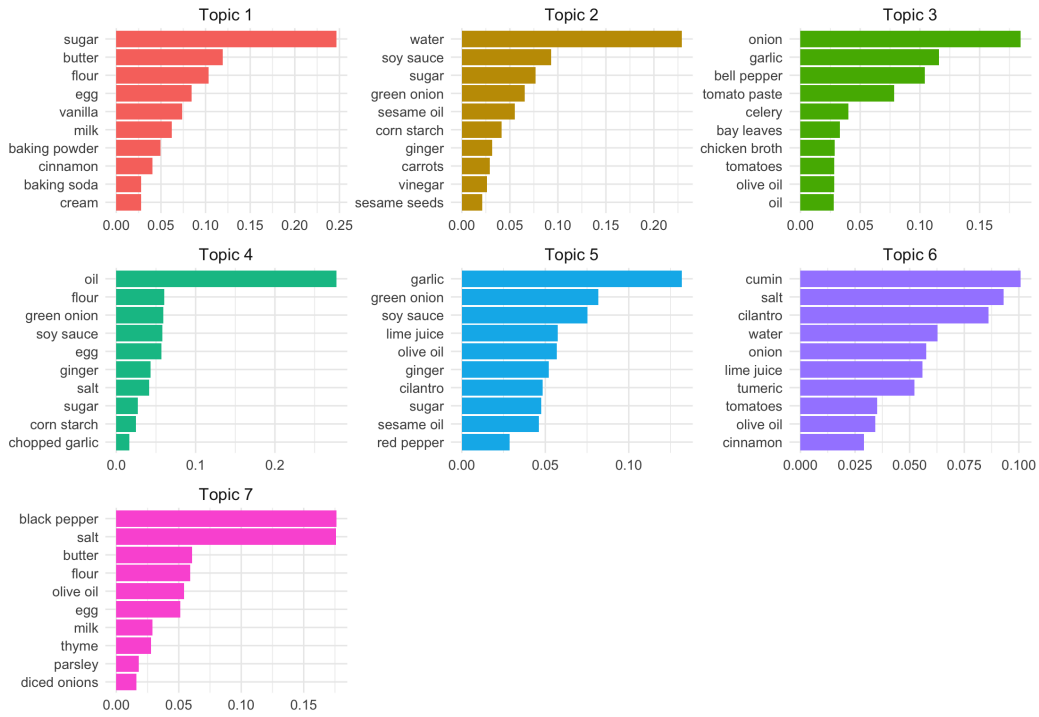


Figure 20: Top ten common words for each topic estimated by GpLSI.

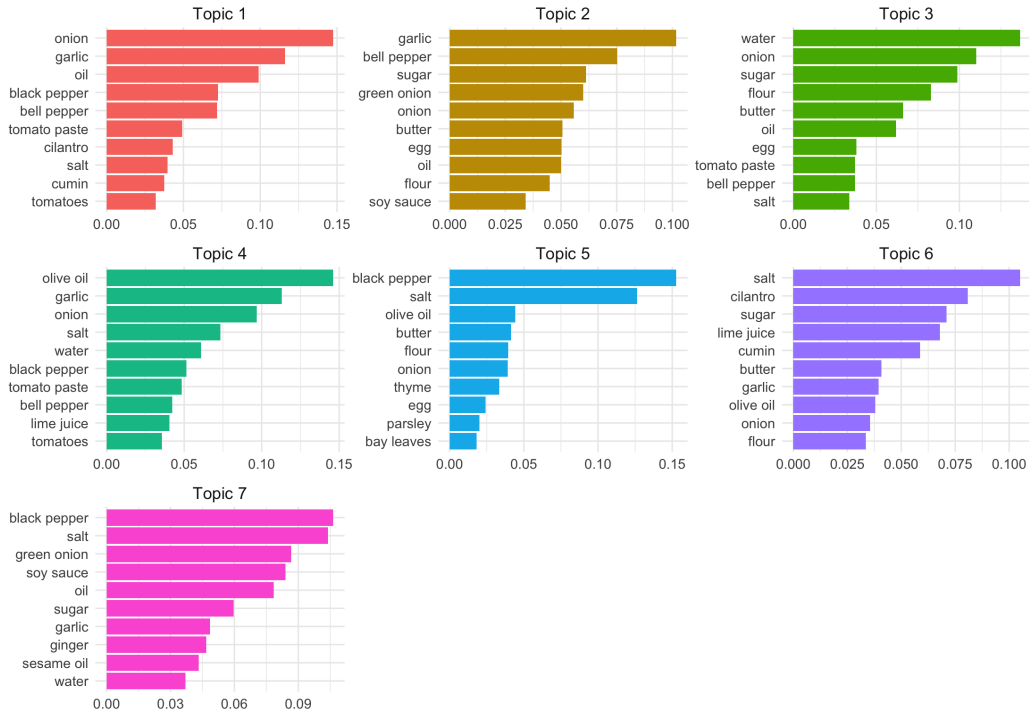


Figure 21: Top ten common words for each topic estimated by pLSI.

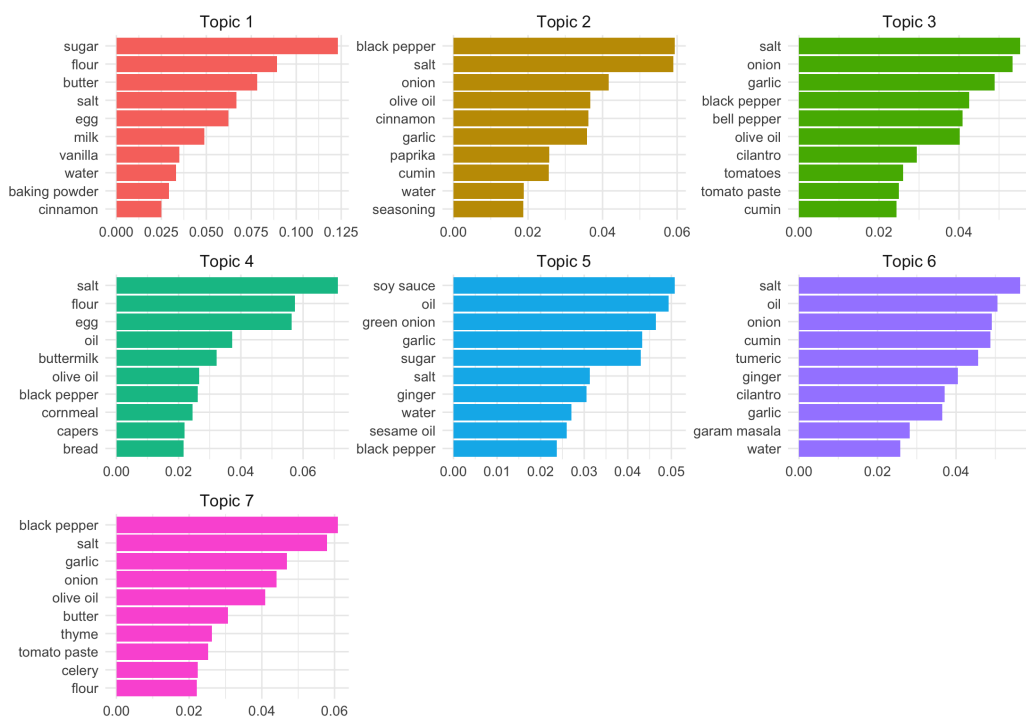


Figure 22: Top ten common words for each topic estimated by LDA.